# Continuum Modeling Techniques and Their Application to the Physics of Soil Liquefaction and Dissipative Vibrations

Daniel Lakeland
University of Southern California

December 2013

# Dedication

This dissertation is dedicated to my dear wife Dr. Francesca Mariani, who supported me during my graduate studies and provided the vast majority of funding for this research. She has a deep and abiding love of scientific discovery, a strong sense of what the truly important questions are in her field, and is extremely generous with her expertise. May you continue to have an endless supply of graduate, undergraduate, and volunteer researchers to enrich.

Thank you to my two doodlers Nicolas and Alexander, the most important products of my research.

I would like to thank Dr. Roger Ghanem and Dr. Amy Rechenmacher who advised me during my graduate career, and especially got me started on the right foot, and helped me to focus on the essential questions that led to my biggest discoveries.

To Dr. Paul Newton, who seemed to always understand where I was going and appreciated the nature of my work. His email saying "I like the way you are approaching it from the ground up. keep working that way - sometimes it's hard to do, and sometimes under appreciated, but I'm a supporter!" provided me with enough encouragement for over a year of grinding out results.

To Dr. Yehuda Ben-Zion whose research group in the Earth Sciences studies earthquakes both in deep details and across the whole breadth of related phenomena. Thank you for your encouragement and many excellent discussions on wide ranging topics and for the environment you create of both nurturing and challenging students.

To Dr. Andrew Gelman whose blog and books introduced me to the practical application of Bayesian Statistics to scientific data analysis, a technique especially suited to statistical analysis in the context of complex physical models and measurement errors. Also, for the Zombies.

To Dr. Edward Nelson whose IST system for nonstandard analysis is sufficiently simple that it can be used for practical purposes by mere mortals.

To Dr. Dennis Hazelett who I've known since 5th grade, who provided me with at least four or five distracting projects in Biology and Bioinformatics during my PhD, which got me my first peer reviewed publications and gave me focused projects where I could refine techniques and software knowledge that ultimately contributed to my ability to finish my own research. Hopefully none of my graphs need to be turned upside down.

To my mother, who always supported my nerdy tendencies, and somehow managed to afford computers for me while I was growing up, even when they cost six months of discretionary spending, and my father, who for all his troubles in life was always proud of my accomplishments, I'm happy that this work validates the importance of his contribution to the UC Davis NEES Geotechnical Centrifuge project.

Also, I would like to thank Dr. Guy Miller, a colleague at Barra Inc. in the late 1990's who first got me thinking about the beauty of physics and the joy of modeling and data analysis, and Dr. Michael Bishop whose undergraduate classes in the Philosophy Of Science gave me an appreciation for getting right to the heart of the matter and not fooling around on the periphery.

Finally, this research would have been computationally painful if it were not for the work of many contributors to the Free Software projects R, Maxima, and JAGS and the contributors to the Maxima mailing list who provide insight into an under-appreciated piece of free software.

# Contents

# Chapter I

# Purpose and Outline

*I go among the fields and catch a glimpse of a stoat or a fieldmouse peeping out of the withered grass — The creature hath a purpose and its eyes are bright with it — I go amongst the buildings of a city and I see a man hurrying along—to what?*

—John Keats

The research in this dissertation encompasses four main thrusts: mathematical modeling techniques for building continuum models of systems that are explicitly acknowledged to be non-continuous at the finest scale of observation, application of a continuum model of water flow in porous media to the problem of "drained vs undrained" processes in soil liquefaction, an example model for the dissipation of waves in a system of molecules decoupled from any radiative process, where the total energy stays constant, and the application of Bayesian Statistics to identifying the parameters of these physical models.

All of this work arises in the context of an original project to analyze how soil liquefaction occurs, and to incorporate physical principles such as energy conversion and entropy generation into the physical description.

The work on soil liquefaction has been submitted to Proceedings of the Royal Society A (Lakeland, Rechenmacher, and Ghanem n.d.). A paper is being prepared on unifying a spectrum of continuum modeling techniques under the umbrella of analysis via Internal Set Theory (IST), and the model for dissipative waves is also being prepared for submission.

The dissertation proceeds by first describing the initial motivation related to soil liquefaction, and the background knowledge that led to the research program. Then, I discuss a generalized modeling technique using the

mathematics of IST which is applicable to building and interpreting continuum models of explicitly non-continuous phenomena. Following that background, a continuum model is presented for the fluid flow through porous media arising during earthquake liquefaction and based on what might be called classical continuum modeling involving Darcy's law, without explicit reference to the IST based technique. Following that, a model is developed using the IST technique explicitly which ultimately leads in a straightforward way to a dynamic model of dissipative waves in molecular scale bars, and a comparison of the continuum type model to the statistics of a detailed Molecular Dynamics (MD) simulation. Finally the comparison to MD is performed by Bayesian analysis to determine the implications of the data for the unknown parameters.

# Chapter 2

# Background

*I remember when our whole island was shaken with an earthquake some years ago, there was an impudent mountebank who sold pills which (as he told the country people) were very good against an earthquake.*

—Joseph Addison *The Tatler*

Although the research encompassed in this dissertation ranges over a wide swath of scales, and includes mathematical, statistical, mechanical, and philosophical topics, all of the research was ultimately motivated by initial inquiries into the way in which soil liquefies during an earthquake. With apologies for the pun, this topic has been considered as "settled" in the Geotechnical field to the extent that textbook definitions and descriptions are consistent and have been for many years. The only problem is that these textbook descriptions do not offer much explanatory power in terms of well known physical principles, especially the thermodynamics of fluids that describes how fluid pressure is generated. The background given here motivates and informs the in-depth physical analysis given in future chapters.

Liquefaction of sandy soils is a serious risk in earthquake prone regions. Soil liquefaction is a range of phenomena all related to the interaction between fluid in the pores of a granular soil and the motion of the grains. The worst consequences occur when grains cease to maintain tight contact and the mixture is able to flow like a slurry, resulting in large deformations of the soil. During my research the footage taken by Brent Kooi of liquefaction in a park during the Tohoku-Oki earthquake in Japan provided a striking real-time example of how quickly earthquake liquefaction can occur (`http://www.youtube.com/watch?v=rn3oAvmZY8k`). This video provides a clear timescale for the liquefaction process as the ground floats on a layer of

water and the water rises all the way to the surface within the first 40 seconds of an earthquake whose shaking lasted several minutes in many places (Nyquist 2012).

So far models of liquefaction in engineering practice have involved primarily statistical prediction rules involving regression or curve fitting to case studies and laboratory tests (cf. (Idriss and Boulanger 2006)). Dynamic models of liquefaction have been built based on continuum models with stress-strain relationships defined based on phenomenological hysteresis models involving "backbone curves" (cf. (Liang 1995)). Several investigators have shown that water pressure build up is highly correlated with energy dissipation, as originally proposed by Nemat-Nasser and Shokooh (1979). In particular, laboratory and field observations inform the work by Figueroa et al. (1994) and Davis and Berrill (2001).

Although the complexity of the phenomenon is widely acknowledged, so far, the physical understanding of soil liquefaction has relied on a core set of assumptions and understanding that is consistent across the field. A critical concept is the effective stress, the total stress across a section minus the portion provided by water pressure. An effective stress of zero means that grain-grain contacts have disappeared and this is more or less the definition of a fully liquefied soil.

**Textbook Definitions** The process of liquefaction has a consistent textbook description involving an assumption of "undrained" pore pressure increase. For example from Holtz and Kovacs "The loose sand trieds [sic] to densify during shear and this tends to squeeze the water out of the pores. Normally, under static loading, the sand has sufficient permeability so the water can escape and any induced pore water pressures can dissipate. But in this situation because the loading occurs in such a short time, the water doesn't have time to escape and the pore water pressure increases." (Holtz and Kovacs 1981, p. 245)

Alternatively from Kramer: "The tendency for dry cohesionless soils to densify under both static and cyclic loading is well known. When cohensionless [sic] soils are saturated, however, rapid loading occurs under undrained conditions, so the tendency for densification causes excess pore pressures to increase and effective stresses to decrease." (Kramer 1996, p. 349).

Both descriptions involve an analogy between the dry sand, which densifies during shearing, and the saturated sand which is assumed to be iso-

volumetric and instead increases in water pressure. Holtz and Kovacs offer a picture of a tabletop tank where a quick blow to the side of the tank instantly liquefies the sand, and piezometers show significant water pressure increase over static conditions. (Holtz and Kovacs 1981, p. 243 fig 7.12).

Unfortunately these standard descriptions do not offer a clear physical picture of what occurs to cause the pressure increase, but they both agree on the undrained nature of the event. The tabletop demonstration of Holtz and Kovacs however occurs with impact loading lasting perhaps 10 or 100 milliseconds, whereas earthquake loading occurs over a timescale of 10 to 100 seconds or more. The maximum water flux which can occur on a millisecond time scale is significantly different from the mass flux possible over a 10 second time scale.

**Problems With The Textbook Description** Although the standard description is quite suggestive, there are many open questions. How are laboratory conditions and field conditions similar or different? Does pore water pressure build-up cause loss of effective stress, or does loss of effective stress cause pore water pressure build up? What is the role of volume changes and mass flow? Kokusho and Kojima offer an example laboratory experiment where water migration is clearly important and water film formation is the primary explanation for soil strength failure (Kokusho and Kojima 2002; Kokusho 1999). These experiments involve a column of soil in the vicinity of 1 to 2 meters high carefully layered, and excited by a blow to the bottom of the column. After a brief transient period, under certain circumstances the bottom layers of soil settle downward and a long-lasting water film forms between the bottom layer and upper layers. Clearly, water has migrated upwards while soil has migrated downwards, all within a timescale of a second or so. Such behavior is inconsistent with the concept of an "undrained" event. How can we explain these phenomena in a physically consistent way?

**The Way Forward** The insight that wave energy dissipation was associated with soil water pressure changes as described by Nemat-Nasser and Shokooh (1979) led me to investigate both the process that causes water pressure changes, and methods of understanding wave dissipation. The process of wave dissipation in soil is difficult to model without a considerable body of physical experiments designed to inform the model building process. Processes that could contribute to wave dissipation in sand include frictional

rubbing of the grains, and reflection, scattering, and geometric spreading of the wave. Processes that could contribute to reflection and scattering include the breakage of force chains between particles that could contribute to both the production of spherically spreading high frequency harmonics (due to impacts between grains when force chains collapse) and increased frictional heat generation as grains rub against each other. With such a wide variety of processes that might contribute, a body of physical experiments are required in order to inform the modeler.

**Contribution To Liquefaction** The model developed in chapter 4 describes how water pressure develops under an assumed grain deformation, which enters in terms of the rate of change of $\varphi$ the porosity of the material. This chapter gives more detailed background on liquefaction history and then proceeds to develop an equation for the rate of change of pore pressure from first principles, fully incorporating the thermodynamics of water and Darcy's law, a well known model for viscously dominated flow. In order to close the system for prediction from first principles, a model for $\frac{\partial \varphi}{\partial t}$ would be needed, and this model would require coupling a physical description of the grain motion to a continuum description of the whole soil deposit.

**Problems With Continuum Models of Sand** However, even if we had a good understanding of the inter-grain interactions, it is hard to understand how to build a continuum model of grains interacting in a way that makes consistent physical sense. We want a continuum model, because a model built on the mechanics of individual grains depends on too many details to be worthwhile. In particular, to be accurate we need to know the irregular shape, and material properties of an enormous number of grains that fill thousands of cubic meters of soil. A continuum model has the property that for any location in space, there is some value of a relevant physical variable, such as density, velocity, and so forth. In a network of grains, it's clearly the case that at a given point either there is a grain, or there is no grain, so that if we are to properly describe the system with a continuum model we need to understand how the continuum model is to correspond to this discrete reality. In later chapters of this dissertation I develop a framework for interpreting continuum models that can inform the process of building continuum models of discrete particles in a consistent way.

**Building an Example Continuum Model of Discrete Particles** A model of dissipation in the simple Lennard-Jones model of molecular interactions is an easier place to start developing these modeling techniques, and the model developed in chapter 5 of this dissertation informs us of an important physical process in wave dissipation, namely momentum diffusion by coupling of thermal and wave motion. This model was built by explicitly using the techniques I developed for interpreting continuum models.

As a first pass at understanding the effect of momentum diffusion, we can consider how kinetic energy that is transferred from a small mass to a larger mass inevitably leads to dissipation. Consider a 3g bullet traveling at 500 m/s impacting a 1 kg block of clay on a frictionless table, and embedding itself. The bulk-scale (non-thermal) kinetic energy of the system before impact is $0.003 \times 500^2/2 = 375\,\mathrm{J}$ and the momentum of the system is $0.003 \times 500 = 1.5\,\mathrm{kg\,m/s}$. The momentum is conserved during impact, so that the final velocity of the clay with bullet embedded is $(1.5\,\mathrm{kg\,m/s})/(1.003\,\mathrm{kg}) = 1.496\,\mathrm{m/s}$ and the kinetic energy is $1.003 \times 1.496^2/2 = 1.12\,\mathrm{J}$ or a loss of $(1 - 1.12/375) \times 100 = 99.7\%$. If momentum is conserved, but becomes distributed over a larger mass, inevitably the kinetic energy associated with center of mass motion must decrease, and this is the effect that predicts the dissipation in the dissipative wave model, though the causes are much different from those operating during a bullet impact.

In the next chapter we will visit this model building technique as background for the models described in later chapters.

# Chapter 3

# Techniques and Philosophical Considerations for Continuum Models

*If you do not look at things on a large scale it will be difficult for you to master strategy*

—Miyamoto Musashi

It isn't generally the practice of Engineers to delve too deeply into the *philosophical* implications of the models or procedures they use. Most of the time, these sorts of questions are simply unnecessary. We can start with some basic description of phenomena which is known to work reasonably well in practice, and we can make modifications or predictions based on those descriptions that are interpreted implicitly in some conceptual framework that is common to our colleagues. For example, the Navier-Stokes equations for the motion of a Newtonian fluid are enormously successful. We can mostly design airplanes without worrying about the fact that air is actually a collection of individual molecules as this fact has no measurable consequences at the scale of a ten meter long wing. Occasionally though, we will ask questions where a continuum description has questionable meaning. What is the meaning of a continuum description of the flow of a fluid through a nanotube only 10 atomic diameters wide? How does a continuum model of fluids make sense at the edge of the atmosphere where the mean free path of a molecule is perhaps 1 meter? And especially in granular materials, how do we describe the flow of fluid and grains as a continuum when we wish to describe features on a similar length scale as the grains themselves?

Jacob Bear explicitly deals with this question in the first chapter of his book on fluid flow in porous media (Bear 1988, p.20). To aid in the development of models in later chapters, I will introduce here several unifying notions that allow us to interpret continuum models even when the non-continuum nature of the material is apparent. In addition to allowing for better comparisons between reality and the model predictions, these philosophical and mathematical issues can inform the development of new models in the initial stages.

## 3.1 Continuum Model as Statistical Mechanics

Whenever we discuss a continuum model of physical phenomena, we necessarily either ignore or must confront the question of what does a continuum mean? Clearly our modern knowledge tells us that air is made of nearly non-interacting molecules bouncing around within the entire volume containing them. Water is made of molecules which interact to maintain a close proximity to each other but do not have long-range order over many molecular diameters. The volume they occupy stays relatively constant as the container size increases due to the formation of a gas-liquid interface. A glass is like a liquid in that it has molecules in close proximity and no long range order, but the molecules are held in place in some kind of local order which is preserved over long time scales. Over extremely long time scales, in the crust of the earth for example, we may have material flow in a material which would normally be considered a solid such as portions of the earth's mantle. A polycrystalline solid has molecules arranged in a lattice with a constant lattice orientation over a significant multiple of the lattice spacing, but varying lattice arrangements from place to place within the solid. A single crystal such as a quartz mineral may have a constant lattice alignment throughout its entire extent. These forms of matter make up the bulk of everyday materials, and yet we frequently describe their behavior in terms of a continuum. The mathematical property of a continuum is that it has a specific value for some variables of interest at any real number spatial coordinate. Since in a Newtonian description, a molecular material can at best be said to have a particular property only at exactly the coordinates of the molecules, clearly the continuum is not a representation of the molecules themselves.

An alternative approach is to consider the quantities of interest in a continuum model as statistical averages over some volume that is small with

respect to the overall body in question but large enough with respect to the elementary particles that make up the body to have well controlled statistics. A continuum model of a physical body is then a description of a large but unspecified number of these small volumes. Averages are the appropriate type of statistic due to the presence of conserved quantities. The total mass, energy, momentum, and angular momentum of a system under ordinary physical conditions is conserved in the absence of external interactions, and the linear nature of Newton's Laws $\sum F = ma$ makes the total of a conserved quantity or its flux the appropriate quantities of interest. The property that makes averaging meaningful for these types of quantities is:

$$\sum_{i=1}^{N} x_i = \sum_{j=1}^{K} n_j \langle x \rangle_j$$

In other words, the total over all N elementary quantities $x_i$ of interest, when that total is a conserved quantity, can also be calculated as the sum of all the K extrapolated averages of groups of varying size $n_j$. We use the average when we are interested in the behavior of the total, so that statistics like the median or other quantiles of the distributions are not appropriate in the presence of conserved quantities, except in so far as they may be effective approximations of the average.

This statistical outlook on continuum models is not new. The notion of a "representative volume element" (RVE) is common in the literature of multi-scale modeling (cf. (Galvanetto and Aliabadi 2010)). However, it should be noted that there is a continuum of sizes of volume element, each with its own degree of "representativeness". A trade off exists between the size of statistical fluctuations expected in the statistic, and the size of the smallest spatial detail that the model can capture. This trade off can be illustrated easily in figure 3.1. In these graphs, 10000 points were placed uniformly at random within the interval $(0, 1)$. Because the points are non-interacting their density is exceedingly noisy compared to typical interacting particles which will tend to arrange themselves into a more ordered and less energetic state. The number density of points can be computed by taking a box centered at a given location with varying size. In addition to the uniformly weighted average, it is also possible to use a smooth kernel weighted average to get a lower noise statistic, but for illustration purposes the uniform box is convenient.

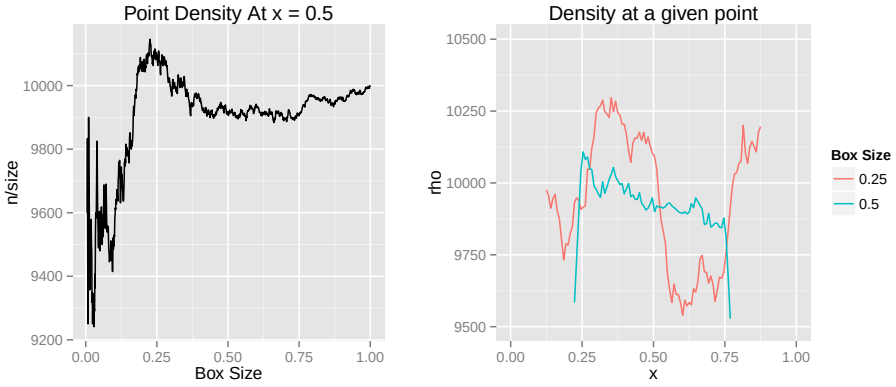


Figure 3.1: As box size increases, the fluctuations in density as a function of box size decreases. In the vicinity of size 0.25 the density at x = 0.5 is relatively insensitive to the specifics of the box size (left graph). At box size 0.25 the density has a large negative gradient in the vicinity of location 0.5 (right graph), for box size 0.5 this gradient is smaller and relatively uniform across the domain.

In any mathematical modeling procedure it is necessary to ignore certain effects which are deemed to be negligible, because if we attempt to include all details, our models become intractable for systems beyond a few thousand or million molecules. Even in MD simulations potentials are typically truncated so that we ignore very small long-range forces. The negligibility of an effect is always with reference to the size of some other effect considered more important. In the graph on the left (figure 3.1), the fluctuations in the density of the material at $x = 0.5$ when $s \approx 0.25$ is approximately $1/10$ of the overall average of 10000 points per unit of x, and the average varies on the order of $1/100$ as s changes by $10\%$ or so. By the time the box size is 0.5 a variation of $10\%$ in box size produces a variation in density of on the order of $2\%$ or so. Furthermore, the variation at $s = 0.25$ is related to the fact that there are more points slightly to the left of 0.5 than there are to the right, producing a gradient across the domain. This shows that even the concept of a "statistical fluctuation" is traded off with the concept of spatial inhomogeneity in this process.

The continuum model then can be thought of as an intermediate asymptotic model (Barenblatt 2003) in which the size of the representative volume

is large enough with respect to the minimum feature size that statistical fluctuations in quantities of interest are $o(1)$ relative to the typical values of the quantities, but the RVE is small enough with respect to the overall phenomenon of interest that predicted results vary from place to place or time to time at similar scales to the measurements which might be used to falsify the model. If no such intermediate range of scales exists, then a continuum model can not be applied, and an explanation in terms of the more fundamental elemental particle description must be used.

It would be useful to have a mathematical framework in which we could express the fact that there is no exact size of the "ideal" RVE. We will frequently want to simply assert that our "RVE" is "small enough" or that the error between measurements and the predictions of our model are "small enough" when the number of RVE elements is "big enough." Such a concept must ultimately depend simultaneously on the overall phenomenon of interest, the measurement apparatus' size and precision, and the degree of statistical uncertainty required by the user to reject the predictions of the model. This means that there is no precise number that can be assigned universally to concepts such as "small enough" or "big enough." In the next section I will introduce the nonstandard number system devised by Edward Nelson in his system for nonstandard analysis known as IST (Nelson 1977) and show how it can inform our modeling and validation procedures.

## 3.2 Non-dimensionalization, Multiple Scales, IST and Nonstandard Numbers

As pointed out by many authors, every physically meaningful equation must be written as a sum of one or more terms in a homogeneous set of units (cf. (Barenblatt 2003; Fowler 1998; Howison 2005; Mahajan 2010)). This means that every physically meaningful equation can be rewritten in a dimensionless form by dividing a dimensional equation by a constant scale factor with the same dimensions as the terms. In particular, based on prior knowledge of the relative sizes of the terms in the phenomenon of interest we can usually find some meaningful combination of the physical variables S, which has the appropriate dimensions and for which in typical conditions $\max_i |x_i/S| = O(1)$. That is to say that any term $x_i$ in the equation is under usual conditions about the size of S or smaller. After converting our

equation to non-dimensional form with appropriate scaling, we can often make progress by asserting that certain terms have an effect that is negligible and removing these terms from the equation. Negligible, like beautiful, is not a well defined formal concept, it must be with respect to some willingness to make errors of some sort. However, we can formalize the concept of negligible by reference to the concept of "infinitesimal" as a fraction of the physically meaningful scale S.

Edward Nelson introduced a simplified system for defining infinite (or "unlimited") and infinitesimal numbers in his paper (Nelson 1977). This system provides most of the power of the earlier system defined by Robinson (1996) without much of the dizzying formal logic foreign to most applied mathematicians. That approach is elaborated upon in application to basic mathematical concepts of calculus by Robert (2011), and in modeling applications by Lobry and Sari (2008). This approach to calculus melds well with the derivation process for physical equations especially ones involving multiple scales.

## Useful Mathematical Concepts from IST

Important concepts from IST are the predicate "standard" written $\mathrm{st}\,()$. All the usual objects of normal mathematics are "standard" and those concepts defined without reference to the predicate $\mathrm{st}\,()$ are called "internal". Any concept which is defined explicitly or implicitly using the predicate $\mathrm{st}(\mathrm{x})$ is called "external". Due to the way in which these concepts are defined, we have the existence of a nonstandard integer, and can show that any nonstandard integer is bigger than any standard integer, and hence is called "infinite" or "unlimited" (Nelson 1977). Furthermore, it follows that if N is a nonstandard integer then $1/\mathrm{N}$ is a nonstandard rational closer to zero than any standard number. It is numbers like these which are called "infinitesimal." Numbers are therefore classified by whether they are "limited" or "unlimited" and "infinitesimal" or "appreciable". A number which differs from a standard number by an infinitesimal amount is called "near-standard". Every near standard number x is infinitesimally close to a unique standard real number called the "standard part" of x and denoted $\mathrm{st}(\mathrm{x})$. In particular the standard part of an infinitesimal number is 0. These concepts are defined by Nelson (1977), and elaborated in the previous references (Lobry and Sari 2008; Robert 2011).

The point of such a number system from our perspective is to turn the usual calculus and asymptotic analysis into an algebraic manipulation of special numbers and thereby facilitate clear thinking in developing and analyzing models. Since IST has been proven to be a conservative extension of Zermelo-Fraenkel set theory with the axiom of Choice (ZFC) there is nothing new that can be proved within ZFC by use of IST (Nelson 1977). However, there *are* new *methods* of proof which can facilitate the development of models. Just as the C programming language is compiled to machine code and therefore is not able to represent any new computer program than the ones representable by writing raw machine code, we nevertheless find that C is a more convenient language in which to program than writing raw binary machine code because it makes concepts clearer *to the humans reading the code*.

## The "effective infinitesimal" and modeling errors

An "infinitesimal" number in IST is formally so small as to be indistinguishable from zero without the fine-grained comb of the st predicate so that no mathematician working in a standard mathematical framework could distinguish it from zero. However, in practical applied terms, it is a formal logical proxy for the concept of negligible within the scale of interest defined by the modeler. Declaring simply that we will treat an expression as infinitesimal allows us to then determine algebraically what other expressions could also be considered as infinitesimal. It defines in some sense a separation of scales into those we can observe or care about, and those too small to matter for our purposes. When taking this approach, we must therefore be careful when multiplying quantities $\varepsilon$ we have arbitrarily tagged as "effectively infinitesimal" by very large numbers of order $O(1/\varepsilon)$ since these must be considered as "effectively infinite".

Since we will always transition from the language of IST ultimately back to the language of standard mathematics, the process of moving into IST (called *transfer*), development of a model, and moving back to standard mathematics (called *standardization*) will if we are talking about physical models where no quantities are *actually* infinitesimal or infinite, automatically mean that we are committing errors. The goal of any mathematical modeling effort is to bound the extent of these errors to be small enough that treating them as if they were infinitesimal is practically justified.

One notion that the infinite numbers of IST can help us with is the near-complete separation of different physical scales as represented by the relative

size of nonstandard integers. If N is a nonstandard integer, and M is a different nonstandard integer, then N/M might be infinitesimal, appreciable, or infinite depending on the relative sizes of these quantities. If $M = N^2$ then $N/M = 1/N \sim 0$ whereas if $M = \sqrt{N}$ then $N/M \sim \sqrt{N} \sim \infty$, and finally if $M = aN$ where a is a standard number, then $N/M = 1/a$ a perfectly good appreciable standard number.

## Examples of Scale Separation

For example, we may be interested in modeling the mixing of the ocean. The mean depth of the ocean may become our length scale of interest so that one non-dimensional unit of length represents about 4km. If we wish to represent the dissolving of carbon dioxide at the atmospheric interface, we may be interested in a length scale of only a few tens of atoms $\approx$ 1 nm. This is approximately $2.5 \times 10^{-13}$ non-dimensional units. Treating this length as infinitesimal will involve essentially no meaningful error in our model. If we wish to include the stirring and mixing effect of strong wind and waves we may need to average over perhaps up to 10 m wave crest height. This is 0.0025 non-dimensional units, a quantity which we may choose to also treat as infinitesimal on the overall depth scale. Finally, perhaps bubbles formed during the breaking of waves are typically 1cm in diameter but can be mixed to a depth of the 10m wave height. The processes occurring in the vicinity of a single bubble takes place on a scale of perhaps 10cm or $2.5 \times 10^{-5}$ non-dimensional length units and a single bubble might be considered infinitesimal relative to the 10m wave height. In this situation, these infinitesimal scales, the molecular mixing, bubble interaction, and wave mixing scale are extremely disparate so that each may be considered infinitesimal relative to the next largest. Hence we have depths of order 1 between the surface and the bottom of the ocean, of order $\varepsilon \sim 0$ near the surface where waves break, of order approximately $\varepsilon^2 \sim 0$ at the bubble scale, and of order approximately $\varepsilon^5 \sim 0$ at the molecular scale.

Another important concept for modeling that we gain from IST is the concept of "s-continuous" (roughly meaning "seems continuous"). An s-continuous function changes by only an infinitesimal amount when its input is changed by an infinitesimal amount (Robert 2011). However, especially for our purposes, this may be true of some non-standard functions that are not actually continuous, such as a step function which is constant between infinitesimal steps, but the size and spacing of the steps is at an infinitesimal

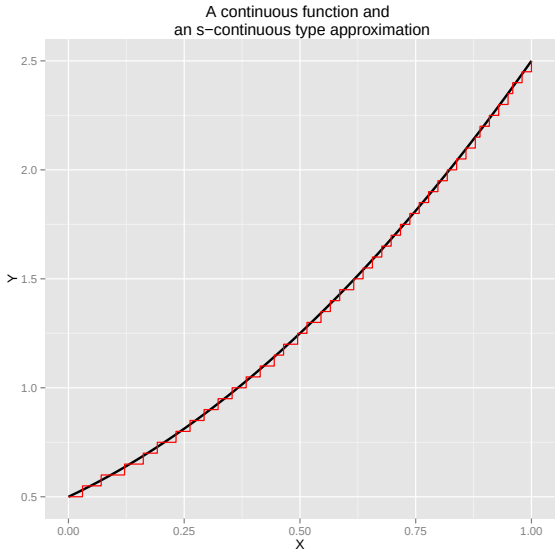


Figure 3.2: An approximation of a continuous function (black) by fine grained steps (red).

scale. Perhaps the difference between the s-continuous function and some standard continuous function remains infinitesimal at every point. We can approximate this concept in the graph of figure 3.2. In fact, the difference between the step function and the continuous function has been accentuated here to make it more visible compared to an earlier version where the step sizes were smaller by a factor of 5.

Mathematically, each bounded s-continuous step-wise non-standard approximation corresponds to some unique standard function that is continuous since every s-continuous *standard* function is continuous (Robert 2011). In the context of the derivation of physical continuum models, a small box in the vicinity of a point defines the region over which an averaged physical quantity is defined. For the purposes of modeling we may treat the quantity defined within the box as a constant over the box. The difference between adjacent boxes when divided by the displacement between the centers of the boxes can define a derivative up to an infinitesimal error. The difference between this derivative of an s-continuous step function and the derivative of the actually continuous function that is the standardization of the s-continuous function can only be distinguished mathematically within

the context of IST.

In building continuum models as models for statistical averages, we will consider small boxes of normally unspecified size defining the spatial extent of the averaged quantities, derive equations for the evolution of the average quantities using the discontinuous step-function approximation implied, treating these functions as s-continuous, and then convert the resulting equations into their corresponding standard equations by the process of standardization.

Since real physical quantities are never actually infinitesimal, the entire process will imply spatial, time, or energy scales below which the equations are not expected to make exact predictions. If the sizes of our errors are large enough that we wish to account for them explicitly, a stochastic component can be included which is infinitesimal only on average but whose error at every point can be described by random variables that are appreciable and potentially correlated. Thus, when describing a physical system using a continuum model there is inevitably a sub-scale structure "within the box" about which we only have average information. There are many potential sub-scale states that are consistent with the average and are naturally described as if they were random since we have little to no information with which to predict them. Depending on the specifics of the system, a variety of distributions and correlation structures may be applicable to describe these fluctuations from the predicted values.

## 3.3 The Model Construction Template: Measurement and Molecules

### The Measurement Region Size

We begin our model construction template with the notion of a control volume (CV) or representative volume element (RVE). However, we specifically interpret this RVE as being the same order of magnitude in size as the region over which our theoretical or actual measurement apparatus averages. In any given scientific problem, we can only validate or falsify our model by reference to physical measurements, a fact sometimes ignored in purely mathematical analysis of continuum models. But the appropriate physical measurement apparatus is necessarily different from one problem to another. A non-contact thermometer for example measures the total infrared radia-

tion coming from some region of a plate, a pressure meter measures the total force on some small flexible membrane of known area, a digital camera takes images whose resolution is limited by the pixel size and the optical properties of the lens, in each case, a measurement is an integration procedure, averaging over some region of space and time. In the finest possible measurements we may get measurements of the approximate locations or forces acting on individual atoms or molecules so that our model must produce predictions at the individual atomic level . However, in the common case, the spatial and time scale over which measurements occur is much larger than those relevant to an atom. Although we often describe continuum models as "infinite dimensional", the real value of a continuum model is that it is a template for or family of finite dimensional models which can give accurate predictions even for those members of the family whose number of dimensions is vastly smaller than the dimensionality of the detailed MD simulation being approximated. Furthermore the convergence of the finite dimensional models as dimension increases implies that answers are approximately independent of the number of dimensions for some large enough dimensionality.

## Dimensionless Length Ratios

Once we define a measurement region size, there are now at least two length scale ratios of interest in the problem. The first is $l_m/l_b$ the size of the measurement region compared to the overall body of interest.

The next is $l_a/l_m$ the ratio of the interatomic or inter-particle distances to the size of the measurement region. This ratio also determines the typical number of elements in an RVE $N \propto l_m^3/l_a^3$ for a 3D problem or $l_m^2/l_a^2$ for a 2D problem. It should be noted that we may instead think of $l_a$ as the "inter-particle" distance if we are considering a model for discrete particles like pellets or sand grains or interacting colloidal suspensions.

As an example of some of these ratios in practice, suppose we are interested in earthquake waves. We have measurements via a seismometer at $100\,\mathrm{Hz}$ sampling frequency. The Nyquist frequency is therefore $50\,\mathrm{Hz}$, and at around $3000\,\mathrm{m/s}$ wave speed, one velocity measurement represents the average velocity over a spatial region of order $60\,\mathrm{m}$. Clearly $60\,\mathrm{m}$ is enormous compared to the interatomic distance in rock, yet $60\,\mathrm{m}$ is tiny compared to the overall length of the wave train lasting perhaps $30\,\mathrm{s}$ and thereby extending over $90000\,\mathrm{m}$ or to perhaps $10^6\,\mathrm{m}$ that the wave might travel through the earth's crust to our seismometer. On the other hand, for a small mechanical

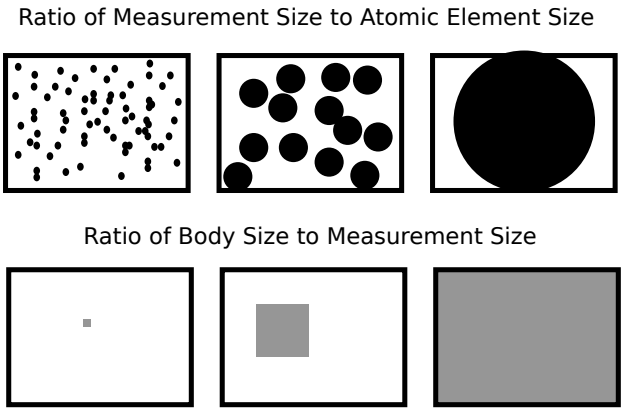


Figure 3.3: Various regimes of size ratio determine which types of models are appropriate. In the upper diagrams the box represents the measurement size, and the circles represent molecules or discrete elements. In the lower diagrams the box represents the body and the grey square represents the region over which measurements average.

part, perhaps a strain gauge is on the order of $1\,\mathrm{mm}$ in size for a part on the order of $100\,\mathrm{mm}$ so that this ratio is more moderate. Sometimes the measurement size is essentially the same size as the system. For example, a large polymer biomolecule with a super-fine laser measurement, or a piston in a machine with a single force gauge on the rod.

Finally, there is the question of the interaction length scale $l_i/l_a$. Typically this ratio is $> 1$ but can sometimes be very large. When this ratio is small, only a few neighbors of an atom contribute to the forces on a molecule, but when it is large, such as when significant electromagnetic forces are involved on bare ions, or when we model the gravitational interactions of asteroid clouds or star clusters, the total force on a particle must include contributions from far away from the particle.

In addition to length scale ratios, there are also timescale ratios of interest. An important one is $dt_{\mathrm{meas}}/t^*$ where $dt_{\mathrm{meas}}$ is the time over which a measurement devices averages when it gives us a measurement, and $t^*$ is the total time that we observe the system and wish to make predictions or explain the system with the model. Modern measurement equipment works

by filtering analog electrical signals to bandwidth limit them, and then sampling this bandwidth limited signal. The filtering inherently delocalizes the signal in time by an amount on the order of $1/f_{cutoff}$ and sampling induces some additional issues including jitter and conversion time, so that even in a classical setting we are subject to Heisenberg type uncertainty between frequency components and their location in the timeseries as is well known. Analog measurement techniques do not provide any way around this issue as we must still somehow define what we mean by the exact value of the measurement and at what time the measurement occurred.

In the subsequent sections, whenever a length is mentioned it is taken to mean a ratio of the related dimensional length to some overall length of the large scale system $l_b^*$, and whenever a time is mentioned it is taken to mean as a fraction of the whole time of some experiment $t^*$. These ratios are therefore dimensionless quantities and generally all less than 1 in size. Occasionally we will make this explicit in statements such as $l_m/l_b \ll 1$ which can be trivially interpreted as $(l_m^*/l_b^*)/(l_b^*/l_b^*) \ll 1$ where starred quantities are dimensional quantities in some units of measurement such as SI.

## The molecular nature of the true dynamics, and the approximate spatial continuity of the measurement

Next, we consider the Newtonian equations of motion for the molecules in some physical system of interest (which we assume have constant mass):

$$\frac{dp}{dt} = m\frac{dv}{dt} = \sum_{i=1}^{N} F_i + F_b \tag{3.1}$$

Here N refers to all the molecules within a distance of the order of $l_i$, the interaction length and $F_b$ is a force that comes from regions far larger than the interaction length and is constant over the measurement volume, generally this involves gravitational forces or occasionally electromagnetic waves propagating from far away.

Finally, we consider the "equation of motion" for the measurement of total momentum P over K molecules in the region of size $l_m$. The linearity of Newton's laws, and the conservation laws of momentum and energy convince us that the measurement must be interpreted as averages, since the average can be linearly extrapolated to the total.

$$\frac{dP}{dt} = \frac{d}{dt}\left(K(l_m)\left\langle mv\right\rangle\right) = \frac{d}{dt}\left(\sum_{i=1}^{K(l_m)} m_i v_i\right) = \sum_{i=1}^{K(l_m)}\left(\sum_{j=1}^{N_i(l_i)} F_{ij}\right) + F_b = F_{net} \quad (3.2)$$

## Conversion of the discrete sum over indices to a nonstandard integral over space

So far, this dynamics takes place in an abstract discrete topology. Each particle is its own "open set" and is disconnected from the other particles. Thanks to finite available energy, and our assumption of approximating quantum mechanics through Newton's mechanics and an appropriate choice of interaction potential, and assuming no nuclear fusion can occur, two particles never approach arbitrarily close to each other. Hence, each particle can be modeled as a very tiny ball or box in 3D space. We can write a mass distribution as

$$\rho_{discrete}(x) = \sum_{i=1}^{N} m_i B(x - x_i) \quad (3.3)$$

Where $B = 1/\varepsilon^3$ when $(x - x_i)$ is inside the cube of side $\varepsilon$ around 0 so that the total integral is 1. Now, in IST, we can assume that $\varepsilon \sim 0$ and recover the Dirac delta function as a perfectly normal but nonstandard function defined pointwise. Physically, nothing is wrong with this because we do not have enough energy to bring two particles close enough together to discover the specific size of $\varepsilon$ so that a nonstandard infinitesimal is a very valid model of the observable physics. The momentum distribution can be defined similarly, by associating a vector velocity to each particle.

$$P_{discrete}(x) = \sum_{i=1}^{N} m_i v_i B(x - x_i)$$

These nonstandard mass distribution functions are trivially integrable provided that we use a small enough elemental volume, one whose side is infinitesimal relative to $\varepsilon$. Since the Dirac function is a nonstandard function, it is not surprising that the integral depends on the particular nonstandard spatial step size.

However, the scientific quantity of interest is not usually the unmeasurable individual particle dynamics, but rather the dynamics of the measurement

$$\begin{aligned}\frac{dp}{dt} + \frac{dp}{dt}_{transport} &= \frac{d}{dt}\left(\int_D p_{discrete}(x)dV(x)_\varepsilon\right) \\ &= \int_{x\in D}\left(\int_{y=x+O(l_i)} F(x,y)dV(y)_\varepsilon\right)dV(x)_\varepsilon + F_b(x) \qquad (3.4)\\ &= \sum_{i=1}^{K(l_m)}\left(\sum_{j=1}^{N_i(l_i)} F_{ij}\right) + F_b = F_{net}\end{aligned}$$

This equation is valid so long as $cdt \gg l_b$ which is to say that an increment of time which is small compared to the total observation time, light can travel a distance which is much larger than the overall size of the body, so that the retardation of forces, and other relativistic effects can be ignored.

So far the equations are exact $\frac{dP}{dt}_{transport}$ represents the change in the measurement purely caused by molecules entering or leaving the measurement region, in situations where $vdt \ll l_m$, this might be neglected as molecules drift only a tiny fraction of a measurement distance in our infinitesimal time. We have simply replaced a standard discrete sum over particle indexes (eq 3.1), with a finite but nonstandard sum (an integral) over locations in space, by associating each particle and its mass, momentum and pairwise force interactions with nonstandard functions of space. Note that if we require multi-body potentials to accurately approximate quantum effects, we can create a force kernel that is a function of any number of locations. For simplicity of exposition we assume pairwise forces are sufficient.

However, in the absence of enormous computing power, and extraordinarily fine measurements for initial conditions, the required molecular dynamics calculations necessary to carry out the exact solution are completely prohibitive. Consider the earthquake dynamics problem, where we must compute the molecular dynamics of the entire earth! A computer to do this is necessarily going to have approximately the same mass as the earth. Fortunately, these detailed calculations are usually unecessary as well since in

the absence of enormously detailed measurements almost all of the computational output is non-falsifiable.

## 3.4 The statistical nature of the model, falsifiability, parameter estimation, and goodness of fit

It goes without saying that to model an actual physical experiment we must have a measurement of some initial conditions, and of boundary or forcing conditions that occur throughout the experiment. To validate the model prediction we must have some measured data to compare with predictions at various space and time points. In the model construction template so far we have emphasized that the predictions of a continuum model are predictions of spatial averages over small regions of space. As is the case in averaging there is always some deviation between the average value of a quantity and the particular value at some point. Failure to predict the exact measured quantities at any given time point can not by itself be construed as a failure of the model. Instead, to validate the model we must compare the predictions and measurements relative to some measure of how likely the deviation is under some reasonable probabilistic model for the variations, and also more generally under some usefulness criterion for predictions with deviations of that magnitude (a utility or decision model).

Frequently some quantities in the model are not precisely known a-priori, quantities such as the Young's modulus of a material, the precise length of a structural element, the characteristic time of some internal process, or the activation energy for some chemical reaction in the presence of a catalyst. Also, initial and forcing conditions may not be precisely known, or only known at a small number of points. Frequently we are in the position of needing to estimate these unknown quantities from the data and then use these estimated quantities to predict what would or did happen under some conditions of interest. Although there are several approaches to the application of probability theory to statistical inference, one which is especially useful for physical modeling is the Bayesian approach in which uncertainty about a quantity which may be either variable or fixed and unvarying from experiment to experiment can nevertheless be given a probability associated to different values, and interpreted as the relative reasonableness of the vari-

ous values that this quantity might have actually taken on.

Validation in idealized detail under this framework is then the process of collecting data, inputting that data into the model's initial, boundary, and forcing conditions, inferring the distribution of important quantities of interest, and then comparing the predictions of the model under high probability values for the unknown quantities to the data collected at various time points, and assessing whether the deviations between the predictions and the data values indicate a well calibrated model or if there is some systematic failure of the model to predict well in certain regimes. Such systematic errors or biases would indicate that a fundamental physical process may be left out or poorly described in the model. Finally we must determine whether any apparent failures are of practical interest, or if the model predicts well enough for the purposes for which it will be used.

One fact of importance is that measurements are never absolutely precise. The finest quality analog to digital converters these days use on the order of 30 or so bits of precision, but accuracy of the low order bits is only guaranteed if thermal and electrical noise are carefully controlled in instrument construction. In any case, we can not imagine a situation in which any measurement will ever in the history or future of humans have anywhere near 190 bits of precision, which corresponds to counting the protons in the sun to within plus or minus one proton or so. It's trivial to say then that statistical error must *logically* enter into every calculation, even if in the end it is of no practical consequence and a decision is then made to explicitly ignore it. From the Bayesian perpective it is possible to assign probabilities to modeling error as well, so that the sum of measurement and modeling error may sometimes be lumped into a single quantity that can inform the likelihood of the data $P(D|a)$ where D is the measured values of the data, and a are the known or unknown parameters in the model including the values of initial, boundary, and forcing conditions, as well as the uncertain fundamental quantities mentioned above.

It is common in almost all circumstances to drop terms from an equation when those terms can be a-priori determined to be of much smaller order of magnitude than the main terms. For example we may ignore the variability in the gravitational acceleration between the bottom of a building and the top of a building when deriving an equation of motion for objects falling off of a skyscraper. Such approximations necessarily define both a bias and an implicit "minimum scale" for allowable deviations between the model and the data even if an extremely precise nanosecond accurate clock is used to

time the fall so that the error in the measurement instrument would seem to be of smaller scale than the observed deviations. Except in cases relevant to metrology or spacecraft orbits or other areas where precision is absolutely necessary, it is rarely of practical benefit to model a process to accuracy better than about 1 part in $10^4$ given the difficulty of collecting sufficiently accurate input data for such purposes. This thought process shows that although we idealize certain quantities as "infinitesimal" in our use of IST, in fact even those who do not adopt the NSA approach already treat quantities whose order of magnitude is a perfectly standard number as if they were infinitesimal, truncating them out of their equations before use.

## 3.5 Conclusion

The goal of this chapter was to introduce an interpretation of continuum models as models for local spatial averages of elementary properties, to argue explicitly for the application of the average due to the presence of conserved quantities, and to introduce the concepts and terminology of IST to give us tools for constructing and describing models that better match mathematical concepts with physical concepts. In following chapters these concepts will be used as needed to describe novel models for the flow of water during soil liquefaction, and for the dissipation of waves in a simulated molecular system which conserves energy to extremely high precision. The molecular dissipation model is meant to be suggestive of methods that could ultimately lead to a continuum model of how wave energy induces porosity changes, which in turn couples to, and induces pore pressure changes and fluid flow during liquefaction.

# Chapter 4

# The Degree of Drainage During Liquefaction

*I am the daughter of Earth and Water,*
*And the nursling of the Sky;*
*I pass through the pores of the ocean and shores;*
*I change, but I cannot die.*

—Percy Bysshe Shelley

In the textbook definitions of soil liquefaction, one assumption is paramount: that during the earthquake no significant quantity of water can flow (Kramer 1996; Holtz and Kovacs 1981). However, water pressure is a function of density and temperature (NIST 2012). In particular, a linear Taylor series for small deviations from some particular typical density and temperature allows us to predict the changes in pressure associated with liquefaction as a simple linear function of density and temperature. Early in my research I took the undrained hypothesis as fact since it is repeated widely and consistently within the literature. However, in order for pressure to change, in the absence of water flow, we must have either the grains getting bigger isotropically so that the volume of voids decreases uniformly everywhere, or we must have heating of the water. The first hypothesis is untenable as there is no physical basis for such an effect. Heating, on the other hand, is tenable and I spent a considerable time thinking about how this effect might work. Eventually, however, I determined that the best starting point was to derive an equation for the rate of change of water pressure and determine

which variables were actually responsible, including all effects that I could remotely consider reasonable.

The starting point for this derivation were the concept of conservation of mass, Darcy's law, and the Taylor series for water's pressure vs density and temperature function.

The resulting model ultimately led to the following paper which is reproduced here in the form in which it was submitted for publication in Proceedings of the Royal Society A (Lakeland, Rechenmacher, and Ghanem n.d.).

## 4.1 Background

The general phenomenon of the liquefaction of granular materials is applicable to a wide variety of grains and fluids. Here, we focus on one of the most important aspects of this phenomenon, namely the role of water flow during earthquake induced liquefaction of sand near the ground surface. Our analysis uses a nondimensional formulation and asymptotic analysis which is adapted to the first few tens of meters of soil where the interplay of gravity, grain rearrangement, water compressibility, and water flow combine to cause these destructive events.

In the Geotechnical Engineering field, soil liquefaction is commonly understood as a consequence of water pressure buildup due to rapid squeezing of pore spaces, without sufficient time for water to flow through the grains and drain the pressure, e.g. (Sawicki and Mierczyński 2006; Kramer 1996; Holtz and Kovacs 1981). When grains are loosely packed, during earthquake motion the tendency is for soil grains to move closer together, squeezing the water and rapidly increasing the pressure due to the high bulk modulus of water.

Taken across a thin horizontal section of the soil, the total vertical force is the sum of the contact forces between grains, and the water pressure times the cross sectional area. This "total stress" minus the water pressure is the so called "effective stress", commonly used in geotechnical analysis (Holtz and Kovacs 1981), which is a measure of the contribution of grain-grain interactions in the soil. If the contact forces drop to zero, then the water pressure carries the entire normal stress, and shear stresses induce flow in the manner of a viscous fluid.

The goal of liquefaction assessment up to now has been to determine how the water pressure in the soil will change during cyclic loading. The

methodology employed has primarily been to build models based on the results of laboratory triaxial, hollow cylindrical, and simple shear tests, as well as more extensive physical centrifuge models. Laboratory tests use samples of sand typically around 10 to 20 cm in characteristic size. The sand is surrounded by an impermeable, flexible membrane to trap the pore water, and the entire sample is contained in a pressurized vessel to simulate the overall pressure conditions in the ground. Cyclic loading of various forms is applied and the total and effective stress states, and evolution of pore water pressure are tracked through the cycling. These experiments have been extensively performed. To complement these small laboratory scale tests, extensive physical modeling in various types of geotechnical centrifuge apparatus have been carried out. These tests use centrifugal acceleration to model the stresses induced in deposits of soil that are 10 to 100 times deeper than the model scale and allow full 3 dimensional geometries to be simulated without the ambiguity of numerical simulations of complex soil materials. Combined with these physical observations, engineers have employed correlations with observed field conditions in post-seismic investigations. An overview of the current state of liquefaction research may be found in Sawicki and Mierczyński (2006).

Implicit in the use of small laboratory samples with impermeable membranes, and explicit in many textbook definitions of liquefaction, is the assumption that during the earthquake there is no significant water flow or change in water volume, which is known as the "undrained" condition (cf. (Kramer 1996; Holtz and Kovacs 1981)). The assumption that soil liquefaction occurs under undrained conditions has lead to extensive research into undrained tabletop experiments such as triaxial and simple shear tests, with several methods suggested to overcome the small volume changes allowed by the compliance of the rubber membrane (Sivathayalan and Vaid 1998). Although centrifuge and laboratory test data have long shown that water migration can occur (Fiegel and Kutter 1994; Kokusho 1999), these situations have been treated as if they were exceptions to the normal situation of undrained pore pressure increase. However, given the thermodynamics of water pressure, the undrained assumption can lead to physically incorrect predictions. If the water is not allowed to change volume whatsoever, then the *only* mechanism for pressurization is heating. This shows that some care is required to determine properly the role of water flow, water compressibility and thermal expansion which was the initial impetus for this research.

With the advent of large computing power, more recent studies of lique-

faction phenomena have used discrete element models (DEM) which operate at the grain scale, and calculate the equations of motion for thousands of individually tracked cylindrical or spherical grains. In (Goren et al. 2011) a 2D DEM model was coupled to a continuum model for fluid flow, and the interactions of grains and fluid were calculated for a sample of a few thousand grains. Their conditions are typical of 200m to 2km deep thin deposits sheared at $\mathrm{ord}(1)$ to $\mathrm{ord}(10)\,\mathrm{m/s}$ [1] which is relevant for fault gouge conditions. Holding boundary conditions of their sample at either zero fluid mass flow, or constant fluid pressure, they were able to observe liquefaction for both dense and loose sheared assemblies under drained and undrained conditions. While their method is in principle applicable to a wide variety of situations, computing the interactions of large deposits of sand over meters or tens of meters would be computationally prohibitive. Their model does show, however, that our understanding of even tabletop sized experiments may be flawed, as they observe liquefaction under all conditions in assemblies whose bulk density was either relatively loose or relatively dense. In an earlier paper (Goren et al. 2010), a nondimensional continuum equation for dynamic fluid flow was derived which is valid for mesoscopic scales and based on conservation of mass together with Darcy's law. Their equation provides much of what is required to analyze a realistic soil deposit, though they explicitly neglect certain aspects such as thermal heating, and they do not extensively analyze the equation in the context of typical near-surface liquefaction conditions.

In this paper, we analyze the liquefaction of saturated sandy and silty soils in the first $\mathrm{ord}(10)$ meters below the ground where initial water pressures are within a few atmospheres of the total vertical stress. Our method is to derive a one dimensional equation for fluid flow in the vertical direction based on the assumptions of mass conservation and Darcy's law for fluid flow through porous media in a manner very similar to Goren et al. (2010). Although the same derivation can be trivially extended to 3D mathematically, it provides no additional qualitative understanding for the main point of this study, which is that fluid flow and soil inhomogeneity are of critical importance in the liquefaction phenomenon. In development of full predictive models for realistic heterogeneous 3D soil deposits however, lateral

[1] Note on our use of asymptotic notation: $x = \mathrm{O}(y)$ means that $|x/y| < C$ for some positive constant C which is expected to be not extremely large, $x = \mathrm{ord}(y)$ means $|x/y|$ and $|y/x|$ should both be treated as close to 1 and $x = \mathrm{o}(y)$ means $|x/y|$ is negligibly small.

water flow must be accounted for as it will influence the water pressure as well.

By treating a comprehensive set of dependencies including temperature effects and the compressibility of water potentially containing some small quantity of gas such as arising from organic processes or dissolved gasses, we arrive at a very general result which leaves no further degrees of freedom that could be expected to contribute significantly to water pressurization in these soils. By nondimensionalizing the model using a distinguished limit (Fowler 1998) we focus attention on the relative size of the various effects that can cause fluid pressurization and transfer of stress from soil particles to the water under the relevant circumstances. By showing that heating and compressibility of water are both perturbation effects, our results clarify that grains collapsing into denser arrangements pressurizes the fluid. Our results also show that pressure diffusion can not be neglected in the liquefaction process. Indeed, we show that for loose sands, diffusion is equally important to densification on timescales significantly shorter than the duration of an earthquake and even shorter than a single loading cycle.

For layered deposits or samples with spatially varying permeability, gradients in the permeability field are critical in determining where liquefaction onset might occur. Though this has been shown in a variety of experiments, it has never been explicitly analyzed mathematically to determine how important the effect is in general. Our model explains the dominant effects in a range of conditions from very low permeability soils typical of silts, through sands, and even in the case of high permeability gravels where diffusion is more dominant. One value of the model is that it predicts certain new features, such as large settlements together with bulk fluid flow to the surface in loose high permeability deposits, and also suggests a new mechanism of liquefaction potentially mediated by heating within silts even if the silt's initial density is such that sustained contractive loading does not occur. We compute solutions for several example scenarios that mimic the observed dynamics in tabletop (Kokusho 1999; Kokusho and Kojima 2002) and centrifuge experiments (Fiegel and Kutter 1994)

Based on the results of these analyses, we believe that liquefaction evaluation approaches should explicitly acknowledge the importance of fluid flow. Future efforts should be placed on evaluating permeability, porosity, and the energetic potential for earthquake-induced porosity changes over entire deposits of soil, not mainly the existence of layers of loose sands and a notional "resistance to liquefaction" based on shear stresses, as is common in

current Geotechnical Engineering practice (Idriss and Boulanger 2006; Seed et al. 2003).

In addition to a description of the fluid flow, the prediction of the grain motions is of great interest, as it is a driving force for the fluid pressurization and migration. At present the authors are unaware of any continuum model which could reliably substitute for the results of fully coupled DEM and yet be computationally tractable for large scales of spatially variable soil deposits. Because of this limitation, we apply an assumed grain deformation, usually a constant in space and time, and investigate the predicted results in terms of the induced fluid flow.

## 4.2 Model Construction

We assume a horizontally layered deposit of soil, and a vertical coordinate axis pointing upward with zero reference point at a deep impermeable layer below the region of interest. We choose this coordinate system rather than one oriented downward from the ground surface since the ground surface may settle downward. We are interested in the first few tens of meters below the ground surface, as this is where small pore volume strains can produce changes in water pressure that can easily produce a zero effective stress condition. We consider a thin horizontal slice of this material with cross sectional area A which is very large compared with the typical size of a grain, and thickness dz which is on the order of several grain diameters. For the saturated sands we consider, the fluid in our differential volume at pressure P and density $\rho$ fills the inter-grain spaces whose volume is $V_f = \varphi A dz$, where $\varphi$ is the bulk porosity (the fraction of total volume occupied by pore space). Since the bulk modulus of the grains is typically an order of magnitude higher than that of the fluid, which is already quite high, we assume that the individual grains do not compress by any appreciable amount. However, grain rearrangement can cause changes in porosity.

While the usual assumption in liquefaction research is that fluid flow does not occur on the time scale of the earthquake, we instead model the rate of change of fluid mass within the volume of a thin slice by examining the difference in the fluid flux out of the top surface and into the bottom surface. We can estimate the fluid flow rate $v_f$ relative to the grains moving at velocity $v_g$ using Darcy's law $v_f - v_g = -\frac{k_d}{\mu}\frac{\partial P}{\partial z}$, where $k_d$ is permeability and $\mu$ is the fluid viscosity. Darcy's law has been established to give an accurate

effective fluid flow velocity $v_f$ which gives the proper "apparent" volumetric flow rate when multiplied by the *total* cross sectional area of a representative volume. This equation represents an approximation of the full fluid flow equation when only viscous effects and pressure gradients dominate.

Assuming that the horizontal slice can be made thin enough relative to the length scale over which fluid velocity varies, the resulting differential equation for change in fluid mass within the differential slice is:

$$\frac{d}{dt}\left(\rho\varphi A dz\right) dt = -\frac{\partial}{\partial z}\left(A\rho\left(-\frac{k_d}{\mu}\frac{\partial P}{\partial z} + v_g\right) dt\right) dz - \Delta M_{static} \tag{4.1}$$

Here the left hand side expresses the change in a short time dt of the total fluid mass in the slice. The right hand side expresses the difference in fluid mass flux which is moving relative to the grains at velocity $\frac{k_d}{\mu}\frac{\partial P}{\partial z}$. To get the absolute velocity in a Newtonian reference frame we add $v_g$. For the actual velocity of the water stream through the restricted cross section of voids we would multiply A by $\varphi$ and $v_w$ by $1/\varphi$ on the right hand side which cancels and leads to the same equation here, but it should be mentioned that the actual velocity of the water through the restricted cross section is the one of interest for anyone seeking to model the fluid drag for grain movement equations.

Because liquefaction of soils takes place over a very small range of fluid density and temperature conditions, we can eliminate the density $\rho$ from the equation by solving for it in terms of pressure and temperature using the Taylor expanded state equation:

$$P(\rho, T) = P_0 + \frac{K_B}{\rho_0}(\rho - \rho_0) + K_B\alpha(T - T_0) \tag{4.2}$$

Where $P_0$, $\rho_0$ and $T_0$ are reference pressure, density, and temperature levels for the water, $K_B$ is the bulk modulus of water $\left(-V\frac{\partial P}{\partial V}_T\right)$, $\alpha$ is the coefficient of volumetric thermal expansion $\left(\frac{1}{V}\frac{\partial V}{\partial T}_P\right)$, and $\rho$ and T are the actual density and temperature. The temperature dependence can be derived from allowing a volume of water to be heated and expand under constant pressure, and then be squeezed back to its original volume at constant temperature. For our purposes we neglect the very small difference between the adiabatic and isothermal bulk modulus of water.

The term $\Delta M_{static}$ is a correction necessary to account for the fact that there is no change in the slice's water mass when static gravitational condi-

tions apply. For example, due to gravity there is a static pressure gradient. Also, the permeability may change with depth, and water density changes minutely with depth. Setting the left side of the equation equal to zero when static gravitational conditions apply and solving for the correction gives

$$\Delta M_{static} = \frac{\rho^2 g A}{\mu}\left(\frac{g k_d \rho_0}{K_B} - \frac{k_d}{\rho}\frac{d\rho}{dz} - \frac{\partial k_d}{\partial z}\right) dt dz \tag{4.3}$$

In equations (4.1) and (4.3), for a vertical cartesian axis z, A, dz, and dt are constant, $k_d$ depends on location z, $\mu$ depends on temperature T, $\rho$ is determined from P and T using the state equation, and P, T and $\varphi$ depend on time t and position z.

Note that we may compensate for the presence of a small fraction of the voids containing gas by adjusting $K_B$. If a volume of water contains small bubbles occupying a small fraction $\varepsilon$ of the volume, then we can approximate the compressibility $(1/K_B)$ using $V_{tot} = V_W + V_g$ and $1/K_{Bmix} = -\frac{1}{V_{tot}}\frac{\partial V_{tot}}{\partial P}$ together with the state equation $V_g = KT/P$ for an ideal gas and the Taylor series state equation for the liquid $V_w = V_0(1 - (P - P_0)/K_B)$. Assuming isothermal gas compression due to the thermal equilibrium with the water, $V_g = V_0 P_0/P$. In a mixture with $\varepsilon$ fraction of gas, this leads to the equation:

$$V_{tot}(P) = (1-\varepsilon)V_{tot0}(1 - \frac{(P - P_0)}{K_B}) + \varepsilon V_{tot0}\frac{P_0}{P}$$

evaluating

$$K_{Bmix} = \frac{-1}{V_{tot0}}\frac{\partial V_{tot}}{\partial P}$$

at $P_0$, we get:

$$\frac{P_0}{K_{B_{mix}}} = \varepsilon\left(1 - \frac{P_0}{K_B}\right) + \frac{P_0}{K_B}$$

This is a strong function of $\varepsilon$ since $P_0/K_B$ is small for atmospheric scale pressures. This may be relevant in situations involving gas bubbles formed by biological organisms or recent rains bearing an excess of dissolved gas, or in tidal areas where fluxes of water and gas bubbles are large.

Since we used the state equation involving P and T to eliminate $\rho$, our equation now includes the temperature T and in expanded form will include both $\frac{\partial T}{\partial t}$ and $\frac{\partial T}{\partial z}$. We use the following heat equation for a flowing fluid to relate these quantities:

$$\frac{dT}{dt} + \frac{\partial T}{\partial z} v_w = \frac{1}{\rho_{avg} c_v} \left( k_T \frac{\partial^2 T}{\partial z^2} + T \frac{\partial S}{\partial t}_Q \right) \tag{4.4}$$

In (4.4) $c_v$ is a bulk averaged specific heat capacity, $\rho_{avg}$ is the bulk average density, $k_T$ is the effective thermal conductivity, and $\frac{\partial S}{\partial t}_Q$ is the change in entropy density due to heat generation.

In addition, the conservation of grain mass was used to replace $\frac{\partial v_g}{\partial z}$ in equation 4.1 with a term involving $\frac{\partial \varphi}{\partial t}$ and a convective term involving $v_g$, which will become a perturbation due to the small settlement velocities.

$$\frac{\partial(1-\varphi)}{\partial t} = -\frac{\partial(1-\varphi)v_g}{\partial z} \rightarrow \frac{\partial v_g}{\partial z} = \frac{1}{(1-\varphi)} \left( \frac{\partial \varphi}{\partial z} v_g + \frac{\partial \varphi}{\partial t} \right) \tag{4.5}$$

In this form, equation 4.1 is not yet useful for analysis and calculation, as within each derivative there are multiple variables whose values are dependent on time or position. Our next task will be to expand the fluid equation (4.1) through the comprehensive application of the chain rule, so we can arrive at an equation for the rate of change of pressure $\frac{\partial P}{\partial t}$ and then make this equation dimensionless to help evaluate the relative importance of various terms. Although it is tempting at this point to try to simplify this equation by making assumptions about the negligibility of certain effects such as compressibility of water, the heat generation rate, and the like to reduce the complexity of the expanded equation, we believe that such early simplifying assumptions have led the field astray in general, and we instead choose to expand the equation fully and deal with the negligible terms only after a full dimensionless analysis.

We employed the freely available Maxima computer algebra system (The Maxima Project 2011) to calculate the expanded version of equation 4.1. By identifying and dropping negligible terms we arrive at a simplified "full" equation which captures all of the dynamics of interest including first order perturbations (equation 4.18 is the fully analyzed dimensionless version below).

In order to arrive at the simplified equation, we needed to understand the dominant balances of effects and identify the negligible terms. To do this a proper nondimensionalization is required. The choice of the characteristic scales for nondimensionalization is one of the critical aspects of our analysis, since it focuses the equation on the specific situations of interest.

To focus our understanding on geotechnically relevant scales, we chose scales for P, $k_d$ and $\varphi$ by reference to the situation in the first several meters of sandy soil, where $P/P_0 = O(1)$ throughout. We introduce $k_{d0}$ which represents a typical order of magnitude for permeability of moderately coarse loose sands, such that the permeability range for most sands falls within about a factor of 4 of this value. We also introduce $\varphi_0$ which represents a typical value for porosity in a loose sand. General sands are between about 70% and 110% of this $\varphi$ value. These values were chosen by reference to tables given in Beard and Weyl (1973).

$$\begin{aligned} P_0 = P_{atm} &= 100\,\mathrm{kPa} \\ k_{d0} &= 1.5 \times 10^{-10}\,\mathrm{m}^2 \\ \varphi_0 &= 0.44 \end{aligned} \tag{4.6}$$

We wrote equations for the dimensional variables in terms of nondimensional "primed" or "hatted" variables as follows:

$$\begin{aligned} &\varphi = \varphi_0 \left(1 + \frac{\Delta\varphi}{\varphi_0}\,\varphi'\right) \qquad z = \Delta z\, z' \qquad v_g = \frac{6\Delta\varphi\Delta z}{\Delta t} v_g' \\ &\hat{\varphi} = \varphi/\varphi_0 \qquad\qquad k_d = k_{d0}\, k_d' \qquad S = \Delta S\, S' \\ &P = P_0 + P_0 P' \qquad\qquad t = \Delta t\, t' \qquad T = T_0 \left(1 + \frac{\Delta S}{C_{v0}}\, T'\right) \end{aligned} \tag{4.7}$$

Here $C_{v0} \approx 1594\,\mathrm{J/kg/K}$ represents a mass weighted average of the specific heat capacity of grains and water. We took numerical values for the heat capacities of water and grains as $C_{vw} = 4156.7\,\mathrm{J/kg/K}$ and $C_{vgr} = 835\,\mathrm{J/kg/K}$. We then substituted these expressions into the expanded dimensional form of equation 4.1 and solved for the dimensionless $\frac{\partial P'}{\partial t'}$.

During liquefaction, due to the high bulk modulus of water, $\varphi$ does not need to change very much in order to induce a unit of dimensionless pressure. We have introduced the variable $\varphi'$ which changes $O(1)$ when $\varphi$ changes by this tiny amount required for pressurization. On the other hand $\hat{\varphi}$ represents a normalized value of $\varphi$ as a fraction of its typical size, a value which can be considered very nearly constant during the event. The scaling of dimensional velocity $v_g$ was chosen so that 1 unit of $v_g'$ represents a ground settlement of about 10 cm during a 30 s earthquake after computing $\Delta\varphi$ as described below.

The remaining scale constants $\Delta z$, $\Delta t$, $\Delta S$ and $\Delta\varphi$ can be chosen arbitrarily, however the situation with the maximal interplay of different effects is the

so called distinguished limit (Fowler 1998), where all of the relevant terms in the equation have coefficient equal to 1 under typical conditions so that one unit of change in any variable or derivative induces the same size of effect compared to changes of any other variable or derivative. By calculating our scale factors to force the equation into this form, we identify the regime in which maximal interplay occurs.

To calculate the scale constants, we evaluate the coefficients under the conditions $k'_d = 1$ and $\varphi = \varphi_0$ as representative of typical conditions, and then require the important terms $\frac{\partial^2 P'}{\partial z'^2}$, $\frac{\partial \varphi'}{\partial t'}$, and $\frac{\partial P'}{\partial z'}\frac{\partial k'_d}{\partial z'}$ which represent the effect of pressure diffusion, grain skeleton contraction, and spatial variability in permeability respectively to have coefficients equal to 1. In addition we require the initial dimensionless gravitational static pressure gradient to be 1. These four equations are sufficient to constrain the values of $\Delta z$, $\Delta t$, $\Delta S$ and $\Delta\varphi$ and we solve for them as follows:

$$\begin{aligned}
\Delta z &= P_0/\rho_0 g && \approx 10\,\mathrm{m} \\
\Delta t &= \frac{\varphi_0 \mu P_0^2}{g^2 k_{d0} K_B \rho_0^2} && \approx 0.14\,\mathrm{s} \\
\Delta S &= \frac{C_{v0} P_0 \gamma_S}{\alpha K_B T_0} && \approx 6.0 \times 10^{-3}\,\mathrm{J/kg/K}\,(\gamma_S = 1) \\
\Delta\varphi &= \frac{\varphi_0(1-\varphi_0)}{(2-\varphi_0)}\frac{P_0}{K_B} && \approx 7.2 \times 10^{-6}
\end{aligned} \tag{4.8}$$

Clearly our assumption that diffusion, contraction, and permeability variation are all important in realistic flow regimes is validated by the magnitude of these scale constants. The value of $\Delta t$, which is a diffusion timescale related to $(\Delta z)^2/D$ where D is the pressure diffusivity, is small compared to an earthquake duration of around 30 s, and even to a single cycle of loading of approximately 1 s. The length scale $\Delta z$ is $O(1)$ relative to the size of deposits of interest, and $\Delta\varphi$ is a reasonably achievable fluctuation in $\varphi$. The fact that $\Delta t$ is small compared to the earthquake duration or the single loading cycle means that a near-steady-state approximation of the flow should be valid for predicting the pressure field at the end of earthquake shaking. This is true even though the forcing may change significantly over a loading cycle as the diffusion term $\frac{\partial^2 P'}{\partial z'^2}$ implies a gaussian weighted averaging over one dimensionless unit of length during one dimensionless unit of time. Therefore all points in the deposit are influencing all other points and no localized pres-

sure changes can last more than $O(0.14)\,\mathrm{s}$ without both rapid and sustained grain skeleton contraction in a single direction to balance the diffusion. We expect that drag forces on particles prevent the sustained contraction in a single direction from becoming too rapid (as will be shown in later examples), and since the typical earthquake loading fluctuates in both directions, the fast fluctuations in loading are averaged out and the pressure field remains near steady state when time averaged over at least a cycle.

Note in the above scales we have left $\gamma_S$ as a nondimensional parameter which measures the fraction of the "distinguished limit" level of heating which actually occurs in practice. If $\gamma_S = 1$, then this implies a characteristic temperature change rate of $1.05\,\mathrm{K/s}$ which for a $30\,\mathrm{s}$ earthquake implies $32\,\mathrm{K}$ temperature change, a clearly untenable quantity: the sand would be scalding hot, a phenomenon not reported previously. The distinguished limit with heating is therefore more relevant for some mechanical apparatus in which external heating is applied, or perhaps a geothermal or fault gouge condition or within rapidly shearing bands where large quantities of energy are being dissipated in small spatial regions, such as in landslides or thin partially liquefied layers. However, as pointed out by Nemat-Nasser and Shokooh (1979) and verified in field observations by Davis and Berrill (2001), dissipated mechanical energy is highly correlated with water pressure development. Clearly, the wave energy is used by the grains as activation energy for rearrangement, and this process is irreversible and must produce *some* heat. To estimate the actual scale of heating within the soil during the early stages of typical liquefaction events, and thereby constrain $\gamma_S$, we made reference to the entropy generated by the flow of water through a characteristic soil under a characteristic pressure gradient. We calculate this entropy scale by assuming that the water flows horizontally for $\Delta t$ seconds through a constant pressure gradient $P_0/\Delta z$ at a velocity given by Darcy's law, and the work done by the pressure field (the change in enthalpy) is completely converted to entropy at temperature $T_0$, via drag from the particles:

$$\begin{aligned}
\gamma_{S_{\min}} &= \left(\frac{P_0}{\Delta z}\right)\left(\frac{k_{d0}}{\mu}\frac{P_0}{\Delta z}\right)\frac{\Delta t}{T_0\rho_w}\left(\frac{1}{\Delta S_{\gamma_S=1}}\right) \\
&= \frac{\alpha\varphi_0 P_{\mathrm{atm}}}{C_{v0}\rho_w} \\
&\approx 6\times 10^{-6}
\end{aligned} \tag{4.9}$$

This is a lower bound for the relative entropy generation in the soil as it

does not include any effect of the grain motion. To bound the range of reasonable values for $\gamma_S$ we assumed that during a 30 second earthquake soil temperature should not change more than $\mathrm{ord}(1)\,\mathrm{K}$ since an order of magnitude more would not be ignorable, and temperature must change at least $\mathrm{ord}(10^{-4})\,\mathrm{K}$ due to the flow entropy calculated above. As a representative value, we therefore chose $\gamma_S \approx 5 \times 10^{-3}$ under the assumption that the grain motion contributes significantly to entropy production but that the temperature change is still a fraction of a Kelvin. The implied characteristic change in temperature for the soil overall is $0.24\,\mathrm{K}$ in $30\,\mathrm{s}$. This would seem to be a large fraction of the amount that could occur while still being neglected in most field or laboratory experiments. Even if the true value is an order of magnitude larger than this, our treatment of the effect as a small perturbation will remain valid.

After nondimensionalizing, we replaced each of four important nondimensional groups with a single nondimensional symbol for each group as follows:

$$\gamma_{vol} = \frac{P_{atm}}{K_B} \tag{4.10}$$

$$\gamma_{\mu_T} = \frac{1}{\alpha\mu}\frac{d\mu}{dT} \tag{4.11}$$

$$G_{gr} = \rho_{grain}/\rho_0 \tag{4.12}$$

$$\beta(\hat{\varphi}) = \frac{1 + \frac{1}{(1-\varphi_0\hat{\varphi})}}{\hat{\varphi}\left(1 + \frac{1}{(1-\varphi_0)}\right)} = \frac{(\varphi_0 - 1)(\varphi - 2)}{(\varphi_0 - 2)\hat{\varphi}(\varphi - 1)} \tag{4.13}$$

Above, $\gamma_{vol}$ expresses the compressibility of water in terms of the volumetric strain required to generate a characteristic unit of pressure, $\gamma_{\mu T}$ represents fractional change in viscosity for a nondimensional unit of temperature change, and $G_{gr}$ is the relative density of grains to water, typically about 2.6 to 2.7; here, we have used 2.655. $\beta$ is the local nondimensional bulk modulus of the mixture. It gives the dimensionless pressure induced by a unit change of $\varphi'$ in the absence of flow, and is a function of the local $\hat{\varphi}$ value ranging in practice between about 1 and 2 for realistic values of $\hat{\varphi} \in [0.5, 1.1]$. For important constants related to water, we used the values of density, heat capacity, viscosity, and other important properties available online from the NIST database of the properties of water for a reference pressure of P=100kPa and temperature T=293.15K (20°C)(NIST 2012).

By construction, for typical conditions of soil liquefaction all the variables and their derivatives are $O(1)$ so that the relative size of each term is determined from its coefficient. In certain conditions these assumptions are violated, such as near sudden transitions in permeability. To eliminate the negligible terms and identify the leading order terms of the perturbation we performed an asymptotic analysis of the equation. Retained perturbation terms are relevant only near large gradients in permeability, large gradients in pressure, or extremely low permeability regions.

To see the development of the fully analyzed equation we first show the full expanded dimensional equation:

$$
\begin{aligned}
\frac{dP}{dt} = {} & \frac{\partial k_d}{\partial z}\left(K_B\left(\frac{\alpha^2 g \rho_0 (T_0-T)^2}{\mu\varphi}+\frac{2\alpha g \rho_0 (T_0-T)}{\mu\varphi}+\frac{g\rho_0}{\mu\varphi}\right)\right. \\
& \left. +\alpha\left(\frac{2 g \rho_0 P (T_0-T)}{\mu\varphi}-\frac{2 g P_{atm}\rho_0 (T_0-T)}{\mu\varphi}\right)+\frac{\frac{g\rho_0 P^2}{\mu\varphi}-\frac{2 g P_{atm}\rho_0 P}{\mu\varphi}+\frac{g P_{atm}^2\rho_0}{\mu\varphi}}{\mu\varphi}\right. \\
& \left. +\frac{2 g\rho_0 P}{\mu\varphi}-\frac{2 g P_{atm}\rho_0}{\mu\varphi}\right) \\
& -\frac{\alpha^2 g^2 k_d \rho_0^2 (T_0-T)^2}{\mu\varphi}+\frac{\partial P}{\partial z}\frac{\partial T}{\partial z}\left(K_B\left(\alpha\left(\frac{k_d(\varphi-1)}{\mu\varphi}-\frac{k_d\frac{d\mu}{dT}(T_0-T)}{\mu^2\varphi}\right)-\frac{k_d\frac{d\mu}{dT}}{\mu^2\varphi}\right)\right. \\
& \left. +\frac{d\mu}{dT}\left(\frac{k_d P_{atm}}{\mu^2\varphi}-\frac{k_d P}{\mu^2\varphi}\right)\right) \\
& +\frac{\alpha\left(\frac{2 g^2 k_d P_{atm}\rho_0^2 (T_0-T)}{\mu\varphi}-\frac{2 g^2 k_d \rho_0^2 P (T_0-T)}{\mu\varphi}\right)-\frac{2 g^2 k_d\rho_0^2 P}{\mu\varphi}+\frac{2 g^2 k_d P_{atm}\rho_0^2}{\mu\varphi}}{\mu\varphi} \\
& +\frac{\partial T}{\partial z}\left(K_B\left(\frac{\alpha\left(\mu v_g - g k_d\rho_0\right)}{\mu\varphi}-\frac{\alpha^2 g k_d\rho_0 (T_0-T)}{\mu\varphi}\right)+\alpha\left(\frac{g k_d P_{atm}\rho_0}{\mu\varphi}-\frac{g k_d\rho_0 P}{\mu\varphi}\right)\right) \\
& +\frac{\partial\varphi}{\partial t}\left(K_B\left(-\frac{\alpha(\varphi-2)(T_0-T)}{(\varphi-1)\varphi}-\frac{\varphi-2}{(\varphi-1)\varphi}\right)-\frac{(\varphi-2)P}{(\varphi-1)\varphi}+\frac{(\varphi-2)P_{atm}}{(\varphi-1)\varphi}\right) \\
& +\frac{\partial^2 P}{\partial z^2}\left(K_B\left(\frac{\alpha k_d (T_0-T)}{\mu\varphi}+\frac{k_d}{\mu\varphi}\right)+\frac{k_d P}{\mu\varphi}-\frac{k_d P_{atm}}{\mu\varphi}\right) \\
& +\frac{\partial k_d}{\partial z}\frac{\partial P}{\partial z}\left(K_B\left(\frac{\alpha(T_0-T)}{\mu\varphi}+\frac{1}{\mu\varphi}\right)+\frac{P}{\mu\varphi}-\frac{P_{atm}}{\mu\varphi}\right) \\
& +K_B\left(\frac{\alpha\left(C_{v0}\frac{\partial\varphi}{\partial z}C_v'(\hat{\varphi})\, v_g T_0+\varphi^2\frac{\partial S}{\partial t}T-\varphi\frac{\partial S}{\partial t}T-C_{v0}\frac{\partial\varphi}{\partial z}C_v'(\hat{\varphi})\, v_g T\right)}{C_{v0}(\varphi-1)\varphi C_v'(\hat{\varphi})}+\frac{\frac{\partial\varphi}{\partial z}v_g}{(\varphi-1)\varphi}\right) \\
& +\frac{\partial P}{\partial z}\left(\frac{\alpha g k_d\rho_0 (T_0-T)}{\mu\varphi}+\frac{\frac{g k_d\rho_0 P}{\mu\varphi}-\frac{g k_d P_{atm}\rho_0}{\mu\varphi}}{\mu\varphi}-\frac{\mu v_g - g k_d\rho_0}{\mu\varphi}\right) \\
& -\frac{2\alpha g^2 k_d\rho_0^2 (T_0-T)}{\mu\varphi}+\frac{\alpha K_T K_B\frac{\partial^2 T}{\partial z^2}}{C_{v0}C_v'(\hat{\varphi})\left(\varphi\rho_0-\varphi\rho_{gr}+\rho_{gr}\right)}+\frac{k_d\left(\frac{\partial P}{\partial z}\right)^2}{\mu\varphi} \\
& +\frac{-\frac{g^2 k_d\rho_0^2 P^2}{\mu\varphi}+\frac{2 g^2 k_d P_{atm}\rho_0^2 P}{\mu\varphi}-\frac{g^2 k_d P_{atm}^2\rho_0^2}{\mu\varphi}}{\mu\varphi}+\frac{\mu\frac{\partial\varphi}{\partial z}v_g P-g^2 k_d\varphi\rho_0^2+g^2 k_d\rho_0^2}{\mu(\varphi-1)\varphi}-\frac{\frac{\partial\varphi}{\partial z}P_{atm}v_g}{(\varphi-1)\varphi}
\end{aligned}
\tag{4.14}
$$

After replacing the dimensionless groups with their dimensionless parameters, and reorganizing, the full dimensionless equation is:

$$
\begin{aligned}
\frac{dP'}{dt'} = {} & \frac{\frac{\partial S'}{\partial t'} T' \gamma_S^2 \gamma_{vol}}{\alpha C_v'(\hat{\varphi}) T_0} + \gamma_S \gamma_{vol}^2 \left( - \frac{k_d' \varphi_0 \frac{\partial P'}{\partial z'} \left( P' \frac{\partial T'}{\partial z'} \gamma_{\mu_T} + T' \right)}{\varphi} - \frac{6 \left(\varphi_0 - 1\right)^2 \varphi_0^2 \frac{\partial \varphi'}{\partial z'} T' v_g'}{(\varphi - 1) \varphi \left(\varphi_0 - 2\right)^2} \right. \\
& \left. - \frac{k_d' \varphi_0 \left( P' \frac{\partial T'}{\partial z'} - 2T' \right)}{\varphi} - \frac{2 \frac{\partial k_d'}{\partial z'} \varphi_0 P' T'}{\varphi} \right) \\
& + \gamma_S \gamma_{vol} \left( - \frac{k_d' \varphi_0 \frac{\partial P'}{\partial z'} \frac{\partial T'}{\partial z'} \left( \gamma_{\mu_T} - \varphi + 1 \right)}{\varphi} + \frac{6 \left(\varphi_0 - 1\right) \varphi_0 \frac{\partial T'}{\partial z'} v_g'}{\varphi \left(\varphi_0 - 2\right)} - \frac{k_d' \varphi_0 \frac{\partial T'}{\partial z'}}{\varphi} \right. \\
& \left. - \frac{k_d' \varphi_0 \frac{\partial^2 P'}{\partial z'^2} T'}{\varphi} - \frac{\frac{\partial k_d'}{\partial z'} \varphi_0 \frac{\partial P'}{\partial z'} T'}{\varphi} + \frac{(\varphi - 2) \left(\varphi_0 - 1\right) \varphi_0 \frac{\partial \varphi'}{\partial t'} T'}{(\varphi - 1) \varphi \left(\varphi_0 - 2\right)} - \frac{2 \frac{\partial k_d'}{\partial z'} \varphi_0 T'}{\varphi} \right) \\
& + \gamma_S^2 \gamma_{vol}^2 \left( \frac{k_d' \varphi_0 \frac{\partial P'}{\partial z'} T' \frac{\partial T'}{\partial z'} \gamma_{\mu_T}}{\varphi} + \frac{k_d' \varphi_0 T' \frac{\partial T'}{\partial z'}}{\varphi} + \frac{\frac{\partial k_d'}{\partial z'} \varphi_0 T'^2}{\varphi} \right) \\
& - \frac{k_d' \varphi_0 T'^2 \gamma_S^2 \gamma_{vol}^3}{\varphi} + \frac{2 k_d' \varphi_0 P' T' \gamma_S \gamma_{vol}^3}{\varphi} - \frac{k_d' \varphi_0 P'^2 \gamma_{vol}^3}{\varphi} \\
& + \left( \frac{6 \left(\varphi_0 - 1\right)^2 \varphi_0^2 \frac{\partial \varphi'}{\partial z'} P' v_g'}{(\varphi - 1) \varphi \left(\varphi_0 - 2\right)^2} + \frac{k_d' \varphi_0 P' \frac{\partial P'}{\partial z'}}{\varphi} + \frac{\frac{\partial k_d'}{\partial z'} \varphi_0 P'^2}{\varphi} - \frac{2 k_d' \varphi_0 P'}{\varphi} \right) \gamma_{vol}^2 \\
& + \left( - \frac{6 \left(\varphi_0 - 1\right) \varphi_0 \frac{\partial P'}{\partial z'} v_g'}{\varphi \left(\varphi_0 - 2\right)} + \frac{6 \left(\varphi_0 - 1\right)^2 \varphi_0^2 \frac{\partial \varphi'}{\partial z'} v_g'}{(\varphi - 1) \varphi \left(\varphi_0 - 2\right)^2} + \frac{k_d' \varphi_0 P' \frac{\partial^2 P'}{\partial z'^2}}{\varphi} + \frac{k_d' \varphi_0 \left(\frac{\partial P'}{\partial z'}\right)^2}{\varphi} \right. \\
& \left. + \frac{\frac{\partial k_d'}{\partial z'} \varphi_0 P' \frac{\partial P'}{\partial z'}}{\varphi} + \frac{k_d' \varphi_0 \frac{\partial P'}{\partial z'}}{\varphi} - \frac{(\varphi - 2) \left(\varphi_0 - 1\right) \varphi_0 \frac{\partial \varphi'}{\partial t'} P'}{(\varphi - 1) \varphi \left(\varphi_0 - 2\right)} + \frac{2 \frac{\partial k_d'}{\partial z'} \varphi_0 P'}{\varphi} - \frac{k_d' \varphi_0}{\varphi} \right) \gamma_{vol} \\
& - \frac{\gamma_{thermC} \frac{\partial^2 T'}{\partial z'^2} \gamma_S}{\left(G_{gr} \varphi - \varphi - G_{gr}\right) C_v'(\hat{\varphi})} + \frac{\frac{\partial S'}{\partial t'} \gamma_S}{C_v'(\hat{\varphi})} + \frac{k_d' \varphi_0 \frac{\partial^2 P'}{\partial z'^2}}{\varphi} \\
& + \frac{\frac{\partial k_d'}{\partial z'} \varphi_0 \frac{\partial P'}{\partial z'}}{\varphi} - \frac{(\varphi - 2) \left(\varphi_0 - 1\right) \varphi_0 \frac{\partial \varphi'}{\partial t'}}{(\varphi - 1) \varphi \left(\varphi_0 - 2\right)} + \frac{\frac{\partial k_d'}{\partial z'} \varphi_0}{\varphi}
\end{aligned}
\tag{4.15}
$$

Simplifying this equation by taking the first order Taylor series in the small parameters produces:

$$\frac{dP'}{dt'} = \left( -\frac{6\left(\varphi_0 - 1\right)\varphi_0 \frac{\partial P'}{\partial z'} v_g'}{\varphi\left(\varphi_0 - 2\right)} + \frac{6\left(\varphi_0 - 1\right)^2 \varphi_0^2 \frac{\partial \varphi'}{\partial z'} v_g'}{(\varphi - 1)\varphi\left(\varphi_0 - 2\right)^2} + \frac{k_d' \varphi_0 P' \frac{\partial^2 P'}{\partial z'^2}}{\varphi} + \frac{k_d' \varphi_0 \left(\frac{\partial P'}{\partial z'}\right)^2}{\varphi} + \frac{\frac{\partial k_d'}{\partial z'} \varphi_0 P' \frac{\partial P'}{\partial z'}}{\varphi} + \frac{k_d' \varphi_0 \frac{\partial P'}{\partial z'}}{\varphi} - \frac{(\varphi - 2)\left(\varphi_0 - 1\right)\varphi_0 \frac{\partial \varphi'}{\partial t'} P'}{(\varphi - 1)\varphi\left(\varphi_0 - 2\right)} + \frac{2\frac{\partial k_d'}{\partial z'} \varphi_0 P'}{\varphi} - \frac{k_d' \varphi_0}{\varphi} \right) \gamma_{vol} + \frac{\frac{\partial S'}{\partial t'} \gamma_S}{C_v'(\hat{\varphi})} + \frac{k_d' \varphi_0 \frac{\partial^2 P'}{\partial z'^2}}{\varphi} + \frac{\frac{\partial k_d'}{\partial z'} \varphi_0 \frac{\partial P'}{\partial z'}}{\varphi} - \frac{(\varphi - 2)\left(\varphi_0 - 1\right)\varphi_0 \frac{\partial \varphi'}{\partial t'}}{(\varphi - 1)\varphi\left(\varphi_0 - 2\right)} + \frac{\frac{\partial k_d'}{\partial z'} \varphi_0}{\varphi} \tag{4.16}$$

Due to the large size of $\gamma_{\mu T}$ the combination $\gamma_S \gamma_{\mu T}$ can not be considered second order in size, and we restore terms related to this combination yielding:

$$\frac{dP'}{dt'} = \gamma_{vol} \left( -\frac{k_d' \varphi_0 \frac{\partial P'}{\partial z'} \frac{\partial T'}{\partial z'} \gamma_S \gamma_{\mu_T}}{\varphi} - \frac{6\left(\varphi_0 - 1\right)\varphi_0 \frac{\partial P'}{\partial z'} v_g'}{\varphi\left(\varphi_0 - 2\right)} + \frac{6\left(\varphi_0 - 1\right)^2 \varphi_0^2 \frac{\partial \varphi'}{\partial z'} v_g'}{(\varphi - 1)\varphi\left(\varphi_0 - 2\right)^2} + \frac{k_d' \varphi_0 P' \frac{\partial^2 P'}{\partial z'^2}}{\varphi} + \frac{k_d' \varphi_0 \left(\frac{\partial P'}{\partial z'}\right)^2}{\varphi} + \frac{\frac{\partial k_d'}{\partial z'} \varphi_0 P' \frac{\partial P'}{\partial z'}}{\varphi} + \frac{k_d' \varphi_0 \frac{\partial P'}{\partial z'}}{\varphi} - \frac{(\varphi - 2)\left(\varphi_0 - 1\right)\varphi_0 \frac{\partial \varphi'}{\partial t'} P'}{(\varphi - 1)\varphi\left(\varphi_0 - 2\right)} + \frac{2\frac{\partial k_d'}{\partial z'} \varphi_0 P'}{\varphi} - \frac{k_d' \varphi_0}{\varphi} \right) + \frac{\frac{\partial S'}{\partial t'} \gamma_S}{C_v'(\hat{\varphi})} + \frac{k_d' \varphi_0 \frac{\partial^2 P'}{\partial z'^2}}{\varphi} + \frac{\frac{\partial k_d'}{\partial z'} \varphi_0 \frac{\partial P'}{\partial z'}}{\varphi} - \frac{(\varphi - 2)\left(\varphi_0 - 1\right)\varphi_0 \frac{\partial \varphi'}{\partial t'}}{(\varphi - 1)\varphi\left(\varphi_0 - 2\right)} + \frac{\frac{\partial k_d'}{\partial z'} \varphi_0}{\varphi} \tag{4.17}$$

The final stages of analysis are an asymptotic analysis of the perturbation terms (those multiplied by $\gamma_{vol}$) to retain only those terms which are leading order. In order for the perturbations to be important, we must have the unperturbed equation (4.19) in near-equilibrium (otherwise it will dominate). Since all the variables themselves are $O(1)$ everywhere, in order for the perturbation terms to be appreciable, we need one of the derivatives to be large. For example, if $\frac{\partial kd'}{\partial z'} = \frac{1}{\varepsilon}$ is large we can zoom into this small spatial region by

rescaling $z' \to \varepsilon\hat{z}$. The dominant terms with the right order of magnitude to balance are those with a factor of $1/\varepsilon^2$ under this rescaling which includes the $\frac{\partial^2 P'}{\partial z'^2}$, $(\frac{\partial P'}{\partial z'})^2$, and $\frac{\partial k'_d}{\partial z'}\frac{\partial P'}{\partial z'}$ terms, as well as the previously mentioned term involving $\gamma_{\mu T}$, hence they are retained. All remaining perturbation terms are dropped, and this, together with some reorganization of terms and simplifying substitutions leads to our final equation:

$$\begin{aligned}\frac{dP'}{dt'} = &-\beta(\hat{\varphi})\,\frac{\partial \varphi'}{\partial t'} + \frac{1}{\hat{\varphi}}\left(k'_d\,\frac{\partial^2 P'}{\partial z'^2} + \frac{\partial k'_d}{\partial z'}\left(\frac{\partial P'}{\partial z'} + 1\right)\right)\\ &+ \frac{\frac{\partial S'}{\partial t'}\gamma_S}{C'_v(\hat{\varphi})} + \gamma_{vol}\left(-\beta(\hat{\varphi})\,\frac{\partial \varphi'}{\partial t'}\,P'\right.\\ &\left.+ \frac{1}{\hat{\varphi}}\left(-k'_d\,\frac{\partial P'}{\partial z'}\,\frac{\partial T'}{\partial z'}\,\gamma_S\gamma_{\mu_T} + k'_d\,P'\,\frac{\partial^2 P'}{\partial z'^2} + k'_d\left(\frac{\partial P'}{\partial z'}\right)^2 + \frac{\partial k'_d}{\partial z'}\,P'\,\frac{\partial P'}{\partial z'}\right)\right)\end{aligned} \tag{4.18}$$

Equation (4.18) describes all relevant features of our model including small first order perturbations due to water compressibility and thermal effects. In this equation $C'_v(\hat{\varphi})$ is the nondimensional relative heat capacity as a fraction of $C_{v0}$ which changes due to spatial changes in porosity, and $\beta(\hat{\varphi})$ is the nondimensional bulk modulus of the mixture defined above (equation 4.13). In equation (4.18) the eliminated terms all had coefficients smaller than about $10^{-9}$.

It is at this point that the assumption of "fluid incompressibility," which is often invoked from the beginning in soil mechanics, can be applied in a rational manner by taking a limit as $\gamma_{vol} \to 0$. This assumption is a helpful one and justified for most purposes involving soil liquefaction. The primary conditions in which compressibility can become significant are high pressure gradients in low permeability soils, such as at the center of thin layers of silt, the spatial regions where these conditions occur are necessarily small as discussed in the oscillating permeability example below. Thus the term multiplied by $\gamma_{vol}$ is dropped, and the resulting simplified equation is:

$$\frac{dP'}{dt'} = -\beta(\hat{\varphi})\,\frac{\partial \varphi'}{\partial t'} + \frac{1}{\hat{\varphi}}\left(k'_d\,\frac{\partial^2 P'}{\partial z'^2} + \frac{\partial k'_d}{\partial z'}\left(\frac{\partial P'}{\partial z'} + 1\right)\right) + \frac{\frac{\partial S'}{\partial t'}\gamma_S}{C'_v(\hat{\varphi})} \tag{4.19}$$

## 4.3 Qualitative Results

Some basic simplified models for the qualitative behavior expected from these equations are now considered. Although researchers such as Zienkiewicz, Chang, and Bettess (1980) have previously investigated the role of drainage and shown that drainage is usually important, these results have not generally been appreciated. Here we examine several key experiments performed by others in the context of the predictions from our equations. First, recall that the characteristic time scale $\Delta t \approx 0.14\,\mathrm{s}$ for this system is smaller than the time scale for a typical earthquake loading period of about $1\,\mathrm{s}$ and much smaller than a typical earthquake duration of around $10 - 60\,\mathrm{s}$. This means that the behavior of the water pressure under realistic loading is always nearly in steady state. The diffusion term in the equation implies gaussian averaging of the pressure field over the entire deposit in time $\Delta t = 0.14\,\mathrm{s}$ so that any localized pressure feature will spread over the whole deposit in this short time via pressure diffusion induced by imbalances in flow described by the right hand side of equation 4.1. Any $\mathrm{ord}(1)$ imbalance in any of the terms of equation 4.19 would induce $\mathrm{ord}(1)$ bars of pressure change over $0.14\,\mathrm{s}$, returning the system rapidly to near steady state. Even for fine sands where $k_d \sim k_{d0}/20$ the time scale would be approximately the same order as a single loading cycle and significantly shorter than typical earthquake duration. Only when permeability is similar to the permeability of silts $k_{d0}/1000$ can we assume that the pressure diffusion time is long compared to earthquake duration. Under those conditions the pressure changes are determined by the tiny volumetric changes caused by squeezing the nearly incompressible water, and the "undrained" approximation $\frac{\partial P'}{\partial t'} \approx -\beta(\hat{\varphi})\frac{\partial \varphi'}{\partial t'}$ might be reasonable. Even in regions of silty soils, as we shall see in examples, when a silt layer is small and in contact with a sandy layer, very high curvature of the pressure field and large gradients generated near these interfaces can cause the silt to reach steady state pressures on the same time scale as the sand. Clearly flow can not be neglected in earthquake liquefaction of sand. In fact for sands quite the opposite case occurs, the flow required to induce steady state pressures happens extremely quickly.

To support this analysis with physical data, we can reference for example the centrifuge model B of Fiegel and Kutter (1994) involving a fine sand overlain by silt. Shaking starts at approximately 2 seconds, and lasts until approximately 12 seconds. By 4 seconds the pore pressure in the sand has come to a locally time-averaged steady state with a fast oscillation superim-

posed due to continued shaking, and the silt has a similar if slightly slower response, achieving a locally time-averaged steady state at approximately 10 seconds which is before the end of shaking at 12 seconds (times given in prototype dimension). A steady state solution of equation 4.19 based on time-averaged rate of change of porosity could be expected to be quite accurate at 10s, even before the shaking stopped, if the loading were taken to be the time average of the actual loading over a few seconds.

Because of this near-steady state, we can approximate the pressure field at liquefaction by solving for the steady state of equation (4.19) numerically to find the average forcing $\frac{\partial \varphi'}{\partial t'}$ required to make the water pressure field tangent to the total vertical stress. Once we have this solution we can find the location of tangency which is where the onset of liquefaction occurs. We use $\frac{\partial \varphi'}{\partial t'}$ constant in space except where noted below. Since heating was earlier determined to be a small perturbation for sands we ignore it here for simplicity except in the example involving thermal liquefaction in silts. Also, we set $\beta(\hat{\varphi}) = \hat{\varphi} = 1$ and ignore the small effect of spatial variability in $\varphi$ except as it influences $k_d$ which is spatially varying as shown in each figure. By adjusting the characteristics of the soil, especially the permeability field and the spatial variation in the forcing, we can determine how the permeability and permeability gradient affect the onset of liquefaction.

**Example 1: Uniform Loose Hydraulic Fill** A model of a uniform loose hydraulic fill such as those found at reclaimed land in bays and port facilities worldwide would be a uniform deposit with $k'_d = 1$ of depth $z' \approx 1$. We assume for simplicity that the water table is at the surface of the ground, and we apply a 0.12 nondimensional pressure unit load on the ground designed to model 1/2 meter of concrete pad to ensure that the effective stress is not zero at the surface (figure 4.1). In this situation, due to the uniform permeability, the term in equation 4.19 involving the spatial derivative of $k_d$ disappears. If we assume the contractive forcing $\frac{\partial \varphi'}{\partial t'}$ is constant in space and we are solving for steady state conditions, then the curvature of the pressure field is constant and we have a parabolic pressure curve.

In figure 4.1 we show the results of this simulation and we find that the soil just initiates liquefaction via loss of grain contacts at $z \approx 0.61$ when $\frac{\partial \varphi'}{\partial t'} = -1.53$ corresponding to a ground surface settlement velocity of $\frac{\partial \varphi'}{\partial t'} \Delta\varphi \Delta z / \Delta t = -0.08\,\mathrm{cm/s}$. Liquefaction occurs at this location not because of special properties of the sand at this point as all sand is treated equally, but rather be-

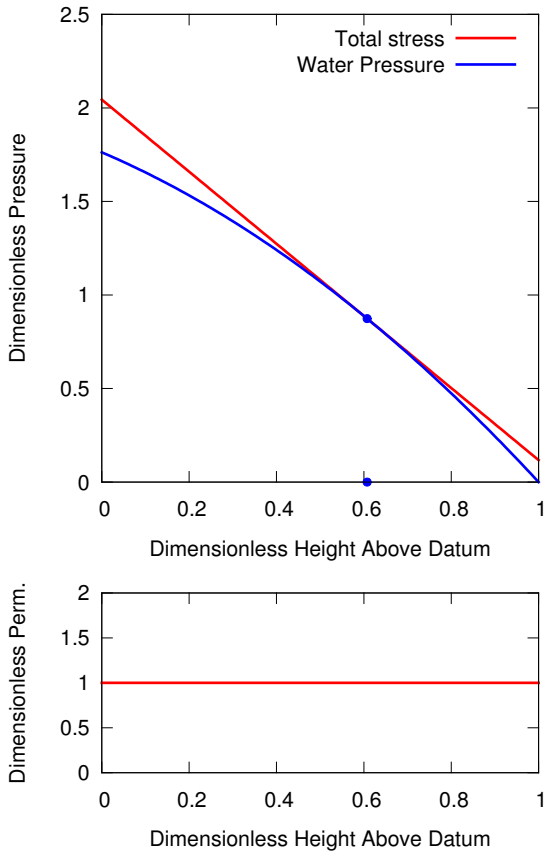


Figure 4.1: Parabolic water pressure is tangent to the linear total stress curve at the point of initial liquefaction in a uniform sand

cause of the flow and its interaction with the boundary conditions as will be explained later. For a 30 second earthquake and a 10 m deposit, this implies a vertical settlement of about 2.4 cm. Normally if the ground drops several centimeters we would see serious consequences for pipelines or structures on spread footings.

**Example 2: Fine-scale variability in permeability around an average value** Due to the importance of permeability variation, we consider a model of a loose hydraulic fill sand whose layering structure causes a fine-scale oscillation in permeability of 30% about a typical value $k'_d = 1 + 3/10 \sin(2\pi 40 z')$.

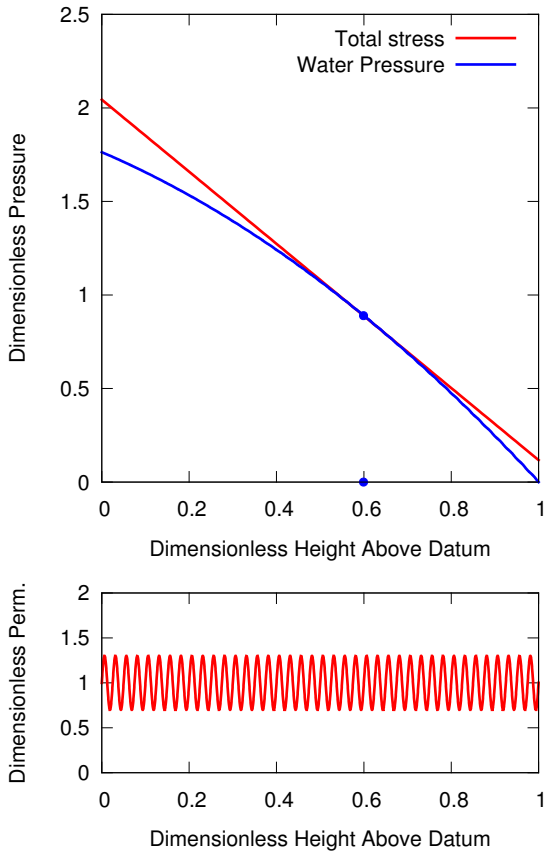


Figure 4.2: Liquefaction initiates at essentially the same place as in the constant permeability example despite a fine-scale oscillation in permeability of 30%. The dominant term in the differential equation is the $k'_d \frac{\partial^2 P'}{\partial z'^2}$ term so long as $k'_d \not\approx 0$ implying that large stable gradients in pressure do not form unless permeability becomes quite small as seen in the silt-layer example.

This oscillation occurs on a small length scale $O(1/40)$ of the total length, and is a simple model for variability in hydraulic fill material and the natural segregation of sandy soil by varying sinking rates due to varying grain sizes as pointed out by (Kokusho and Kojima 2002). Note that the water pressure curve for this case is very similar to that of figure 4.1.

This example allows us to highlight the role of the variability in permeability. If the permeability field is $O(1)$ throughout, but has a fine scale os-

cillation of dimensionless length scale $\lambda \ll 1$ then the term $\frac{\partial k'_d}{\partial z'}$ becomes $O(1/\lambda)$ which can be quite large. To balance this we can either generate curvature of the pressure field to induce diffusion, or if diffusion is quenched by $k_d \frac{\partial^2 P'}{\partial z'^2} \sim 0$ then $(\frac{\partial P'}{\partial z'} + 1)$ must be $O(\lambda)$ to keep $\frac{\partial k'_d}{\partial z'}(\frac{\partial P'}{\partial z'} + 1) = O(1)$.

Suppose that a fine scale variation in $P'$ develops so that $P' = F(z'/\lambda) + G(z')$ where F is an $O(1)$ function representing the fine scale variation and G is $O(1)$ representing the large scale variation. Then $|\frac{\partial^2 P'}{\partial z'^2}| = O(1/\lambda^2)$ with a factor $1/\lambda$ coming from each derivative of F with respect to $z'$. In order for diffusion to be quenched we must have $k'_d \ll \lambda^2$ so that $k'_d \frac{\partial^2 P'}{\partial z'^2} \approx 0$ in equation 4.19. Since in real materials $0 < k'_d < O(1)$, necessarily the region where both $k'_d \ll \lambda^2$ and $|\frac{\partial k'_d}{\partial z'}| = O(1/\lambda)$ is extremely small. To see this, consider that if $k'_d$ is small, and the derivative of permeability is negative, then it must become nonnegative quickly to keep $k'_d > 0$; or if the derivative is positive, $k'_d$ increases rapidly so it does not remain small for long.

If the overall size of $k'_d$ is small everywhere, then we can rescale the $k'_d$ variable everywhere, and by rescaling the $t'$ variable the equation remains symmetric though now all processes take longer in dimensional time. This shows that for lower permeability soils an overall lower level of forcing is required for liquefaction as the same change in $\varphi'$ would liquefy the soil if imposed over a longer dimensional time. In general, the conclusion is that large stable gradients in pressure occur primarily in small regions of very low permeability soils surrounded by higher permeability as shown in a later example with a thin silty layer.

By using a Fourier series approach to approximate the analytical solution we find that the oscillations in permeability are completely dominated by the tendency for pressure diffusion in the steady state case so that the pressure field is nearly indistinguishable from the earlier constant permeability field figure 4.1, and does not develop an important fine scale oscillation since the permeability never becomes small enough; in this example $\frac{\partial \varphi'}{\partial t'} = -1.45$ and $z' = 0.599$ compared to the constant permeability model where $\frac{\partial \varphi'}{\partial t'} = -1.53$ and $z \approx 0.61$. Since the figure for this example is very similar to figure 4.1, it is reproduced in the supplement.

**Example 3: Silty Inter-Layer** Another case of interest is a simple model for the experiment of Kokusho (1999). In this situation we have loose sandy soil with $k'_d = 1$ and a thin layer of much lower permeability $k'_d \sim .001$ with a large gradient in permeability around this minimum (see figure 4.3). Be-

cause of the large permeability gradients, there can be fast changing boundary layers in which the pressure gradients are high and develop over small regions so that the curvature of pressure is quite large. If we solve the steady state equation we find that with $\frac{\partial \varphi'}{\partial t'} = -1.23$ the confining of pressure by the inter-layer forces a localized loss of grain contacts at $z' = 0.497$ just below the center of the layer. In the experiment of Kokusho (1999) there is the formation of a thin water film below the silt inter-layer in a manner consistent with these results.

A follow up to the above experiment considered a silt inter-layer in a fine sand, in which a long lasting sable layer of water below the silt layer was observed (Kokusho and Kojima 2002). The water layer will be long lasting if the upper soil can not fall quickly through the water due to drag. This can be explained in general by the ratio of drag force to weight for small particles. If we consider a single spherical soil particle of radius R, the well known formula for Stokes drag is $f_d = -6\pi\mu Rv$ (Brinkman 1949) whereas the weight for a spherical grain is $w = \frac{4}{3}\pi R^3 \rho g$. If we take the fluid velocity to be the velocity in the water layer immediately above the sand $v = \frac{k_d}{\mu}\frac{\partial P}{\partial z}$ the characteristic value of $f_d/w$ for one nondimensional unit of each variable is therefore: $\frac{9k_{d0}}{2G_{gr}R^2}$. For sand grains with $R \sim 0.5\,\mathrm{mm}$ this ratio is $0.001$ whereas for a silt grain with $R \sim 0.01\,\mathrm{mm}$ the ratio is 2.5 indicating that silt particles which fall down into the water layer are easily pushed back up by the drag caused by fluid flow whereas the sand will easily sink under these conditions. In addition to this basic interpretation, Brinkman (1949) and Verschoor (1951) show that the drag on the particle increases dramatically as it integrates into the porous medium at the water-silt boundary so that once a layer is formed, the particles above are unlikely to detach and sink. The effect of grain sizes is discussed more comprehensively in an additional section below.

In another experiment by Kokusho and Kojima (2002), which involved a fine sand overlying a coarse sand, a transitory turbulent water layer was observed at the interface between the sands. The differences between this coarse and fine sand case compared to the fine sand and silt case can be understood in terms of two factors: the lack of a long-term strong gradient in pressure which would induce a large flow velocity, and the larger grain sizes involved in the coars and fine sand experiment. In further cases, involving a fine sand inter-layer in a coarse sand, the results were substantially similar to the sand with silt inter-layer experiment with an altered timescale due to the different permeabilities involved (Kokusho and Kojima 2002). Finally, the

authors alter their fine sand overlying a coarse sand experiment where only transient turbulent water films formed at the interface by reducing the height of the water table. In this case the water layer at the interface is stabilized (Kokusho and Kojima 2002). The lack of water above the water table means that the effective size of the upper fine sand layer is only 7 cm compared to 90 cm in the original experiment, since the unsaturated sand above the water level does not affect the flow and the fluid pressure drops to atmospheric at the fluid/air boundary. This effectively thinner upper soil layer means a larger pressure gradient can form and higher fluid velocities develop, thus higher drag develops on the upper sand particles which stabilizes the water film.

**Example 4: Liquefiable Sand Inter-Layer** A typical warning sign for Geotechnical engineers is the existence of a loose sand layer between layers of denser and especially lower permeability material. This is the inverse of the silty inter-layer example given above. When we make permeability $k'_d = 1/8$ outside of a region of width about 20cm (10 times as wide as the silty inter-layer) where permeability is 1 we find that the contraction of the deposit pushes water upwards out of the coarse sandy layer and the deposit liquefies in the fine sand above at $z' = 0.65$. Also $\frac{\partial \varphi'}{\partial t'} = -0.198$ which is *much* lower loading than in either the uniform or silty layer case. In this case, the location and manner of liquefaction is less important than the magnitude of the loading required (see figure 4.4)). Due to the lower permeability of the main deposit, the diffusion is less dominant, and with less drainage, it is easier to cause liquefaction. However, since the gradients in pressure remain $O(1)$ the perturbation terms do not become important here. This highlights the phenomenon that "drainage" is a non-local phenomenon which is affected by the entire permeability field. Sand itself may be locally well drained, but can be confined by low permeability boundaries.

**Example 5: Sand overlain by silt** This model (figure 4.5) is modeled after the centrifuge results of Fiegel and Kutter (1994) in which a silt overlies a loose sand, and is subject to shaking in a geotechnical centrifuge. In these experiments, pore water pressure was recorded in several locations within the sand and silt. For our model of this case we have rescaled the z axis to correspond to the depth of the experiment and correspondingly rescaled $P'$, $\varphi'$ and $t'$. Contractive forcing $\frac{\partial \varphi'}{\partial t'}$ is spatially varying and appreciable only in

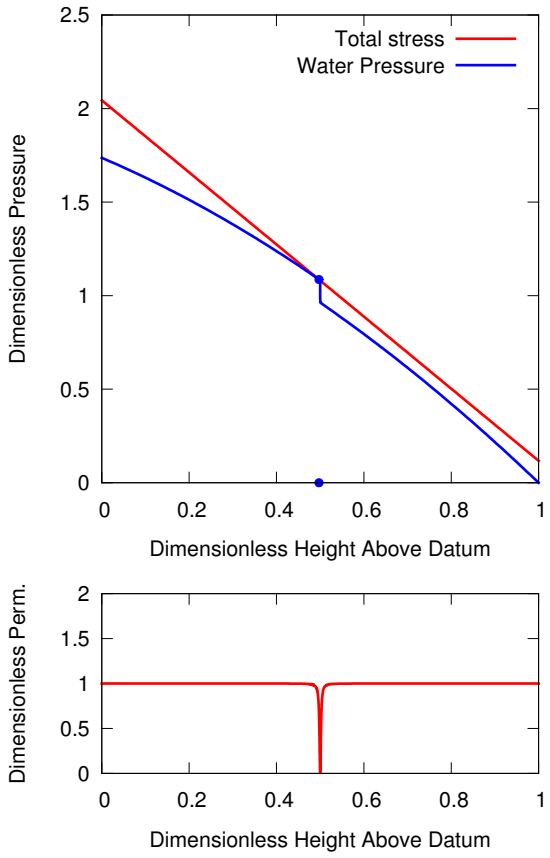


Figure 4.3: Silt layer embedded within loose sand. Liquefaction initiates below the region of lowest permeability where the large gradient in permeability induces a large second derivative of pressure, and a thin water film forms.

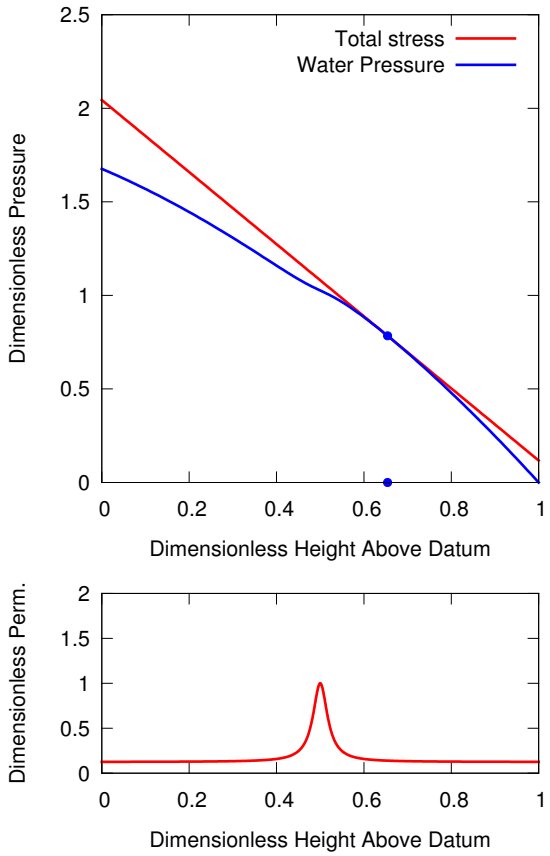


Figure 4.4: A high permeability layer acts as a drain for water pressure in the lower region and a source for water pressure in the upper region. Liquefaction occurs above the high permeability layer. This result occurs whether we use uniform forcing throughout or localized forcing only within the high permeability layer.

the lower sand region, the silt region is assumed not to contract, and hence the water pressure curve is nearly linear in the silt which implies fluid flow at constant velocity. Clearly then, water is squeezed out of the lower sand and pressure diffuses into the upper silt, liquefying it at the base. The experimental results of Fiegel and Kutter (1994) qualitatively agree with this steady state solution. Note that the consequences of liquefaction, a failure via a sand-boil, were observed to occur much later, presumably near a localized weakness within the silt layer. In our example, liquefaction occurs at $z' = 0.695$ which is slightly above the center of the permeability transition, which is located at $z = 0.629$. The required loading is $\frac{\partial \varphi'}{\partial t'} = -0.011$ which ultimately is unrescaled (both $\varphi'$ and $t'$ are rescaled by the same factor, hence canceling). This is significantly smaller than in the uniform sand example (figure 4.1) where $\frac{\partial \varphi'}{\partial t'} = -1.53$. The relatively thick silty layer makes drainage difficult as expected, and this contributes to a large reduction in the necessary loading.

**Example 6: Theoretical process of thermal liquefaction of silt** By substituting $k'_d = \varepsilon \hat{k}_d$ in the incompressible equation 4.19 we can consider the case when typical permeability is small relative to sand, such as $\varepsilon < .001$. When this is the case, diffusion does not act on the same time scale, and in fact the diffusion time scale $\Delta t/\varepsilon > 140\,\mathrm{s}$ is larger than the typical duration of the earthquake. This rescaling process also makes the $\gamma_{vol}$ term more dominant, and the full compressibility effects might become important though we ignore them in this example as our purpose is simply to highlight a new phenomenon which could provide an avenue for further study. If a silt is somehow precluded from sustained grain skeleton contraction $\frac{\partial \varphi'}{\partial t'}$, perhaps due to its initial porosity being near the equilibrium state, it could still theoretically liquefy by absorption of wave energy into thermal energy. The simplest case is a single homogeneous layer of silt similar to the homogeneous layer of sand above. Instead of contractive forcing, we apply $\frac{\partial S'}{\partial t'}$ and attempt to liquefy the silt via heating. The equation is similar to uniform contraction, and produces the same pressure field as figure 4.1. We find that the homogenous layer liquefies at $z' \approx 0.61$ when $\frac{\partial S'}{\partial t'} = 1.53\varepsilon/\gamma_S$. The question arises then as to whether $\varepsilon/\gamma_S = \mathrm{ord}(1)$ in some regimes of shaking and grain size implying that silt might thermally liquefy by absorbing wave energy to heat. This is an interesting question for which a simple centrifuge experiment using a well insulated bucket and measuring before and

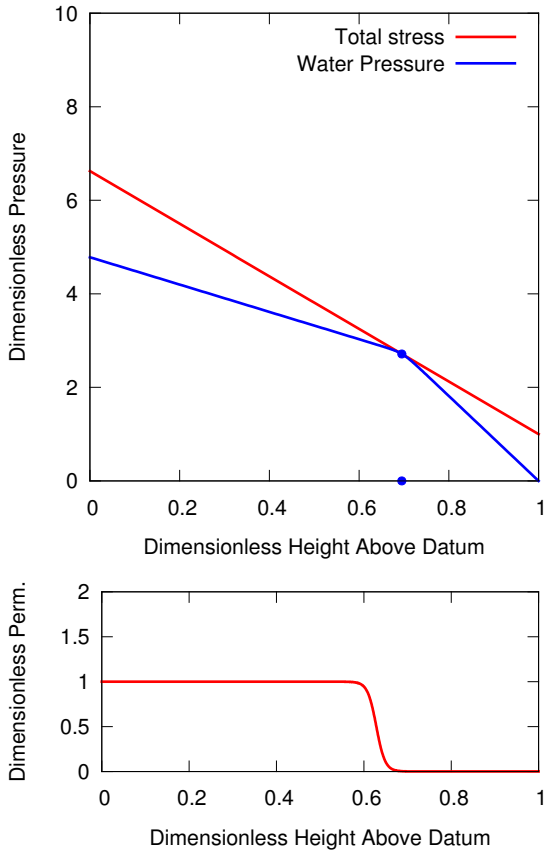


Figure 4.5: A model for the experimental results of Fiegel and Kutter (1994) in which the step in permeability induces liquefaction at the sand-silt boundary where a sharp kink in pressure occurs. Here the spatial dimension has been rescaled by a factor $\varepsilon \approx .34$ so that $z' \in [0,1]$ corresponds to $z \in [0, 3.5]\,\mathrm{m}$, the dimensions of the experiment. Pressure, $\varphi'$, and time have been rescaled by $\varepsilon^2 \approx 0.12$ to maintain the order of magnitude of the coefficients in the equation. Scaling of the forcing $\frac{\partial \varphi'}{\partial t'}$ cancels out so that numerical values are directly comparable to other examples. Forcing is constant in the sand, and drops to near zero just below the permeability transition, hence only the sand contracts appreciably. The gradients stay small enough that the perturbation terms do not become important.

after temperatures could give insight, or perhaps borehole measurements of thermal changes during an earthquake might be available to provide insight.

## 4.4 The role of grain sizes and drag forces for liquefaction consequences

Since we are considering the liquefaction of silt, it should be mentioned that pure silts and pure gravels are generally thought to be lower risk for liquefaction than sands, though a more nuanced view of silt and gravel liquefaction is developing (cf. (Idriss and Boulanger 2006; Seed et al. 2003)). Examining the cases for different grain sizes within the context of simple steady state water flow described here can be instructive.

In order for sustained contraction of the grain skeleton to occur we need gravitational and over-burden forces on the particles to be balanced by drag forces of the water so that the grains travel downwards at a slow terminal velocity while the water is pressurized and travels upwards towards the surface. Because of this balance of forces, and the rapidity of pressure diffusion, the details of grain motion at each point in the loading cycle are less important than the overall average contractive trend.

In the examples by Kokusho and Kojima (2002), the sand particles descend rapidly through the water while the silt particles sit on top of the water layer. These settlement velocities are related to the drag forces on the particles. However when all particles are silt sized, even if all particle contacts are lost, settlement will be extremely slow and particles will not move far from their initial positions during a loading cycle due to high drag forces relative to gravitational settlement forces. Consequences of such an event on level ground may be significantly less destructive than in sand where drag forces do not affect mobility as strongly and settlement is more rapid. For gravels mobility is even more rapid than sand, but contraction of the gravel does not induce strong pressurization since the pressure dissipates extremely rapidly due to the high permeability, unless surrounding lower permeability soils impede flow. This implies we should expect fast settlements but only transient liquefaction in contractive gravels.

Although in the vertical direction we expect rapid settlement from gravel particles and slow settlement from silt, in terms of shear displacements the roles may be reversed. The rapidity with which gravel particles descend

may allow them to regain contact more rapidly thereby reducing the time during which shear strength is lost, whereas silt particles will take a long time to regain their shear-transferring ability through settlement. Soils with a wide range of particle sizes will be more complex. The development of a soil behavior model which takes the fluid drag forces into account explicitly is a worthy goal. Whatever the case, this analysis highlights the gradient in particle size, which is also related to the gradient in permeability, as playing an important role in the liquefaction process especially with regards to the development of fluid lubrication layers as seen in Kokusho (1999); Kokusho and Kojima (2002).

## 4.5 The problems with small scale empirical tests

To understand the role of water flow on small scale samples, consider the example in figure 4.1 where all the sand is uniformly similar in initial porosity and permeability conditions. If we take a slice of dimensionless length 0.01 from this example, it corresponds to a sample similar in size to a hypothetical triaxial sample of about 10cm characteristic length. Recall that all points in the model of example 1 were squeezed equally since $\frac{\partial \varphi'}{\partial t'}$ was a constant in space. The rate of squeezing in example 1 was 1.53 units of $\Delta\varphi$ per 1 unit of dimensionless time, or a volumetric strain of about 1% in 130 s which is perhaps a reasonable timescale for a tabletop undrained liquefaction experiment. In the absence of drainage, at this volumetric strain rate, we would generate in our hypothetical sample 100kPa of additional pressure every 0.6 seconds, and at the end of 130s we would have about 22.5 MPa of water pressure. Instead, in example 1, we have about 100 kPa of excess pressure (1 dimensionless unit over atmospheric) at infinite time, as shown in figure 4.1 at $z = 0.6$ where liquefaction occurs. This discrepancy is due to drainage in steady state conditions. Note that the pressure field in example 1 is influenced by three factors: the rate of squeezing ($\frac{\partial \varphi'}{\partial t'} = -1.53$), the constant permeability, and the boundary conditions (impermeable at $z = 0$, constant atmospheric pressure at $z = 1$ and zero lateral flow). This is in contrast to the triaxial test where drainage is prevented (impermeable at top and bottom), and the boundary conditions are much closer, and more complex, due to the surrounding rubber membrane and constant pressure bath.

In example 1, the reason the point at $z = 0.6$ has liquefied is not that it has been squeezed harder, or that its grain skeleton was more susceptible

than other points, it is that fluid is flowing continuously through the sample, and due to a combination of squeezing, and imbalance in fluid flow, the density of water at this point is just slightly higher than it was before we began squeezing the sample. The role of water flow is highly nontrivial even in this extremely simple example.

In contrast, consider taking our slice of dimensionless length 0.01, removing it from the ground, and placing it into a triaxial machine. Now, the boundary conditions have been brought 100 times closer to the sample (about 10cm instead of 10m) and have been changed. In a triaxial test, we have an impermeable but stretchy membrane surrounded by a constant pressure on the sides, with a rigid base and loading cell below and above. This can be compared to the layered soil in our mathematical model where lateral symmetry implies zero flow horizontally, and we have an impermeable layer below and constant atmospheric pressure above. Although a triaxial test is not really a 1D system, we can begin to qualitatively analyze the effect of investigating the small scale samples using the same equation 4.19 by choosing new scale constants to interpret the results.

We leave the characteristic pressure at $P_0 = 100\,\mathrm{KPa}$ since this is the order of magnitude of pressure we must induce to liquefy the sample. Since $\Delta\varphi$ depends only on the pressure scale, it remains unchanged. We ignore heating for these purposes. We are left with re-evaluating $\Delta z$ and $\Delta t$. The characteristic size of our sample is $\Delta z = 0.1\,\mathrm{m}$, and the new value of $\Delta t$ is determined from $\Delta z$ and equal to $\Delta t = \frac{(\Delta z)^2 \varphi_0 \mu}{k_{d0} K_B} \approx 1.3 \times 10^{-5}\,\mathrm{s}$ or 13 microseconds. The triaxial boundary conditions are now complex because they involve the interaction of a pressure bath with a rubber membrane which then interacts both with the grains and the pore water, and they are no longer 1D. However, it is safe to say that the pressure exerted by the membrane on the pore water is relatively uniform. Next we consider the loading, $\frac{\partial \varphi'}{\partial t'}$. It is safe to say that this is nearly zero on our new scales, as the loading is such that the order of magnitude of pressure changes that these experiments induce is enormously less than $P_0 = 100\,\mathrm{kPa}$ in 13 microseconds.

In the absence of any significant loading, the water pressure inside the sample is in gravitational equilibrium at all times, since the equilibriation time is 10 million times shorter than the duration of the experiment, and since our new length scale is $\Delta z = 10\,\mathrm{cm}$ the gradients in pressure are tiny as we will never induce anywhere near 100 kPa fluid pressure differences across the 10cm sample.

Just as in the full scale equation, the water pressure in our impermeable-membrane-wrapped triaxial sample is dependent on three things: the dynamics of the loading which we have shown to be essentially zero, the uniform permeability which remains unchanged, and the pressure induced by the boundary conditions which involve both grains and water interacting with a highly compliant impermeable membrane surrounded by a constant pressure bath. In the triaxial test the fluid pressure is entirely determined by this boundary condition as all points are in equilibrium with the boundary. To the extent that we are not interested in how rubber membranes interact with grains and water under constant external pressure conditions, we should also be highly skeptical of any results from tabletop triaxial or similar specimens in so far as they are supposed to represent how the soil behaves in the ground. As we have shown at the beginning of this section, under the ground, water flow is extremely important, and tabletop experiments, as currently performed, simply can not model this process.

In contrast to triaxial type experiments, geotechnical centrifuge experiments such as Fiegel and Kutter (1994) instead use scaled fluid viscosity so that the diffusion time from a point deep in the model to a point on the surface where constant atmospheric pressure exists will scale appropriately. Also the model is built in layers, so that the permeability field of the entire deposit is modeled correctly, including permeability gradients. Therefore fluid flow can be properly accounted for in geotechnical centrifuges through the proper application of scaling laws.

## 4.6 Conclusions

By deriving a comprehensive equation for the water pressure development within layered soils and analyzing some critical examples we have shown that fluid flow driven by porosity changes and permeability changes is the main factor that causes pore pressure change during liquefaction. By comparison with experimental results (Fiegel and Kutter 1994; Kokusho 1999; Kokusho and Kojima 2002) we show that sandy soil is well drained enough that this soil comes to steady state on the same time scale as the earthquake. Also, due to our model of this drainage, we can identify several modes of liquefaction, from fluid flow induced "fast settlement" to localized water film formation at permeability boundaries, to flow induced liquefaction of low permeability layers that overly a high permeability layer, and even poten-

tially thermally induced liquefaction when permeability is very low. In each of these example cases, we do not attempt to couple the behavior of the grains to the behavior of the water, or provide time-varying dynamic solutions, as no large scale continuum model is available for grain-fluid interaction behavior comparable in quality to the DEM model of Goren et al. (2011). Our intention in this paper has been to highlight the importance of fluid flow and spur an understanding of the need to develop soil models that can account for flow.

Modeling a 1/4 m square cross section 10 meters long with 1mm diameter typical grain sizes would require perhaps $10^8$ grains and be computationally prohibitive. However for qualitative understanding of the liquefaction process it is sufficient to perform a careful analytical analysis of a continuum model of water flow through soil driven by changes in pore volume. Our analysis provides tremendous insight without supercomputing requirements, from which we make several important conclusions:

- Soil liquefaction in water saturated sands is a process usually involving fluid flow due to gravitational pumping, not purely fluid stagnation in an "undrained" event. Thin regions of low permeability silt do not prevent drainage, as large pressure gradients will develop to force fluid through these layers. However, their presence significantly influences the location and ease of onset of liquefaction. Large regions of low permeability soil can significantly reduce drainage, leading to liquefaction at significantly lower rates of grain contraction.

- Due to water pressure diffusion, we can not examine the liquefaction process by simply considering local properties of soil in a small sample on a tabletop apparatus, given the characteristic length scales of $\mathrm{ord}(10)$ meters, and corresponding characteristic time scales of tenths of seconds. In a tabletop apparatus with samples on the order of 10cm the timescale for diffusion of pressure to the impermeable rubber boundary and hence to the constant pressure boundary conditions is on the order of 10 microseconds, so that the pressure throughout the sample is equal to the boundary pressure at the membrane. Therefore, geotechnical centrifuge experiments are the only meaningful physical experiments for this phenomenon.

- In lower permeability materials such as thick regions of fine sand or silt, the time scales for the water flow process can be longer. These long

characteristic times occur when the typical permeability throughout the material is $\mathrm{O}(10^{-13})\,\mathrm{m}^2$ which is well below the sandy range (Beard and Weyl 1973). Due to grain size effects, fluid flow in silt causes high drag on the particles, limiting their mobility. Liquefaction in extensive silt deposits is an interesting and different flow regime.

- Impedance to flow caused by local sharp reductions in permeability is the main driving force in localized liquefaction events, and can cause the formation of water films that lubricate layers of soil allowing large lateral spreading. For level ground, failure is expected via localized sand boils at fissures, or the liquefaction of overlying layers as fluid flow stagnates. This phenomenon can only be explained by explicitly acknowledging the flow of water.

- "Liquefaction" as the term is commonly used is not necessarily associated with total loss of effective stress as is already known. Large settlements could occur without the formation of a fully liquefied layer if loose soil settles while water flows to the surface. This may especially occur in contractive gravel or coarse sand fills.

- In silts, where permeability is small and diffusion can not act on the earthquake duration timescale, extensive shaking might concievably cause liquefaction through heating effects, a previously unexplored phenomenon.

# Chapter 5

# Dissipation of Waves in a Molecular Test Problem

*What are the wild waves saying*
*Sister, the whole day long,*
*That ever amid our playing,*
*I hear but their low lone song?*

—Joseph Edwards Carpenter

## 5.1 Introduction

When thinking about how to model the interactions between grains and earthquake waves which lead to the dissipation of wave energy and rearrangement of grains it became clear that stepping directly to this complicated problem was prohibitive. Instead, during discussions with earthquake physicists a simpler test problem emerged. In this problem we attempt to model the cause of dissipation in waves traveling through a molecular polycrystalline medium, which can be simulated to high precision using MD techniques. In the absence of wave spreading, external radiation, and scattering, where all energy remains within the bar, any wave dissipation must be described via some other mechanism. The results of this investigation are reproduced below and are being prepared in substantially similar form for further publication.

## 5.2 The Problem

A thin rod with a square cross section made of polycrystalline molecular material sits in free space and the two ends are tapped to induce two opposite-traveling compression waves. The net momentum and angular momentum of the rod is zero and we assume no mechanism for the total energy of the system to change, such as acoustic or thermal radiation or other coupling to the surroundings. The classic wave equation derived from linear elasticity is:

$$\frac{\partial^2 u}{\partial t^2} = \frac{\partial v}{\partial t} = v_w^2 \frac{\partial^2 u}{\partial x^2} \tag{5.1}$$

Where $v = \frac{\partial u}{\partial t}$ is a velocity field along the length of the bar, $v_w = \sqrt{\frac{E}{\rho}}$ is the wave velocity and u is the displacement field of the material from equilibrium position.

This classic equation, derived from the assumption of stress proportional to strain $\frac{\partial u}{\partial x}$ predicts no dissipation whatsoever and the bulk scale waves continue to travel back and forth forever in such a model. However even without having performed the experiment, we are fairly sure that there is some long-time limiting behavior in which the rod ceases to have a discernible bulk-scale wave, and instead is simply at higher temperature than before. The wave equation is therefore the asymptotic limit where observational size is much larger than molecular size so that measurements are not made of individual molecules, and dissipative effects are negligible on the observational time scale. Depending on the size of the rod, the temperature, and the material it is made of, the time scale for dissipation may be anything from fractions of a second to perhaps years. The question is, how can we use our knowledge of the molecular nature of the material to produce predictions for the bulk scale decay of waves in a medium where dissipation is non-negligible, and what are the scaling laws that determine when dissipation is important?

In realistic situations, in addition to the fundamentals of local entropy generation, geometric spreading, diffraction, and scattering of waves by inhomogeneities in the material operate simultaneously. At large length and energy scales in a 3D medium, geometric spreading over the spherical wave front, diffraction, and scattering completely dominate over local entropy generation. When adding formal damping terms to the wave equation, the choice

of damping coefficient is usually made by reference to statistical fitting of observational data in which these larger scale processes dominate. Such statistical fitting does not give us a satisfactory description of the inherent local entropy generation rate. Only a model built on our knowledge of the micro-scale interactions can inform the causal questions of how dissipation occurs in the absence of spreading and scattering.

## 5.3 The Approach

We simulate a solid built of uniform Lennard-Jones (LJ) particles, interacting with a truncated potential, using the LAMMPS molecular dynamics simulator (Plimpton 1995). Units are the non-dimensional "Lennard-Jones" units described in the LAMMPS manual. In particular $3T/2$ is the average kinetic energy per molecule at thermal equilibrium, all molecules have mass 1, and 1 unit of energy is the escape energy required to separate two molecules in free space initially at equilibrium distance. Lengths are measured as multiples of the zero-crossing length for the potential, and time is defined by $mv^2/2 = 1$ unit of energy when one molecule travels at velocity $v$ equal to one unit of distance in one unit of time.

We repeatedly choose a random number of particles $N$, an initial temperature $T_0$ and a velocity pulse strength $v_0$ to run 120 different simulations. The parameters were chosen so that $N = 2500 + n$ where $n$ was exponentially distributed with average 50000. Using LJ walls, we confine the particles into a region whose dimensions are approximately $(\delta, \delta, 10\delta)$ in the $x, y, z$ directions where $\delta = (N/10)^{1/3}$. After initially equilibriating a bar at higher temperature, and removing the boundary walls, we slowly lower the temperature and bring the bar to a new state of equilibrium at temperature $T_0$. We choose $T_0 \in [0.025, 0.25]$ uniformly so that molecules are not generally hot enough to boil off the surface of the bar in any sample simulation. Then we select the molecules in a region of length $3\delta/2$ at the two ends of the z axis of the bar and superimpose a velocity $v_0$ on top of their thermal velocity distribution, oriented toward the center of the bar. The velocity pulse strength was chosen uniformly at random in $[0.05, 0.25]$. Finally we zero out the linear and angular momentum exactly so that the bar does not move in space and watch the time evolution of the system. At each slice of width $\delta/2$ along the z axis, we output the number of molecules, the net kinetic energy, the net potential energy, and the center of mass velocity within

each slice at each recorded timestep. We define the total wave kinetic energy as $W = \sum_{i=1}^{N_{slice}} n_i v_i^2/2$. Due to fluctuations in the initialization process $N_{slice}$ is not always 20. For example, occasionally a 21st box might have a few molecules in it, but we can idealize the system as nominally having $N/20$ molecules in each of 20 slices of width *exactly* $\delta/2$ along the length and this idealization is good to within a few percent.

The total kinetic wave energy decays with time according to a consistent pattern of time evolution which varies with N, T, and $v_0$. If we assume a perfect linear elastic wave equation then we can define a new time scale by $t_w = (L/2)/v = (L/2)/\sqrt{K/\rho}$. We find experimentally that $\rho \approx 1.05$ in these systems, and assume that $K = \frac{\partial^2 U}{\partial r^2}|_{r_{min}} = 9(2^{(8/3)}) \approx 57.15$ leading to a wave speed of about 7.38 in molecular units. The time scale $t_w$ is the molecular time required for our waves to travel from the ends of the idealized bar to the center. In performing statistical inference later we will fit the $t_w$ time scale more precisely.

With precisely calibrated timescale, we therefore expect the total wave kinetic energy to reach minimum at times $t/t_w = \{1, 3, 5, \ldots\}$. If we choose a bar scale length of $l_w = \delta/2$ then the wave speed in our new bar scale units is nominally 10, and a system which is purely linear elastic would collapse down to a single solution having a wave traveling from the end to the center in one unit of time and bouncing back and forth within the bar infinitely.

If dissipation occurs however, the dissipation need not be independent of N in the new time and length units as dissipation may depend on N in a different way, as well as on T or other properties. Our next task is to determine how this bar behaves including dissipation as a function of N and T. We mention for completeness that we ignore the effect of surface energy and surface tension here, and find that it does not make a large difference in our results.

## 5.4 The Model

The dynamics of our bar are represented at the bulk scale as 20 measurements of different properties, but especially the number of particles and center of mass velocity of each slice. Of course it is possible to choose another number of boxes, but so long as the number is fixed across the different samples and is large enough in every sample to contain a nontrivial statistical sample of particles then it makes no difference what the number

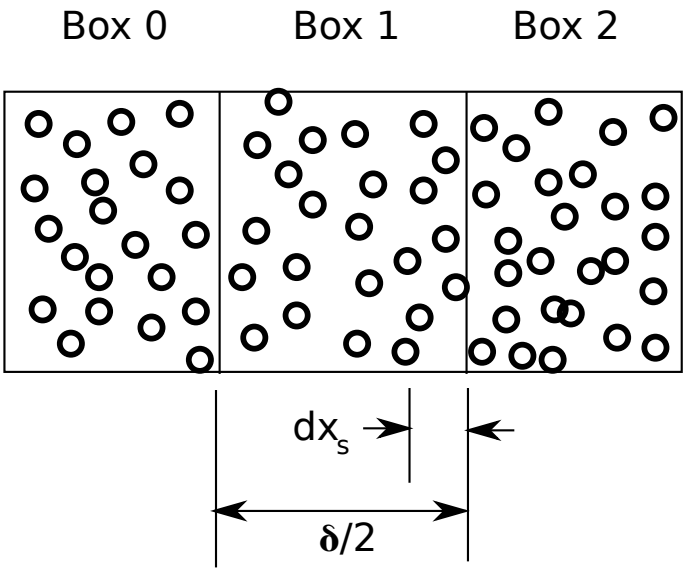


Figure 5.1: An idealization of three slices of the bar from which statistical averages are calculated in the molecular dynamics simulation

is. What does matter however is the width of the slices relative to the interaction length of the LJ potential as well as to the feature size of the initial wave pulse. The non-dimensional size of the slice $\delta/2 = (N/10)^{(1/3)}/2$ and non-dimensional temperature T are therefore the parameters of interest for our dissipation model.

The derivation of our model proceeds according to a template described in chapter 3. We start by taking into account the molecular processes within a slice. The bulk scale average statistics are formed from averages over the molecules in our slice. We choose a slice on the interior of the bar and call it slice 1, so that the slice to the left is slice 0 and the slice to the right is slice 2 (see figure 5.1). The slice is fixed in space in an Eulerian coordinate system. Assume that the bulk scale measurements at time $t = 0$ are $n_i, v_i, T_i$. We choose a short time dt which is small compared to the time that the wave

takes to travel the width of the slice $\delta/2$ and treat it as if it were a nonstandard dt in the IST model of nonstandard analysis (Nelson 1977).

The expected momenta P at times t, and $t + dt$ in box 1 are:

$$P_1(t) = n_1 v_1 \tag{5.2}$$

$$P_1(t + dt) = n_{11}(v_1 + dv_1) + dn_{01}v_{01} - dn_{10}v_{10} - dn_{12}v_{12} + dn_{21}v_{21} \tag{5.3}$$

Here $n_{11}$ refers to the number of particles that start in slice one and end in slice one. The small changes $dn_{ij}$ refer to the number of particles moving from slice i to slice j, and the velocities $v_{ij}$ refer to the mean velocities of those particles which start in slice i and end in slice j.

Since counts such as $n_1$ are $O(100)$ to $O(10000)$ in our simulations it is not reasonable to immediately ignore their discrete nature and treat them as continuous without further analysis.

The only truly continuously divisible fundamental quantities in the system are time and length. Derived quantities momentum and energy are therefore also continuously divisible, but both also depend on the quantized mass [1].

We consider the changes in momentum on time scales that are short compared to the time it takes a molecule to go a significant fraction of the typical inter-molecular distance (the $\mu dt$ time scale) and on longer time scales that are still short compared to the time it takes the center of mass of the box to travel half the box length at its initial velocity (the dt time scale).

There are two contributions to the change in momentum, the first is the quantized transport of momentum across the box boundary by transport of mass. Namely when a molecule enters or leaves the box its momentum becomes part of or ceases to be a part of the average over the box. These transitions involve jumps of size proportional to $1/n$ where n is the number of molecules in the box, and are a Poisson-like process with the particles being discrete, however when n is reasonably sized the jumps are not large relative to the average, and therefore $1/n/dt = O(1)$ so that we can treat the momentum function as if it were an s-continuous nonstandard function. This "convective derivative" portion of the momentum transport occurs at

[1] The use of the term "quantized" refers to the fact that mass comes in discrete molecules, but all calculations are based on classical physics without any of the wave-function or other aspects of quantum mechanics. The main issue is that due to the discrete masses, statistical averages over a box will be discontinuous when molecules cross box boundaries.

velocities related to the center of mass velocity of each slice so that the dt time scale is the one of interest.

Secondly, there is momentum transport at infinite speed due to the force fields from the LJ potential. We do not consider relativistic effects and retardation of the forces, especially at the tiny distances modeled by the LJ interaction. Although this transport is at infinite speed, the range is still on the order of a few molecular lengths. Force-based momentum fluxes through the boundaries of the box are therefore dominated by the interactions near the surface of the box within a distance of $dx_s \approx 1$ molecular lengths. In-between jump events caused by molecules crossing the boundary, this momentum transport is a continuous function, but due to the fact that there are multiple molecules in the box and each one is moving at a different speed and at a different distance from the boundary we expect detailed fluctuations in this force which occur on the $\mu dt$ time scale. From the perspective of modeling the increments at the dt time scale each increment is itself an integral over the finer time scale. Nonstandard numbers supply us with a model of this type of scale separation. If $t^*$ is one unit of non-dimensional bar time, then $dt = t^*/I_1$ and $\mu dt = dt/I_2$ with $I_1, I_2$ being nonstandard integers, and $I_1/I_2 \cong 0$ is a model of three separate time scales each smaller timescale infinitesimal with respect to the next larger one. We think of the $t^*$ time scale as the time it takes the wave to move half the bar length, dt as the time it takes the wave to move a microscopic bar length, and $\mu dt$ as on the order of the time it takes for the smallest oscillation in the force along a boundary due to tiny rearrangements of the molecules. Although in reality neither $I_1$ nor $I_2$ are truly nonstandard, the concept of a nonstandard integer is a good model for a "large but not exactly specified" number which aligns well with the asymptotic ideas we use to build this model.

## Momentum Transport by Mass Transport

Although the analysis of the momentum transport by particles crossing the slice boundaries is interesting we find that for our purposes it can be ignored in these simulations. If we let the slice move with the center of mass, in a Lagrangian frame of reference, then the standard equation connecting the rate of change of the Eulerian momentum average P to the net forces is:

$$\frac{\partial P}{\partial t} + v\frac{\partial P}{\partial x} = F_{net}$$

Since for typical experiments, $v = O(0.1)$ and $n > 100$ whereas $dx > 5$, the contribution of the convective portion $v\frac{\partial P}{\partial x} < 0.1/500 < .0002$ whereas we can estimate the order of magnitude of the typical force as the change in momentum from the peak of the wave to zero as the wave passes our slice, $F_{net} = O(\Delta P/\Delta t) = nv/(3dx/v_w) = (100)(0.1)/(15/7.4) = .5$. Convective transport of momentum is therefore a small fraction of the total transport and will be considered as part of the noise for simplicity.

## Momentum Transport by Forces

Consider a time increment in which no molecules cross any boundaries, so that all the momentum transport is via forces. In a time dt the net force on the molecules in box 1 can be described as:

$$F_{1net} = \left( \frac{(\rho_1 + \rho_2)}{2} F_{lj}(r_{e12}) + \frac{(\rho_0 + \rho_1)}{2} F_{lj}(r_{e01}) \right) (Adx_s + \varepsilon_n)$$

Here A is the effective cross sectional area of the bar $\rho_n$ is the number density of the bar in box n, $F_{lj}$ is the Lennard-Jones force function, and $r_{e_{ij}}$ is the effective distance between the boxes which gives the per-molecule force needed to account properly for the actual total force. The variable $dx_s$ is a short length of $\mathrm{ord}(1)$ molecular length such that a volume $Adx_s$ contains the vast majority of the molecules in box 1 that are interacting appreciably with molecules in the neighboring box on each side. Our $\varepsilon_v$ is the error in the interaction volume which we take to be small enough that it can be modeled as infinitesimal relative to $Adx_s$.

If we follow all the molecules through their complex motions on the $\mu dt$ time scale as is done in the molecular dynamics simulation, and calculate the effective r values we would see a continuous trajectory of $r_e$. However we wish to make our model at a longer time-scale, one more appropriate for the motion of the center of mass of the molecules in the box. This dt time scale is a large multiple of the $\mu dt$ time scale. For theoretical purposes, the $r_e$ values at the end of our dt time step can be modeled as some drift, which is closely related to the center of mass velocity, and some random component which is related to the detailed wiggles of the continuous path of $r_e$. We take then:

$$dr_{01} = (v_1 - v_0)dt + \sigma(T) \circ dQ_{01} \tag{5.4}$$

$$dr_{12} = (v_2 - v_1)dt + \sigma(T) \circ dQ_{12} \tag{5.5}$$

$$\rho_{01} = (\rho_0 + \rho_1)/2 \tag{5.6}$$

$$\rho_{12} = (\rho_1 + \rho_2)/2 \tag{5.7}$$

$$dP_{1force} = \left( \frac{\rho_{01}(F_{lj}(r_{e01}) + F_{lj}(r_{e01} + dr_{01}))}{2} + \frac{\rho_{12}(F_{lj}(r_{e12}) + F_{lj}(r_{e12} + dr_{12}))}{2} \right) A dx_s dt \tag{5.8}$$

The increment in momentum of molecules in the box due to forces is therefore a Stratonovich stochastic increment, with stochastic portion dQ intended to approximate the micro-integrated effect of the complicated but continuous micro-time-scale wiggling of the individual molecules near the surface of the box. The use of a Stratonovich increment, rather than an Itô increment is due to the fact that the random increment is a model for the details of a rapidly fluctuating continuous function, and the rules of standard calculus should apply to increments derived from such a process.

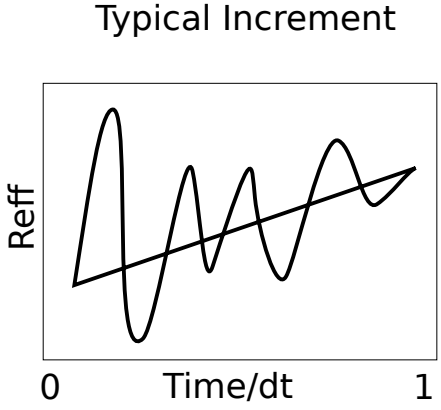


If we wish to eliminate the stochastic portion of this model we can take an expectation with respect to the random increment to find an "effective average force" during the increment. When the stochastic portion is not too large, this will produce a reasonable deterministic approximate model, in

addition we assume that density is relatively uniform across the bar, which is how we proceed.

Next, we argue that not only is the $r_e$ value dependent on center of mass displacement, but also on temperature, and the velocity difference between the centers of mass of adjacent boxes. The physical argument for this model goes as follows:

Suppose that we have two boxes of molecules next to each other and that the first one is instantaneously heated to a higher temperature than the other. The molecules in this box now have more energy and can on a micro-increment of time occupy a larger volume because they can reach higher into the potential energy field produced by atoms in neighboring boxes. Thus molecules near the boundary will immediately begin to expand in space, pushing harder on the neighboring box. The effective distance, which describes the forces between boxes, is therefore a function of temperature. The fact that this occurs on a micro time increment is due to the fact that temperature is a non-local property of the entire box. Similarly, center of mass velocity is a non-local property, an average over all the molecules in the box. The assumption is, therefore, that molecules on the boundary between the boxes couple to several molecules within the volume and these molecules all couple indirectly to the center of mass energy by thermal mixing. This coupling to center of mass energy allows the molecules to occupy higher potential energy states in the boundary region than they otherwise would, which means they can exert larger forces, altering the effective distance between boxes on a time scale much faster than the movement of the center of mass.

If we linearly Taylor expand the $r_e$ values in the variables $T, x, v$ we can assume the following dimensionless relationship (for interaction between box 1 & 2 for example):

$$\frac{\delta r_{e12}}{x_m} = \frac{A_x}{\delta/2}(u_2 - u_1) + \frac{B_v}{v_m}(v_2 - v_1) + \frac{C_T}{T_0}(T_2 - T_1) \tag{5.9}$$

In this expression, $\delta r_{e12}$ is the change in $r_e$ from its equilibrium value, $x_m$ is the molecular unit length, $\delta/2$ is the width of the RVE, and is also the equilibrium separation between successive u measurements, $v_m$ is the molecular scale velocity unit, and $T_0$ is the initial temperature of the system. The quantities $u_2$ and $u_1$ are the displacements of the centers of mass of the molecules that started in slice 1,2. And $A_x, B_v, C_T$ are dimensionless constants. In later analysis we will define the model in terms of the bar time scale $t_w$ which

will fix the numerical value of the coefficient $A_x$ exactly. Our question then becomes what are $B_v$, and $C_T$. Thinking first about the temperature dependence, if we convert all the initial center of mass velocity into thermal energy using numerical values typical for these simulations and ignoring potential energy thermal capacity, thereby over-estimating the dT increment conservatively, we have $3/2nT + dT)/T = (3/2nT + nv_0^2/2)/T \rightarrow dT/T = 2/3(0.1)^2/2/(0.1) \approx 0.033$. We therefore conclude that changes in temperature are not important for the problem at hand as the temperature will be constant to within a few percent throughout the experiment and we expect $C_T = O(1)$ so we drop the T dependence term for this model.

Finally, we take $B_v$ to be of the order $\frac{t_m}{t_0}$ where $t_0$ is the time it takes for a thermal wiggle at the center of mass to have a probability $\frac{1}{e}$ of propagating to the edge of the box by Gaussian diffusion since it is the coupling of thermal wiggles on the edge of the box to center of mass motion that causes the velocity dependence of $r_e$. If we assume the center of mass is near the center of the box, then the time it takes for a 1D Gaussian random walk to have $1/e$ probability of exiting a box of side $\delta/2$ can be calculated easily as.

$$t_e = \frac{Q(\delta/2)^2 m_m}{T t_m}$$

$m_m$ is the molecular mass which is taken as 1 in our simulation, $t_m$ is the molecular mean free path time which we take to be of the order of the molecular time unit. The constant $Q = \frac{1}{8}[\mathrm{erf}^{-1}(1 - 1/e)]^2 \approx 0.308$ is due to the $1/e$ probability chosen for exiting the box.

However, notice that due to the non-zero range of the LJ forces when the box is small enough, thermal motion throughout the box immediately affects the surface. We therefore propose the following modification which has constant behavior asymptotically for small boxes and similar asymptotic behavior for large boxes as the previous result:

$$t_0 = \frac{Q(1 + (\delta/2/x_0)^2) x_0^2 m_m}{2 t_m T}$$

Where $x_0$ is of the order of the box size at which the Lennard-Jones forces permeate the entire box.

Substituting the expression for the change in $r_e$ (equation 5.9) into the model for dP (equation 5.8) and dividing by dt we have:

$$\frac{dP}{dt} = (\rho A dx_s) K x_m \left( A_x \frac{(u_2 - 2u_1 + u_0)}{\delta/2} + \frac{B_v}{v_m} \frac{2t_m^2 T}{m_m Q (1 + (\frac{\delta}{2x_0})^2) x_0^2} (v_2 - 2v_1 + v_0) \right) \quad (5.10)$$

Here $K \approx 57.15$ is the stiffness for the quadratic Taylor expansion of the Lennard-Jones potential about the equilibrium location at its minimum, in the dimensionless LJ "units." We let $dx_s = x_0$ in our statistical model. If in defining the model above, we express time in units of $t_w$ and distance in units of $\delta/2$ then necessarily the square of the wave velocity $\rho A x_0 K A_x = 100$. We specified this form in our statistical model, and proceeded to fit the behavior of the model to the observed wave decay time-series, including inferring both $B_v$ and the precise value of $t_w$ for each bar.

## 5.5 Equivalent Continuum Model

To make the transition from a discrete model for a small fixed set of observations in a tiny bar (where the RVE was an appreciable fraction of the length on the order of 1/20) to a continuum model for an unknown number of measurements over a very long distance in a very thin bar, we can reinterpret the algebraic quantities in equation 5.10 by allowing $\delta \cong 0$ when measured at the bulk scale. We begin by rewriting the dimensionless model in equation 5.10 using new dimensionless variables in terms of fractions of the bulk scale distance, time, and mass. Also we factor the mass of the RVE slice out of the momentum variable $P = dm'v$.

$$dm' \frac{dv}{dt} = (\rho A m_m dx_s) K x_m \left( A_x \frac{(u_2 - 2u_1 + u_0)}{\delta/2} + B_v \frac{2t_m^2 T}{m_m Q (1 + (\frac{\delta}{2x_0})^2) x_0^2} \frac{(v_2 - 2v_1 + v_0)}{v_m} \right) \quad (5.11)$$

We begin by noticing that $dm' = \rho A m_m \delta/2$ the dimensionless mass of the slice, and dividing both sides by this quantity to get a model that is invariant to the mass scale:

$$\frac{dv}{dt} = dx_s K x_m \left( A_x \frac{(u_2 - 2u_1 + u_0)}{(\delta/2)^2} + B_v \frac{2t_m^2 T}{m_m Q(1 + (\frac{\delta}{2x_0})^2)x_0^2} \frac{(v_2 - 2v_1 + v_0)}{v_m(\delta/2)^2} \delta/2 \right) \quad (5.12)$$

Next we convert the entire equation to dimensional form on the bulk scale, by multiplying all lengths, and times by dimensional quantities $dL = \varepsilon_L L$ and $dt = \varepsilon_t t^*$. The coefficient K is multiplied by $1/dt^2$ as it expresses a force per unit mass per unit displacement as a fraction of the molecular units. On the bulk scale $x_m = 1dL$

$$\frac{dL}{dt^2}\frac{dv}{dt} = dL dx_s dL \frac{K}{dt^2} \left( A_x \frac{(u_2 - 2u_1 + u_0)}{(\delta/2)^2} \frac{dL}{dL^2} + B_v \frac{t_m}{t_0(T,\delta)} \frac{(v_2 - 2v_1 + v_0)}{v_m(\delta/2)^2} \frac{1}{dL^2} \delta/2dL \right) \quad (5.13)$$

Now we interpret $dLdx = dL\delta/2$ as an infinitesimal displacement at the bulk scale, and rewrite the ratios of the differences using the definition of the derivative in IST $dy/dx \cong (y_1 - y_0)/dx$. We also cancel the factor $dL/dt^2$.

$$\frac{dv}{dt} = dx_s dL K \left( A_x \frac{\partial^2 u}{\partial x^2} \frac{1}{dL} + B_v \frac{t_m}{t_0(T,\delta)} \frac{\partial^2 v}{\partial x^2} \frac{\delta}{2dL} \right) \quad (5.14)$$

canceling the dL we arrive at the continuum model:

$$\frac{dv}{dt} = dx_s K \left( A_x \frac{\partial^2 u}{\partial x^2} + \frac{B_v \delta}{2} \frac{t_m}{t_0(T,\delta)} \frac{\partial^2 v}{\partial x^2} \right) \quad (5.15)$$

Finally, assuming the length scale is fixed at L, the bar scale length, we can rescale again the time scale, replacing the dimensionless t with $\varepsilon_{t2} t'$ and the dimensionless v by $v'/\varepsilon_{t2}$, and multiplying both sides by $\varepsilon_{t2}^2$ with $\varepsilon_{t2}$ chosen so that $dx_s K A_x \varepsilon_{t2}^2 = 1$. The model in simplified bar length and time scales is:

$$\frac{dv}{dt'} = \frac{\partial^2 u}{\partial x^2} + \frac{B_v \varepsilon_t dx_s K \delta}{2} \frac{t_m}{t_0(T,\delta)} \frac{\partial^2 v'}{\partial x^2} \quad (5.16)$$

Now we examine the coefficient $B_v \varepsilon_{t2} dx_s K \delta/2$, and ask whether this is infinitesimal, appreciable, or unlimited? Clearly K and $dx_s$ are limited as

$K \approx 57.15$ and $dx_s = \mathrm{ord}(1)$ was the multiplier for the molecular length that gave the surface region thickness of the RVE. Statistically $B_v$ was $O(1)$ (see chapter 6) and $\delta/2 > 1$ is an appreciable finite RVE thickness as a fraction of the molecular width. The question remains only how large is $\varepsilon_{t2} = 1/(dx_s K A_x)$ but since we expect $A_x = \mathrm{ord}(1)$ it appears that this whole coefficient should be considered near-standard. Incorporating the constants into a single constant that depends on the observational scale $\delta$, $B'_v(\delta)$ we have the final model:

$$\frac{\partial v}{\partial t} = \frac{\partial^2 u}{\partial x^2} + B'_v(\delta)\frac{t_m}{t_0(T,\delta)}\frac{\partial^2 v}{\partial x^2} \tag{5.17}$$

It should be noted that this model depends on $\delta$ which is a measure of the ratio of the scale of observations to the scale of the inter-molecular spacing. When $\delta$ is large the asymptotic behavior of the coefficient in front of $\frac{\partial^2 v}{\partial x^2}$ is proportional to $1/\delta$, so that at large observational sizes the momentum diffusion effect becomes negligible. For seismic waves traveling in the crust of the earth, thermally driven momentum diffusion is completely ignorable. However for waves traveling through a small crystal and arriving at a tiny micro-electro-mechanical (MEMS) accelerometer the effect could be important. This knowledge may help inform sensor based crack formation and crack propagation models in structural monitoring or similar applications.

This continuum equation came about by reinterpreting an intermediate scale molecular model, which we developed in the context of a very well defined MD simulation, where the observational scale was known exactly. This continuum equation can be used when we have a thin molecular bar which is much longer than its thickness, and where we have a measurement apparatus which measures displacements or velocities over a length of the bar which is small relative to the full bar length. In such a context, as described in chapter 3 it is reasonable to treat the measurement region as an infinitesimal region relative to the total length, and to apply the IST techniques when building our model. This allows us to transition from discrete difference equations for a small set of measurements to a differential equation, but only so long as the intermediate asymptotics that are assumed by that transition hold to sufficient approximation. The IST based approach makes this type of reasoning straightforward, replacing confusing limiting ideas about a non-physical continuum idealization, into a combination of algebraic mathematics and asymptotic approximate reasoning about real physical quantities.

## 5.6 Conclusion

Our goal was to generate a mathematical model that explains the dissipation of wave energy in a system that is decoupled from the environment, where internal entropy generation is the only mechanism of dissipation. By using the mathematical tool of Nonstandard Analysis as an aid to our formulation, we were able to account for and describe the separation of scales that occurs in a system where molecules undergo detailed undulations that are much faster than the changes in the regionally averaged quantities derived from those molecules. To couple the detailed dynamics to the averaged dynamics we made reference to energetic arguments that provided a scaling law valid asymptotically for large regions. By modification of this asymptotic law to have constant behavior for smaller regions we arrived at an equation which, when fit to data, provides a quite accurate description of the rate of dissipation of waves across observational scales from between about 1000 and 100000 molecules, and a wide range of temperatures in the solid range for Lennard Jonesium. In the next chapter, I will discuss the fit of this model to the actual data from MD simulations, and the Bayesian statistical techniques used to compare the model to the data.

# Chapter 6

# Comparing Dissipating Wave Model to Detailed Timeseries

*To understand God's thoughts we must study statistics, for these are the measure of his purpose.*

—Florence Nightingale (attr.)

In chapter 5 I developed a model for bulk-scale kinetic energy dissipation in a vibrating molecular bar. The model has three principal degrees of freedom that should be considered in order to fit the data. The most important and fundamental degree of freedom is $B_v$ the multiplier for the momentum dissipation process. The assumptions of the model imply that this should be a number in the vicinity of 1 thanks to the dimensional analysis that went into the model construction. The other degrees of freedom for fit-to-data are the precise time-scale $t_w$ which depends on the precise size of the bar and the wave speed, and the thermal kinetic noise level KT which is a small multiple of $20T/2$ since we are measuring 20 degrees of freedom each of which contributes $T/2$ to the kinetic energy on average. In addition to these per-bar degrees of freedom, the overall model has a length scale $x_0$ which specifies the asymptotic bahavior of the model for small bars whose observational slices are $O(x_0)$ wide or smaller.

Using Markov Chain Monte Carlo methods, we fit a Bayesian statistical model for the error between the predictions from the ODE model above and the actual statistics of the molecular dynamics time-series, giving values for the $B_v$, $t_w$, KT, and $x_0$ parameters. This model was fit to 40 randomly chosen time-series from the total list of available experiments. The model had $x_0$ as

a global parameter, and $B_v$, $t_w$, KT, and $E_0$ as bar specific parameters. The parameter KT is the minimum thermally derived energy that would be present even if the wave were absent and was specified as a multiple of $20T/2$. The parameter $E_0$ is a fitting parameter that multiplies the initial wave energy to account for noise in the initial conditions of the molecular dynamics simulation that result in small differences between the actual and nominal values. A prior was assigned for each of these parameters which was common to the values across all bars. The $B_v$ values were given a common log-normal prior, and the standard deviation of the underlying normal was a hyperparameter and given its own exponential prior with mean value $\log(1.5)$.

In figure 6 (top) we see that the mean $B_v$ values for the 40 simulations form an ensemble whose distribution is significantly narrower than the prior used, such that $B_v \in [0.5, 2]$ for the majority of cases. Variability in $B_v$ may in part be accounted for by the details of the size and arrangement of polycrystalline domains in the bar. In the lower graph we see the distribution of posterior samples of $B_v$ for four example bars, by color, indicating that not only are the mean values for each bar concentrated in the range $[0.5, 2]$ but the individual bars also have individual samples that are concentrated in a subset of this range.

Using the posterior means of the parameters, we graph the wave decay time-series and the velocity time-series for the third bar slice in four randomly chosen bars. Clearly the behavior is qualitatively and quantitatively correct. Although the model is fit to the total wave decay energy time-series only, the equations also correctly predict the details of the forces on slice 3, resulting in the proper velocity time-series shown on the right. The correctness of the velocity time-series gives us confidence that the momentum diffusion process we model is substantially correct.

As can be seen in figure 6.2 in our four randomly chosen example bars, when the posterior mean values are used for $B_v$ and $t_w$ not only is the predicted time-series of kinetic energy closely matched to the observed data, but the time-series for the predicted velocity in the third spatial measurement is closely matched to the observed value.

Finally, we examine trends in the mean $B_v$ values with either T or $\delta$ and find that no strong trends exist.

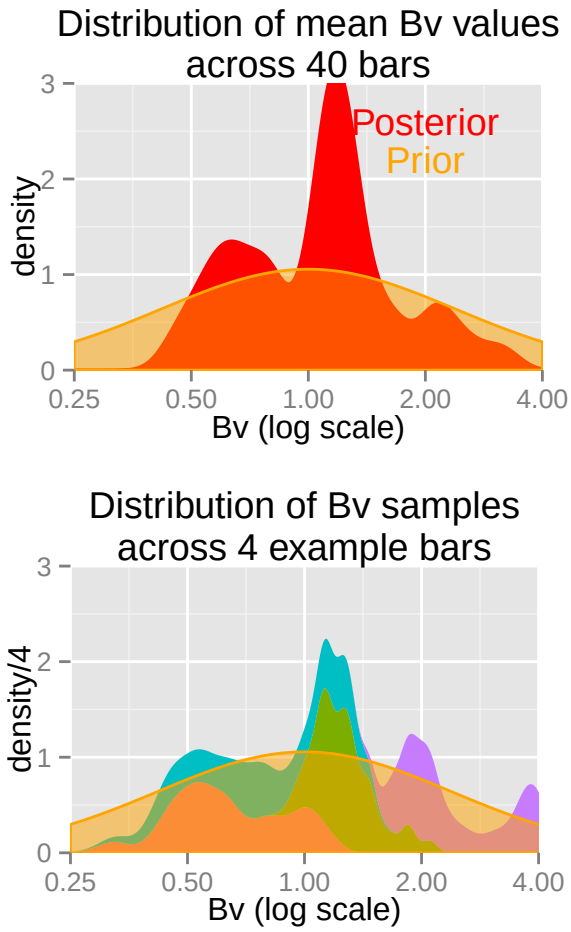


Figure 6.1: Distribution of the posterior mean of the $B_v$ values for each of 40 example bars, compared to the prior distribution (top). And distribution of the $B_v$ samples for the same 4 example bars as shown below (individual colors, bottom). Each bar has its own $B_v$ but they are concentrated in the region [0.5,2]. The $B_v$ value distribution in any given bar is probably influenced by the random polycrystalline structure induced by the initialization conditions. The prior is evaluated at the posterior mean of the hyperparameters that define it.

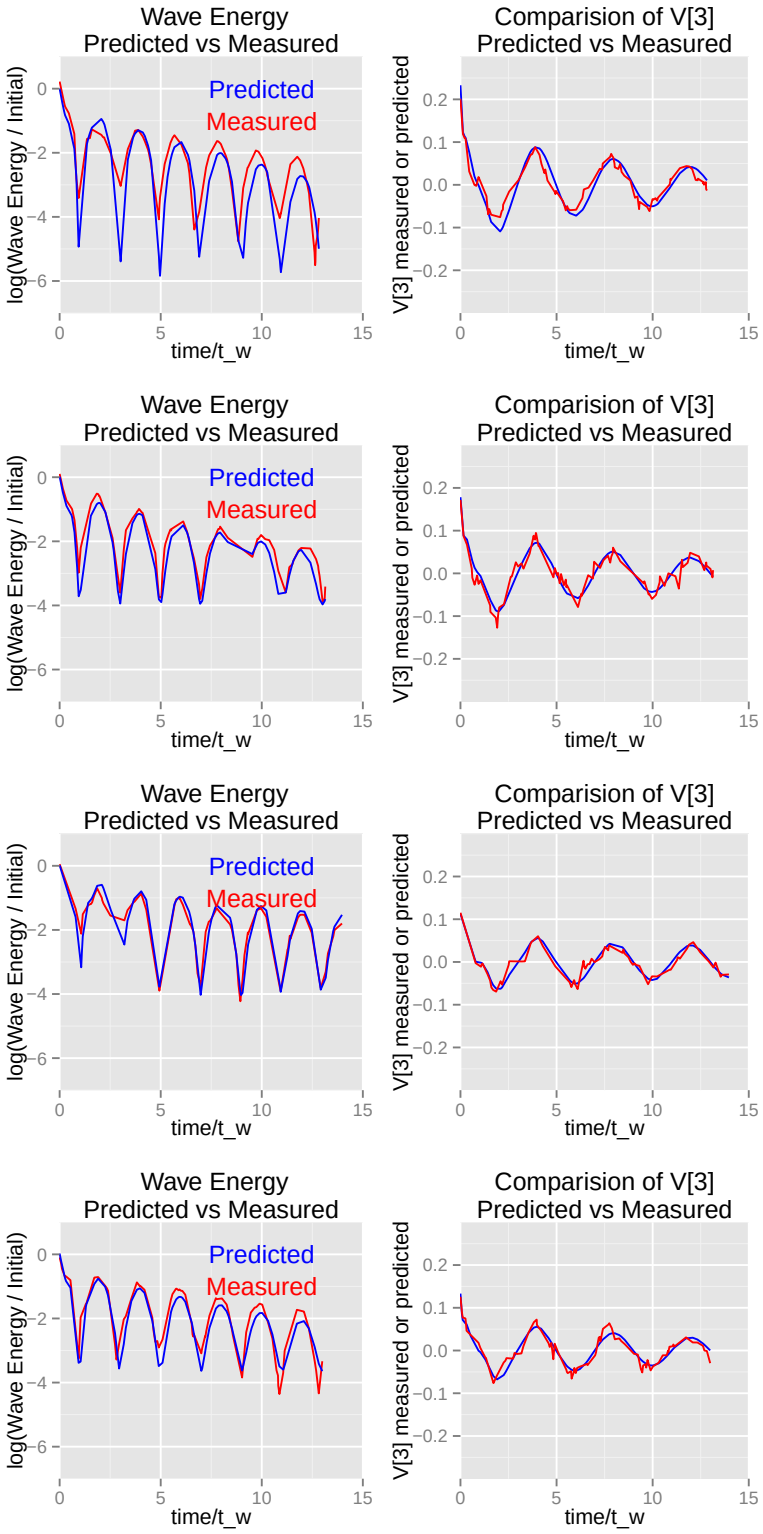




Figure 6.2: Molecular Dynamics vs the 20 D model in 4 randomly chosen examples.

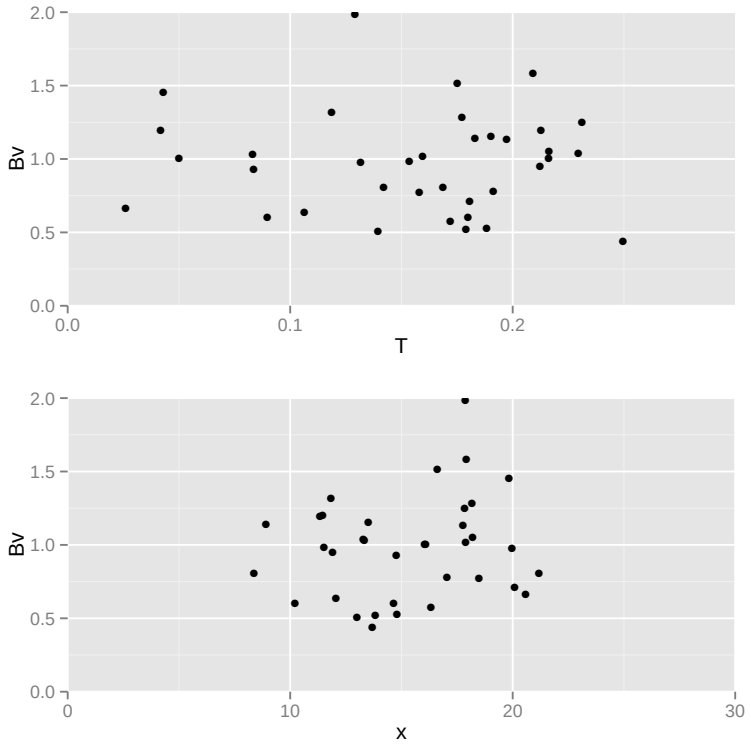


Figure 6.3: Examination of residual trends in $B_v$ reveal no systematic biases with varying T or $\delta$ across the 40 bars used, indicating that the average effects of temperature and size are well accounted for in the model.

## 6.1 Issues With Fitting Bayesian Models to Dynamics

### The Chosen Technique

In order to determine the $B_v$ values in the model for wave dissipation, it was necessary to run the ODE predictions and try to discover which $B_v$ values were consistent with actual behavior, and then whether those values were consistent with the assumptions of the dimensional analysis and modeling that led to the model.

In attempting to fit the Bayesian statistical model certain interesting aspects of the problem became clear and were considered illuminating for the nature of fitting dynamic models in general. The Bayesian model was fit using Markov Chain Monte Carlo (MCMC) and had the following structure. The ODE was run to produce position and velocity estimates at all of the observed time points for all 40 example bars. The predicted wave energy was calculated as the sum $W_p = \sum_{i=1}^{20} v_i(t)^2/2$ and this energy divided by its initial value to get an energy on the scale of the initial conditions. The mass values for each degree of freedom were assumed to be the same, and are normalized away by this rescaling.

The wave energy data from MD simulations was similarly rescaled as a fraction of the nominal initial energy $W_d = (W_i/(6/20Nv_{init}^2/2))_i$ for all of the bars indexed by i.

A prior for bar timescale $t_i$ was specified for each bar using a nominal value for $t_w = 5(N/10)^{(1/3)}/v_w$ as the center of the prior distribution with coefficient of variation of 0.133, $v_w$ was taken to be the nominal value $\sqrt{\frac{K}{\rho}} \approx 7.38$.

The likelihood for a given set of $t_i$ and $B_{v_i}$ was specified as independent Gaussian processes on transformed errors in the log ratio of the wave energies.

$$p(q_N(p_t(\log((W_p + KT)/(E_i W_d))/S, n))|B_v, t_i, S, ...) = N(0, C) \tag{6.1}$$

where $p_t$ is the CDF for the standard student t distribution (with n degrees of freedom, which was given a hyper-prior), $q_N$ is the quantile function of the standard normal (inverse of the CDF), S is an error scale which includes effects both for modeling error, and thermal noise, $E_i$ is an initial energy multiplier accounting for differences in the initial wave energy from its

nominal value, and KT is a thermal base energy level added to the noise-free predictor.

This might be called a "Gaussian Copula t-Process" since the marginal distribution at any time point of the log ratio is t distributed, but the dependency in the model comes from a Gaussian process through the probability integral transform. The student t transformation was used in order to account for the fact that as the kinetic energy reaches a minimum at each cycle (when the waves overlap in the center of the bar) the log ratio becomes $\log(W_p + KT) - \log(E_i W_d)$ and $W_d$ is a small positive noisy value, and therefore outliers are to be expected and should not excessively affect the fit.

The covariance matrix C was built using the following covariance function:

$$\mathrm{cov}(t_1, t_2) = 0.1 \exp(-((t_1 - t_2)/0.2)^2) + 0.9\delta(t_1, t_2) \sin^2(\pi t_1/2) \tag{6.2}$$

This covariance function reflects our knowledge that a well-fitting model will predict the peaks of the wave energy very well at time points $0, 2, 4...$ when the $\sin$ term is at a minimum so that the marginal standard deviation is also at a minimum at those time points, and will have larger variation away from these time points, with maximum variation near the energy minima. Furthermore it predicts correlations between errors that are nearby in time on the order of 0.2 times the cycle length. The overall scale of the variation is already accounted for by S in equation 6.1.

Fitting the MCMC model required tuning this covariance function, and the jumping scales for the metropolis diffusion. The "mcmc" package (Geyer and Johnson 2013) was used in the statistical software R to implement the Markov Chain because it allowed for defining the log posterior density via running the ODE solver to calculate the errors. Because of the evaluation of 40 ODE based time-series twice for each jump (forward and backwards to ensure detailed balance) the computation proceeded slowly on the desktop computer on which it was run, ultimately taking about a week for the final run to generate on the order of 10,000 samples.

In carrying out this statistical investigation, several things became clear through experience. The first was that in many problems, especially problems in dynamics, there is no a-priori correct likelihood. In these cases, the procedure for fitting a statistical model have a different meaning than they do in a more well defined context such as a randomized controlled clinical

trial of one condition vs another. We choose a model to fit some purpose, rather than because of some particular prior belief about the form of the model. Furthermore, when the model is an indirect or approximate model of some more detailed phenomenon, as with the dissipative wave model of the more detailed MD simulation, there do not exist "true" values of the parameters, especially $B_v$ which is the main non-nuisance parameter. As pointed out in Kilminster and Machete (2005) under this condition, it makes sense to adjust the statistical process to achieve some goal. Although they specify some particular goals relevant to their problem, in general we will have some types of fits considered acceptable for our purposes, and other types of fits considered unacceptable.

The criteria for choosing the particular covariance function here were that the statistical model should not allow or prefer for the timescales to become significantly mismatched between the data and the predictive model, and that the peak wave energy values should be fit well for all of the available observation time, so that the decay rate of the wave energy was well predicted. The fact that constraining only the wave energy decay led also to substantially correct time-series for the individual velocities at each point on the bar lends credence to the form of the model and the existence of the physical process that was considered.

## Relationship to Approximate Bayesian Computation (ABC)

It should be mentioned that there is a sense in which this procedure fits within the Approximate Bayesian Computation (ABC) framework (for a review see eg. Marin et al. (2012)). Each bar has 20 velocity measurements at each of about 80 time points both in the data and in the ODE model. There are also displacement measurement in the ODE model, but these are not observed in the MD model with fixed Eulerian measurement boxes. We have no way to write down the likelihood of particular data given $B_v$ and other nuisance parameters since there is no a-priori random data generating process to prefer, but we can simulate pseudo-data from the approximate model so that we get the full 20 dimensional velocity vs. time trajectories under an assumed value of $B_v$ and suitable initial conditions. As is common in ABC, rather than fitting our simulation to the entire data set of observation, including the entire 20 D velocity time-series, we choose a summary statistic equal to the time-series of total wave kinetic energy. Instead of a single $\varepsilon$ value giving a tolerance for deviation between a small dimensional sum-

mary statistic of actual data (from MD) and predicted pseudo-data (from the ODE model) we specify a kind of kernel in this 80 dimensional wave energy time-series using a particular transformation of a Gaussian process with a particular covariance structure. In doing so, we construct a kind of kernel-density-likelihood in which we have implicitly described the character of the modeling errors that our ODE model is allowed to introduce. The result leads to excellent inference on $B_v$ and good agreement with the wave energy decay time-series as well as the time-series in the 20 additional velocity dimensions for each bar.

## Efficiency of MCMC Calculation with Expensive Simulations

Another issue which became obvious in running the MCMC simulation was that the log posterior density (LPD) was calculated (up to a normalizing constant offset) at a large number of points, but these values were thrown away immediately after each jump. Each evaluation involved calculating the full time series of 40 different ODE models and then comparing them to the data. The results are continuously dependent on every parameter, so that two evaluations which are close in parameter space must be close in LPD. By storing the LPD value with each evaluation, we can quickly approximate the LPD when a proposal brings us close to a region we have previously seen (although this was not done in our fit). Various proposals for methods related to this insight have been made in the literature. For example in Taddy, Lee, and Sansó (2009) the authors suggest a method whereby the support of the parameter space is discretized onto a set of values where the simulation results are known, and then the posterior distribution over those discrete locations is determined using resampling. In Higdon et al. (2004) the authors propose fitting a surrogate statistical model, so that pseudo-data which would normally come from expensive simulations instead comes from some form of interpolation of a set of fixed simulation runs. In essence their interpolation technique involves the use of a Gaussian process prior on the unobserved simulation output conditional on the observed simulation output, this can be viewed as a form of interpolation. A useful discussion of Gaussian process models, and their equivalence to various forms of parametric spline or radial basis function smoothing techniques is available in MacKay (2003). In certain circumstances it can be useful to model unknown functions as nonlinear transformations of Gaussian processes, so called "warped Gaussian processes" (Snelson, Rasmussen, and Ghahramani 2004). This can

help to account for non-Gaussian error distributions, and is a generalization of the technique used to account for outliers when building the error model in the dissipative bar experiment.

# Chapter 7

# Future Directions for Continuum Modeling of Sand Grains During Liquefaction

*We have no right to assume that any physical laws exist, or if they have existed up until now, that they will continue to exist in a similar manner in the future.*

—Max Planck *The Universe in the Light of Modern Physics (1931)*

The model developed in chapter 5 was intended to be a testbed for modeling ideas developed in chapter 3 and for fitting of Bayesian statistical models to dynamics. The original motivation for developing the modeling techniques however, was to explore how sand grains could be modeled in a continuum framework in a consistent way so as to couple a grain motion continuum model to the pore-pressure equations of chapter 4. Clearly, grains of sand are discrete, yet we have very limited information about their individual size, shape, and arrangement so that models involving individual discrete particles are artificially simplified to spheres, incapable of dealing with realistic shapes, or prohibitively computationally expensive. Also, we have usually at best coarse measurements of displacements corresponding to spatial averages over many many grains so that the details of grain motion are generally non-falsifiable anyway. In this setting, when interpreting a continuum model as spatially averaged over spatial scales much smaller than the full scale, a continuum model seems ideal so long as we can develop one which

gives accurate predictions while maintaining a causal connection to the sub-scale processes that produce the averages.

In this chapter, we consider some mechanical issues that should be taken into account when trying to build such a continuum model for grain motion.

## 7.1 The Setting

Imagine a slice of soil similar to the one used to develop the water flow model in chapter 4. The cross sectional area is much larger than the cross section of a single grain, and the thickness is much smaller than the overall thickness of the soil deposit, but the thickness is modeled as some standard or non-standard multiple of the typical sand grain diameter D, we will investigate both options. The soil slice is in dynamic equilibrium so that the net force on the slice is zero. The mass of the slice is $M = A\rho_g(1-\varphi)dz + A\rho_w s\varphi dz + \varepsilon_m$ where s is the degree of saturation with water (air is neglected) and $\varepsilon_m$ accounts for the errors induced by small fluctuations, for example when grains cross the slice boundary. Because of the large cross sectional extent there will be a large absolute number of grains over which we average so that the central limit theorem implies an approximately normally distributed error in the average $\varepsilon_m \sim N(0,\sigma)$ with $\sigma$ small relative to the overall M value. If the slice averages over a nonstandard number of grains then we expect $\sigma/M$ is infinitesimal, whereas for a standard multiple the scale of the statistical noise will be appreciable.

We divide the slice into a possibly nonstandard number of sub-slices. There are a certain number of sub-slices near the bottom and the top which define a volume "at the surface" of the slice. The inclination at this point is to treat the "surface volume" as infinitesimal relative to the total slice volume, but this assumption may turn out to be untenable. The reason for defining a "near-surface volume" rather than simply a "surface area" is that all physical objects occupy some volume. The contacts between slices are not all planar along a surface area, and it is the contact forces which will drive the mechanical behavior. See figure 7.1 for a graphical representation.

The net momentum of the grains in the slice of interest is affected by forces transmitted from grains in the near-surface volume of neighboring slices to grains in the near-surface volume of the slice of interest via contact forces. These surface forces are then transmitted into the volume where they cause the acceleration of the whole slice. If instead we model the slices as

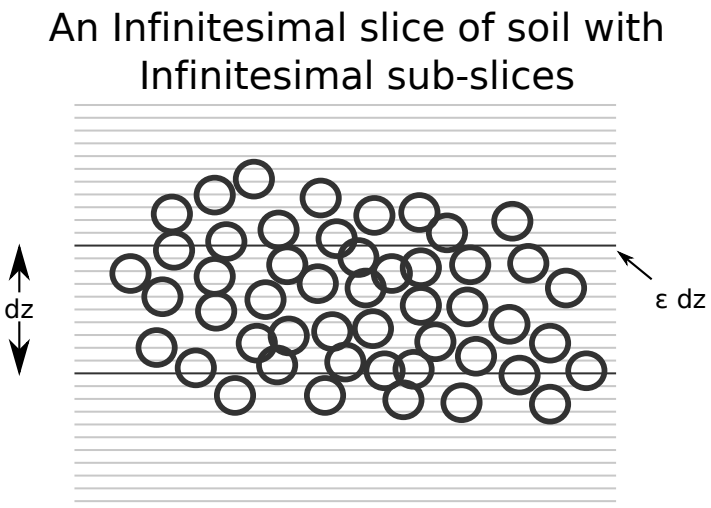


Figure 7.1: An illustration of the basic concept of an infinitesimal slice of soil of thickness dz broken into infinitesimal sub-slices of thickness εdz. The "near surface volume" would be perhaps one or two sub-slices thick. (actual scales relative to grain size chosen for convenience of illustration not quantitative accuracy)

approximately the thickness of a few grains, so that all of the volume of the slice is "near-surface" we may have a more difficult time with the model since some interactions extend over 5 to 10 grain lengths in realistic granular materials possibly cutting through entire slices (Majmudar and Behringer 2005).

Next we consider a time dt which is infinitesimal with respect to the scale of the overall event of interest. Typical earthquakes last tens to up to hundreds of seconds so perhaps 1 unit of non-dimensional time representing 30s is the order of magnitude of a reasonable time scale. Deposits of interest for soil liquefaction are on the order of 10 m deep, and important deposits can be as thin as 1 cm or less. Treating $\mathrm{dx} = 0.01\,\mathrm{m}$ as infinitesimal relative to 10m deposit depth, suggests that the infinitesimal time should be on the order of $\mathrm{dx}/\mathrm{v}$ where v is the bulk scale wave speed in sand. Typical wave speeds in solid minerals of the same type as sand grains are on the order of $3000\,\mathrm{m/s}$, but the empirical bulk wave speed through loose sand is much lower than

$3000\,\mathrm{m/s}$, and is maybe typified by on the order of $300\,\mathrm{m/s}$ instead. The "infinitesimal time" is therefore on the order of $.01/300 = 3.3 \times 10^{-5}\,\mathrm{s}$, or 33 microseconds.

However, in 33 microseconds, within the body of a single sand grain, deformations should travel at the bulk wave speed in the mineral. The implied distance is $3000 \times 3.3 \times 10^{-5} \approx .1\,\mathrm{m}$ or about 100 times the diameter of a 1mm sand grain. The implication is that waves entering a single sand grain must be reflected, scattered, and transmitted in such a way that the overall bulk wave is in essence the interference pattern caused by all of this reflection and scattering.

It's known that in sand grains, force chains form where several sand grains in a row are coupled together tightly by strong contact forces, and other grains are nearly un-loaded (Majmudar and Behringer 2005). The flux of momentum through the boundary of the soil slice consists of a set of impulses produced by the contact forces in our infinitesimal surface volume. Along some of these strongly coupled chains, the impulse should travel quickly, closer to the mineral wave speed than to the bulk speed. And, along other less tightly coupled chains the impulses will travel more slowly. Similarly for the net angular momentum transport caused by the torques due to the off-center nature of the contact forces. If a force chain is tightly supported, it may transmit torque, whereas a torque on a less tightly coupled chain may cause chain collapse.

We consider a coordinate system where z points upwards towards the surface, x is to the right, and y goes away from the viewer. We assume a vertically traveling plane wave whose direction of vibration is transverse to y in the x direction.

$$M dv_x = \sum_{i=1}^{N_b} F_{xi} dt - \sum_{i=1}^{N_t} F_{xi} dt \tag{7.1}$$

$$M dv_z = \sum_{i=1}^{N_b} F_{zi} dt - \sum_{i=1}^{N_t} F_{zi} dt - M g dt \tag{7.2}$$

Where in the above equations, $N_b$ is the number of contact forces at the bottom surface volume of the slice and $N_t$ is the number of forces at the top surface volume.

We assume that the net torque on the slice is zero, since the soil does not rotate as a whole, however individual torques are definitely non-zero and

can cause individual grains to rotate which in turn causes the rotation of other grains, and ultimately the rearrangement of the particles into denser or looser packing.

## 7.2 A sliding thought experiment

Imagine then, two slices of soil stacked on top of each other, with the bottom slice of soil accelerating at an imposed horizontal acceleration $a_l(t) = t$ linear in the time. Let a be non-dimensional in fractions of the steady state acceleration of the upper slice, and t non-dimensional in fractions of $t^\dagger$ the time it takes for the bottom slice to reach the same acceleration as the upper slice's eventual steady state. In order for this parameterization to work there must be a steady state acceleration for the upper slice. Why would this be so?

Instead of two slices of soil, imagine a conveyor belt, and a block of wood with sand paper wrapped around it. The conveyer belt begins to accelerate, and initially it takes the block of wood with it. Eventually, as the conveyer belt is accelerated faster and faster, the force necessary to keep the block of wood accelerating with the conveyor belt exceeds what we think of as the force due to the static coefficient of friction, and the force on the block becomes nearly constant so that the block accelerates at a constant asymptotic acceleration. We assume a similar thing will happen with our two blocks of soil although the details of the grain motion near the boundary between the two slices will be very much more complicated without a glue matrix to hold them in place.

What is the acceleration of the upper slice? Consider the first $\varepsilon \ll 1$ units of time. Due to the very stiff nature of individual grains we will ignore the shear deformation of the grains themselves. When $t = O(\varepsilon)$ the contact forces between the lower slice and the upper slice are able to transfer sufficient momentum that the upper slice accelerates like $a_u(t) = t$ together with the lower slice. Eventually as t gets bigger so that $\varepsilon \ll t < 1$ the grains at the interface between the two slices begin to slip, turn, and rearrange as the contact forces exceed the available contact strength. This occurs not all at once but rather each of the many contacts breaks at some random time so that the acceleration of the upper slice is still relatively smooth on the $O(1)$ scale. Viewed under the microscope of very short time scales and very small acceleration deviations, the acceleration curve is actually rough, so that we

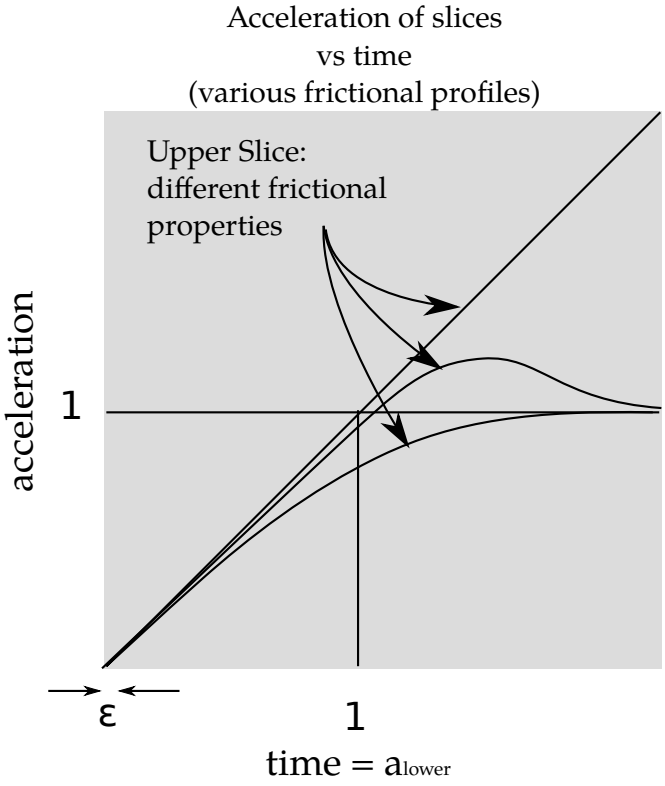


Figure 7.2: Acceleration of sliding blocks of soil in unidirectional loading: The lower slice is constrained to accelerate linearly in time, the upper slice reaches an asymptotic sliding regime at acceleration 1. Intermediately, the upper slice may approach the asymptote from above or below, depending on the configuration. For small times $O(\varepsilon)$ where acceleration is small, the blocks are locked. During liquefaction, the upper slice must be loaded beyond the locked regime to at least initiate sliding and rearragement so that $\varphi$ can change.

can model it as an s-continuous function.

As time $t = O(1)$ the demand placed on the contacts increases to the point where more and more of them begin to slip and as they slip they transfer forces to other stronger contacts, some of which will fail due to the higher demand. Since the acceleration of the upper slice is less than the acceleration of the lower slice, as time goes on the velocity of the upper slice lags the bottom slice more and more.

Eventually, when $t \gg 1$ the relative velocity $v_l - v_u$ is so large that in a microscopic increment of time $t^\dagger dt$ the bottom slice moves relative to the upper slice by a significant fraction of a grain diameter $(v_l - v_u)t^\dagger dt \sim D$. At this point the momentum transfer is quite dynamic so that grains are bouncing and rolling over each other.

Now consider instead the lower slice accelerated by a sinusoidal wave form $a_l(\hat{t}) = \delta \sin(2\pi f t)$ here acceleration is measured on the same scale, and $\delta < 1$ so that the maximum demand on the inter-slice momentum transfer is less than the asymptotic sliding amount imagined above but potentially much greater than the demand for time $\varepsilon$. Also, we assume that we do not enter the dynamic bouncing grain regime described above. This is the regime we expect to operate in during an earthquake at least initially prior to the formation of liquefied soils where the inter-grain forces are small relative to the total stress, and the displacements can grow very large.

The goal of a continuum model for grain motion relevant to liquefaction research then is to describe the transition from a locked pseudo-static assembly to a semi-mobile assembly and the consequences for that evolution on the pore pressure, strength, and mobility of the soil.

The traditional "backbone curve" model of stress vs strain in soil is based on prescribing rules that approximate the time dependence of the stress-strain behavior of the soil through ultimately statistical means. An example of the comparison of various numerical dynamic models to real data and to each other is given in (Stewart et al. 2008) and these types of rules were applied extensively in comaprison to centrifuge data by Liang (1995).

However, if we wish to have a micromechanical explanation for the behavior of soil, it is insufficient to simply prescribe a set of rules which taken as a whole predict the bulk scale observations, we would like also to have some sort of *causal connection* between the micromechanics and the bulk scale rules.

## 7.3 Basic Mechanical Models Compared

The pore pressure equation derived in chapter 4 shows that in order for pore pressure to build up, the porosity must decrease in time, so that the water is squeezed by the grains. In this section we will consider dimensional analyses of various potential physical processes which could contribute to bulk-scale wave-energy dissipation, and compare them to the scale of dissipation which is reasonable in actual practice, thereby hoping to eliminate simple physical models that predict the wrong scale of energy dissipation, and focus on models that produce reasonable dissipation rate scales which might be further refined in future research.

### The Sliding Glass Plate Model

Consider a sinusoidal wave of $f = 1\text{Hz}$ traveling through a loose sand with average wave speed of $c = 200\ \text{m/s}$. Consider a large amplitude of maximum displacement of $A_{max} = 10\text{cm}$. Then the strain is the gradient of the displacement:

$$\gamma = \frac{d}{dx} A_{max} \sin(2\pi f(x/c - t))$$

So that the peak amplitude of strain is $2\pi f A_{max}/c \approx 0.003$. Two layers of grains considered as homogenous sheets of material would move relative to each other on average on the order of $0.003$ grain diameters. What is the fractional kinetic energy dissipation of such sheets with a representative kinetic friction coefficient?

We calculate the ratio $E_{dissip}/E_K$ for two sheets of glass 5mm thick sliding over each other during one cycle of a 1Hz wave under a compression of $P_{atm} = 1\ \text{bar} = 100\ \text{kPa}$, assuming continuous sliding at a kinetic friction coefficient of $\mu = 0.65$ to arrive at an average energy dissipation per cycle:

$$E_{dissip} = \int_{cycle} \mu A V_{rel} P_{atm} dt$$

For our previous sinusoidal wave and a displacement between plates of 5mm we arrive at a total of $3.8\ \text{J}/\text{m}^2$. The average kinetic energy over a cycle is:

$$E_K = \frac{1}{t_{cycle}} \int_{cycle} \rho A V^2/2 dt$$

For an average of $0.81\,\mathrm{J/m^2}$, and a ratio of $E_{dissip}/E_K \approx 4.6$ meaning that we expect 4.6 times as much energy to be dissipated as is present as kinetic energy in the wave. Clearly a wave can not propagate under such enormous dissipation, and in reality two actual glass plates would instead be locked together under such vibrations, and have a much faster wave-speed.

## Fractionally Fractured Plate Model

Although it is not an entirely accurate description, an alternative description which has appealing aspects of realism is that we may treat the layers of grains as if they were two plates which are sliding essentially locked, except at a random number of locations, where the sliding velocity is high, so that during a cycle two sliding grains displace by approximately a grain diameter.

We divide the plates into a large number of small squares, and imagine each one is either locked, or sliding. The number of sliding grains is binomially distributed with some $p$. The $p$ value is small so that the net average displacement is of the appropriate order even though we assume during a cycle that the displacement of a sliding fragment is $O(D)$ the grain diameter. We require that the net overall displacement be according to the strain as before $\gamma \approx 0.003$ so that the displacement of two slipping plates one diameter apart is 1 diameter, but non-slipping plates displace 0. Therefore, $p = \gamma = 0.003$. The problem here is that although we've replaced a large fraction of the plate slipping at small velocity, by a small fraction of the plate slipping at large velocity, then if $v$ is the overall relative velocity of the two plates, $v/p$ is the relative velocity of two slipping parts, and only $p$ fraction of the plate is slipping, therefore the dissipation rate is $p(v/p)F(v/p)$, where $F(v/p)$ is the frictional force between two sliding fragments. Since the $p$ cancels in the coefficient, for this to be dependent on $p$ we must have *velocity dependent friction*, and furthermore, to achieve a much lower, sustainable rate than before, we must have $F(v/p) \ll F(v)$. At high speeds, friction must decrease substantially, by orders of magnitude. Most frictional surfaces do not have such drastic velocity dependent decrease so that this model is unappealing on physical grounds.

## Rolling Wheel Analogy

Instead of considering two adjacent slices as sliding over each other in the manner of rigid plates, or using a model of fragmented plates to capture the

heterogeneity of interactions, we may consider several grains in a chain that crosses the slice barrier as forming a sort of wheel on which the upper slice rolls over the lower slice. Clearly the friction experienced by a rigid block rolling on tiny bearing balls over the floor is usually much reduced from the friction experienced when we slide the same block without the bearing balls. Perhaps such a model can give us a better order-of-magnitude estimate of dissipation and is therefore relevant for future study and refinement.

Consider a wheel formed by a group of grains whose diameter is nD a small multiple of the grain diameter. Let the order of magnitude of the relative velocity of the two ends of the wheel be $\gamma nDf$. If two wheels are adjacent, then at their region of contact, they are rubbing and the relative velocity is $O(2\gamma nDf)$. We can imagine the contact area as of order $D^2$, related to a single grain size. In a slice of square cross sectional area A the total number of slipping locations is related to $\frac{A}{(nD)^2}$ and therefore the total slipping area is proportional to $D^2\frac{A}{(nD)^2}$. The dissipative power per unit area is therefore of order:

$$\frac{1}{A}\frac{AD^2}{(nD)^2}\mu(2\gamma nDf)\sigma_v \propto \frac{1}{n^2}$$

For wheels in the range of 5 to 10 grains in diameter, if $\mu$ is not strongly velocity dependent, we can get dissipation rates in the range of $1/25$ to $1/100$ of the amount in the sliding plate example, thereby reducing the dissipation rate per cycle from about 4 times the mean kinetic energy to perhaps 5-10% of the mean kinetic energy in a cycle.

Although a rolling-wheel model is perhaps too simple, this analysis does suggest that relatively rigid interactions on lengths of around 5 to 10 grain diameters might cause a reduction in dissipation by reducing the sliding surface area as a fraction of the cross sectional slice area while retaining a similar friction coefficient to that involved in pure sliding. Future directions should concentrate on the role of these meso-scale semi-rigid interactions which have been observed in Rechenmacher et al. (2011). Other models involving these meso-scale structures might include a bending beam analogy for force chains, with frictional dissipation during bending, or a wave-trapping-scattering model in which wave energy injected into tight clusters of grains bounces around and is delayed in propagating, and at each bounce the kinetic energy is spread over larger and larger masses while conserving momentum, thereby dissipating bulk scale energy in a manner similar to the

model in chapter 5.

## 7.4 The Role of Entropy-like Quantities in Modeling Sand

Several authors have introduced an entropy-like quantity in models of granular materials. For example, the very succesful application of information entropy to predict the distribution of contact forces in random granular packings of frictionless spheres by Ngan (2004) which was verified via experimental measurements by Chan and Ngan (2005). Real sands are composed of non-spherical and decidedly frictional particles, and so direct application of these ideas to mechanical models of sand is difficult. However, it is useful to consider the connection of bulk-scale observables to non-unique granular micro-states q specified as a position, orientation, temperature, and velocity of specific grains having specific shapes. At a particular point in time, perturbations to a particular arrangement of grains $q \rightarrow q + dq$ will tend to produce a new arrangement. We may consider certain statistics of these arrangements, such as $\varphi(q)$, the porosity. There is an enormous set of possible states consistent with bulk-scale measurements such as porosity, total volume, and bulk stresses or stiffnesses. Given a state q in the possible set, and a particular wave-perturbation with energy dE, we have a transition $q \rightarrow q + dq$ which will imply $\varphi(q) \rightarrow \varphi(q + dq)$. If we give all q values consistent with the initial bulk-scale statistical observations equal probability, we can use the statistical entropy of the distribution $S = -\langle \log(p(q)) \rangle$ to quantify the size of the set of possible states. If we consider a quantity of mechanical energy dE put into the system as activation energy for rearrangement, then there is a set q′ of new states reachable by some path where the total energy is $E_0 + dE$ throughout the path, and this is partitioned into grain kinetic energy, gravitational and contact potential energy, surface energy (if grains are breaking), and thermal energy. If we imagine equal probability of all reachable paths, this will induce a probability distribution on the transition $\varphi(q) \rightarrow \varphi(q + dq)$. Although it is quite difficult to imagine getting this complicated expression from first principles, we nevertheless expect that certain transitions will be more likely than others: the $\varphi$ value will tend towards the most common $\varphi$ reached by all the possible paths.

A simple analogy is the game of "Jenga" in which standardized wooden

blocks are stacked on top of each other. The initial stacking is alternating layers of three blocks. Allowable transitions are those where one block is taken from anywhere in the middle and placed on top of the stack. If there are N identical blocks, there are N! states in which the height of the stack is N units (corresponding to all the blocks stacked on top of each other, but the blocks are identical so labels can be rearranged, we ignore the horizontal rotations of the blocks). There are also N! initial states, where the blocks are stacked 3 per layer and have height $N/3$. However, as soon as we make our first move, the height will be $N/3 + 1$ and the number of possible states is $N \times N!$ corresponding to the fact that we can choose any of the N blocks to move to the top. As the game progresses the height varies from $N/3$ to N and the number of possible states for a given height varies from a minimum of N! to some maximum value corresponding to the "most probable" height of a uniformly randomly chosen legal Jenga state. Considering height as very similar to porosity in a sand, we therefore expect that there are intermediate porosities which are more probable than either more dense or more loose arrangements.

Considering only bulk-scale observations over a large number of grains, we would expect that certain trajectories of $\varphi$ would tend to occur more often than others. Since overall grain rearrangements are small during the initial stages of liquefaction we may be able to explain the linear relationship between dissipated energy density and pore water pressure development observed by Davis and Berrill (2001) by a simple Taylor series argument.

Suppose that for small perturbations from a most-probable value of $\varphi$ for a given bulk scale stress state under the prevailing conditions of static equilibrium, that we can define a "free energy" $E - TS(\varphi)$ for some "mechanical temperature" T, then for a certain external energy input, we may reach states corresponding to a certain region of the free energy potential. For small perturbations from $\varphi'$ the highest entropy value for $\varphi$ we may have the possibility to represent S as a second order Taylor series about $\varphi'$, $S = S_0 - \frac{S_2}{2}(\varphi - \varphi')^2$. We can then define a generalized "entropic restoring force" which acts on the $\varphi$ coordinate as the negative derivative of this "free energy" with respect to changes in the $\varphi$ coordinate, $F(\varphi) = -S_2(\varphi - \varphi')$. Our vibratory perturbations would then act by a combination of this entropic restoring force, and some random forcing related to the details of the vibration. $d\varphi = -S_2(\varphi - \varphi') + \sigma(dE) \circ dQ$ for some stochastic dQ and a scale $\sigma(dE)$ that depends on the energy input in each increment. Particularly if $\varphi$ is observed on a bulk scale involving many sand grains, the scale of the stochastic

perturbation $\sigma(dE)$ might be negligible so that $\varphi$ might be expected to trend strongly towards its maximum entropy value and then undergo only very small oscillations around that value once it is achieved. This model would be one way to understand the previously well-described tendency for soils to come to equilibrium at a "critical state" with either cyclic or continuous direct shearing of approximately constant amplitude and frequency or rate. Although this model is perhaps too simple, it could in a straightforward way be compared to experimental data with the appropriate apparatus, and modified appropriately. Future work should keep in mind this granular microstate viewpoint and consider whether it can be expanded by considering other state variables besides $\varphi$. Furthermore because during liquefaction the changes in $\varphi$ required to induce pore pressure are actually quite small, the model need only work over a small range of $\varphi$ values relative to the initial value, so that the Taylor series approach becomes a valid means of simplifying the dynamics.

# Chapter 8

# Conclusion

**Desdemona:** *Oh most lame and impotent conclusion!*

—William Shakespeare *Othello*

By applying mathematical modeling techniques suitable for general mechanical problems to specific problems in soil liquefaction and thermal wave dissipation this work highlights two important fundamental physical phenomena: the flow of water through soil during liquefaction which contradicts the undrained assumptions of standard liquefaction research, and the dissipation of wave energy through thermally driven momentum diffusion which potentially explains the detectability of very tiny fractures in crystalline materials. These discoveries provide a whole new direction for the study of soil liquefaction and a starting point for further study of nano-scale wave propagation.

Future directions for research include the possibility of applying the NSA based continuum modeling approach to the derivation of continuum models for grain motion. These could couple to the fluid flow equations for the prediction of liquefaction in realistic heterogeneous deposits. In addition, the Bayesian computational techniques used to identify the parameters of the wave dissipation model could be utilized to identify the parameters of grain motion equations based on observations in either real earthquakes via boreholes, or in geotechnical centrifuge models.

Further investigation of micro-scale wave propagation and dissipation could include observing the distribution of small magnitude events in tabletop experiments such as the stress fracturing of a crystal in Åström et al. (2006) and pseudo-static sliding on a simulated fault in Voisin, Renard, and Grasso (2007). By specifying a threshold for detection of a wave, we can esti-

mate the effect of small-signal censoring and determine how this censoring of very small events affected the observed histogram of event sizes.

In the context of Bayesian modeling of dynamical systems, the difficulties that arise in doing efficient inference whenever computational models are used to obtain predictions suggests an area of research involving making model errors explicit through a choice of kernel or pseudo-kernel such as the Gaussian process model utilized here. In the presence of such a modeling-error model perhaps the continuity of the models can be used together with a fixed database of runs to interpolate the errors for intermediate values of important parameters, and obtain better inference without enormous amounts of computation. Future research could include software packages that automatically use these techniques to provide fast efficient inference for dynamic models.

# Bibliography

Åström, J., P.C.F. Di Stefano, F. Pröbst, L. Stodolsky, J. Timonen, C. Bucci, S. Cooper, et al. 2006. "Fracture processes observed with a cryogenic detector." *Physics Letters A* 356, no. 4–5 (August): 262–266. ISSN: 0375-9601, accessed January 25, 2013. doi:10.1016/j.physleta.2006.03.059. http://www.sciencedirect.com/science/article/pii/S0375960106005007.

Barenblatt, G. I. 2003. *Scaling.* Cambridge texts in applied mathematics. Cambridge: Cambridge University Press. ISBN: 0521826578.

Bear, Jacob. 1988. *Dynamics of fluids in porous media.* Dover books on physics and chemistry. New York: Dover. ISBN: 0486656756.

Beard, D.C., and P.K. Weyl. 1973. "Influence of Texture on Porosity and Permeability of Unconsolidated Sand." *AAPG Bulletin* 57. ISSN: 0149-1423, accessed September 18, 2011. doi:10.1306/819A4272-16C5-11D7-8645000102C1865D. http://search.datapages.com/data/doi/10.1306/819A4272-16C5-11D7-8645000102C1865D.

Brinkman, H. C. 1949. "A calculation of the viscous force exerted by a flowing fluid on a dense swarm of particles." *Applied Scientific Research* 1 (December): 27–34. ISSN: 0365-7132, 0003-6994, accessed September 19, 2011. doi:10.1007/BF02120313. http://www.springerlink.com/index/10.1007/BF02120313.

Chan, S. H., and A. H. W. Ngan. 2005. "Statistical distribution of contact forces in packings of deformable spheres." *Mechanics of Materials* 37 (4): 493–506. ISSN: 0167-6636.

Davis, R. O., and J. B. Berrill. 2001. "Pore Pressure and Dissipated Energy in Earthquakes—Field Verification." *Journal of Geotechnical and Geoenvironmental Engineering* 127 (3): 269. ISSN: 10900241. doi:10.1061/(ASCE)1090-0241(2001)127:3(269). http://link.aip.org/link/JGGEFK/v127/i3/p269/s1&Agg=doi.

Fiegel, Gregg L., and Bruce L. Kutter. 1994. "Liquefaction Mechanism for Layered Soils." *Journal of Geotechnical Engineering* 120 (4): 737. ISSN: 07339410. doi:10.1061/(ASCE)0733-9410(1994)120:4(737). http://link.aip.org/link/JGENDZ/v120/i4/p737/s1&Agg=doi.

Figueroa, J. Ludwig, Adel. S. Saada, Liqun Liang, and Nitin M. Dahisaria. 1994. "Evaluation of Soil Liquefaction by Energy Principles." *Journal of Geotechnical Engineering* 120 (9): 1554–1569. http://dx.doi.org/10.1061/(ASCE)0733-9410(1994)120:9(1554).

Fowler, Andrew. 1998. *Mathematical models in the applied sciences.* (Repr.) Cambridge: Cambridge Univ. Press. ISBN: 9780521467032.

Galvanetto, Ugo, and M. H. Aliabadi, eds. 2010. *Multiscale modeling in solid mechanics: computational approaches.* Computational and experimental methods in structures, vol. 3. London : London ; New York: Imperial College ; Distributed by World Scientific. ISBN: 9781848163072.

Geyer, Charles J., and Leif Johnson. 2013. *mcmc: Markov Chain Monte Carlo,* March. Accessed July 30, 2013. http://cran.r-project.org/web/packages/mcmc/index.html.

Goren, L., E. Aharonov, D. Sparks, and R. Toussaint. 2010. "Pore pressure evolution in deforming granular material: A general formulation and the infinitely stiff approximation." *J. Geophys. Res* 115.

———. 2011. "The Mechanical Coupling of Fluid-Filled Granular Material Under Shear." *Pure and Applied Geophysics* (June). ISSN: 0033-4553, accessed September 9, 2011. doi:10.1007/s00024-011-0320-4. http://www.springerlink.com/index/10.1007/s00024-011-0320-4.

Higdon, Dave, Marc Kennedy, James C. Cavendish, John A. Cafeo, and Robert D. Ryne. 2004. "Combining Field Data and Computer Simulations for Calibration and Prediction." *SIAM Journal on Scientific Computing* 26, no. 2 (January): 448–466. ISSN: 1064-8275, 1095-7197, accessed July 29, 2013. doi:10.1137/S1064827503426693. http://epubs.siam.org.libproxy.usc.edu/doi/abs/10.1137/S1064827503426693.

Holtz, R, and W Kovacs. 1981. *An introduction to geotechnical engineering.* Englewood Cliffs N.J.: Prentice-Hall. ISBN: 9780133539127.

Howison, Sam. 2005. *Practical applied mathematics: modelling, analysis, approximation.* Cambridge texts in applied mathematics. New York: Cambridge University Press. ISBN: 0521842743.

Idriss, I. M., and R. W. Boulanger. 2006. "Semi-empirical procedures for evaluating liquefaction potential during earthquakes." *Soil Dynamics and Earthquake Engineering* 26 (2-4): 115–130.

Kilminster, Devin, and Reason Machete. 2005. "Prediction, Behaviour, and Ignorance." In *Proceedings of 2005 International Symposium on Nonlinear Theory and its Applications.* Bruges, Belgium. ISBN: 4-88552-215-3, accessed July 26, 2013. http://www.ieice.org/proceedings/NOLTA2005/HTMLS/paper/7115.pdf.

Kokusho, Takeji. 1999. "Water Film in Liquefied Sand and Its Effect on Lateral Spread." *Journal of Geotechnical and Geoenvironmental Engineering* 125 (10): 817. ISSN: 10900241. doi:10.1061/(ASCE)1090-0241(1999)125:10(817). http://link.aip.org/link/JGGEFK/v125/i10/p817/s1&Agg=doi.

Kokusho, Takeji, and Tetsuro Kojima. 2002. "Mechanism for Postliquefaction Water Film Generation in Layered Sand." *Journal of Geotechnical and Geoenvironmental Engineering* 128, no. 2 (February): 129–137. http://link.aip.org/link/?QGT/128/129/1.

Kramer, Steven. 1996. *Geotechnical earthquake engineering.* Upper Saddle River N.J.: Prentice Hall. ISBN: 9780133749434.

Lakeland, Daniel L., Amy Rechenmacher, and Roger Ghanem. n.d. "Towards a Complete Model of Soil Liquefaction: the importance of fluid flow and grain motion." *Proceedings of the Royal Society of London. Series A, Mathematical and Physical Sciences.*

Liang, Liqun. 1995. "Development of an energy method for evaluating the liquefaction potential of a soil deposit." PhD diss., Case Western Reserve University. http://rave.ohiolink.edu/etdc/view?acc_num=case1058541489.

Lobry, C., and T. Sari. 2008. "Non-standard analysis and representation of reality." *International Journal of Control* 81 (3): 519–536. ISSN: 0020-7179. http://www.informaworld.com/10.1080/00207170701601728.

MacKay, David. 2003. *Information theory, inference, and learning algorithms.* Cambridge UK ;;New York: Cambridge University Press. ISBN: 9780521642989.

Mahajan, Sanjoy. 2010. *Street-fighting mathematics: the art of educated guessing and opportunistic problem solving.* Cambridge, Mass: MIT Press. ISBN: 9780262514293.

Majmudar, T. S., and R. P. Behringer. 2005. "Contact force measurements and stress-induced anisotropy in granular materials." *Nature* 435, no. 1079 (June): 1079–1082. ISSN: 0028-0836. doi:10.1038/nature03805. http://www.nature.com/doifinder/10.1038/nature03805.

Marin, Jean-Michel, Pierre Pudlo, Christian P. Robert, and Robin J. Ryder. 2012. "Approximate Bayesian computational methods" [in en]. *Statistics and Computing* 22, no. 6 (November): 1167–1180. ISSN: 0960-3174, 1573-1375, accessed July 26, 2013. doi:10.1007/s11222-011-9288-2. http://link.springer.com.libproxy.usc.edu/article/10.1007/s11222-011-9288-2.

Nelson, E. 1977. "Internal set theory: a new approach to nonstandard analysis." *AMERICAN MATHEMATICAL SOCIETY* 83 (6): 1165.

Nemat-Nasser, S., and A. Shokooh. 1979. "A unified approach to densification and liquefaction of cohesionless sand in cyclic shearing." *Canadian Geotechnical Journal* 16 (4): 659–678. ISSN: 1208-6010. doi:10.1139/t79-076. http://www.nrc.ca/cgi-bin/cisti/journals/rp/rp2_abst_e?cgj_t79-076_16_ns_nf_cgj16-79.

Ngan, A. H. W. 2004. "On distribution of contact forces in random granular packings." *Physica A: Statistical Mechanics and its Applications* 339 (3-4): 207–227. ISSN: 0378-4371.

NIST. 2012. *Thermophysical Properties of Fluid Systems.* Accessed February 14. http://webbook.nist.gov/chemistry/fluid/.

Nyquist, Christina. 2012. *The March 11 Tohoku Earthquake, One Year Later. What Have We Learned? | Science Features.* Accessed January 11, 2013. http://www.usgs.gov/blogs/features/usgs_top_story/the-march-11-tohoku-earthquake-one-year-later-what-have-we-learned/.

Plimpton, Steve. 1995. "Fast Parallel Algorithms for Short-Range Molecular Dynamics." *Journal of Computational Physics* 117, no. 1 (March): 1–19. ISSN: 0021-9991, accessed February 1, 2013. doi:10.1006/jcph.1995.1039. http://www.sciencedirect.com/science/article/pii/S002199918571039X.

Rechenmacher, Amy L., Sara Abedi, Olivier Chupin, and Andrés D. Orlando. 2011. "Characterization of mesoscale instabilities in localized granular shear using digital image correlation" [in en]. *Acta Geotechnica* 6, no. 4 (December): 205–217. ISSN: 1861-1125, 1861-1133, accessed August 19, 2013. doi:10.1007/s11440-011-0147-2. http://link.springer.com.libproxy.usc.edu/article/10.1007/s11440-011-0147-2.

Robert, Alain. 2011. *Nonstandard analysis.* Mineola N.Y.: Dover Publications. ISBN: 9780486432793.

Robinson, Abraham. 1996. *Non-standard analysis.* Rev. ed. Princeton N.J.: Princeton University Press. ISBN: 9780691044903.

Sawicki, Andrzej, and Jecek Mierczyński. 2006. "Developments in Modeling Liquefaction of Granular Soils, Caused by Cyclic Loads." *Applied Mechanics Reviews* 59 (2): 91. ISSN: 00036900. doi:10.1115/1.2130362. http://link.aip.org/link/AMREAD/v59/i2/p91/s1&Agg=doi.

Seed, R.B., K.O. Cetin, R.E.S. Moss, A.M. Kammerer, J. Wu, J.M. Pestana, M.F. Riemer, R.B. Sancio, J.D. Bray, R.E. Kayen, et al. 2003. "Recent advances in soil liquefaction engineering: a unified and consistent framework." In *Proceedings of the 26th Annual ASCE Los Angeles Geotechnical Spring Seminar: Long Beach, CA.*

Sivathayalan, S., and Y.P. Vaid. 1998. "Truly undrained response of granular soils with no membrane-penetration effects." *Canadian Geotechnical Journal* 35 (5): 730–739. ISSN: 12086010. doi:10.1139/cgj-35-5-730. http://www.nrc.ca/cgi-bin/cisti/journals/rp/rp2_abst_e?cgj_t98-048_35_ns_nf_cgj35-98.

Snelson, Edward, Carl Edward Rasmussen, and Zoubin Ghahramani. 2004. "Warped gaussian processes." *Advances in neural information processing systems* 16:337–344. Accessed August 2, 2013. http://books.google.com/books?hl=en&lr=&id=0F-9C7K8fQ8C&oi=fnd&pg=PA337&dq=%22a+form+well+modelled+by+a+GP.+Making+such+a+transformation+should+really+be+a%22+%22and+asymmetric+noise+in+general.+It+is+not+however+just+a+GP+with+a%22+&ots=TGKvoYRa50&sig=7CqnWm3_OWmbDU6iAg1cHPzJeZo.

Stewart, J. P., A. O. L. Kwok, Y. M. A. Hashash, N. Matasovic, R. Pyke, Z. Wang, and Z. Yang. 2008. "Pacific Earthquake Engineering Research Center." *University of California, Berkeley.* Accessed January 22, 2013. http://128.32.145.86/publications/peer_reports/reports_2008/web_PEER804_STEWARTetal.pdf.

Taddy, Matthew A., Herbert K. H. Lee, and Bruno Sansó. 2009. "Fast inference for statistical inverse problems" [in en]. *Inverse Problems* 25, no. 8 (August): 085001. ISSN: 0266-5611, accessed July 31, 2013. doi:10.1088/0266-5611/25/8/085001. http://iopscience.iop.org/0266-5611/25/8/085001.

The Maxima Project. 2011. *Maxima, A Computer Algebra System. Version 5.25.0. http://maxima.sourceforge.net.* http://maxima.sourceforge.net.

Verschoor, H. 1951. "Experimental data on the viscous force exerted by a flowing fluid on a dense swarm of particles." *Applied Scientific Research* 2 (January): 155–161. ISSN: 0365-7132, 0003-6994, accessed September 21, 2011. doi:10.1007/BF00411979. http://www.springerlink.com/index/10.1007/BF00411979.

Voisin, Christophe, François Renard, and Jean-Robert Grasso. 2007. "Long term friction: From stick-slip to stable sliding" [in en]. *Geophysical Research Letters* 34 (13): n/a–n/a. ISSN: 1944-8007, accessed January 25, 2013. doi:10.1029/2007GL029715. http://onlinelibrary.wiley.com/doi/10.1029/2007GL029715/abstract.

Zienkiewicz, O. C., C.T. Chang, and P. Bettess. 1980. "Drained, undrained, consolidating and dynamic behaviour assumptions in soils." *Géotechnique* 30, no. 4 (January): 385–395. ISSN: 0016-8505, 1751-7656, accessed September 3, 2013. doi:10.1680/geot.1980.30.4.385. http://www.icevirtuallibrary.com.libproxy.usc.edu/content/article/10.1680/geot.1980.30.4.385.